Passive Fire Protection of Metallic Structures

WAN NURSHEILA BINTI WAN JUSOH

A Thesis Submitted for the Degree of Doctor of Philosophy (PhD) in Mechanical Engineering at Newcastle University, United Kingdom

School of Engineering

February 2018

Abstract

This study evaluates the different approaches of Passive Fire Protection (PFP) on aluminium and steel. The first investigation determines effectiveness of newly developed multi-layer laminates made of aluminium, titanium and stainless steel foils insulating aluminium plate. This new means of fire protection is lighter than conventional flame retardant materials, such as intumescent coatings. Fire tests were conducted using a propane burner to provide 35 and 116 kW/m^2 constant heat flux on the samples with and without loading. Results show that laminate with titanium and stainless steel as front face gives better protection against fire compared to aluminium in vertical orientation testing.

The second studies focus on steel substrate temperature profile simulation using two newly developed models; Model I (Insulated Rear Face) and Model II (Uninsulated Rear Face). The accuracy of the models simulating the heat conduction were evaluated using three different PFP on 10 mm thickness steel substrate exposing it to 116 kW/m^2 constant heat flux. In this study, kaowool, furan microsphere and a commercial intumescent coating at different thicknesses are used as PFP. The results show that, although the three PFP thermal mechanism responses are different upon exposure to fire, the temperature-time profiles of each PFP show similar patterns. Simulation results demonstrate a reasonably good fit with experimental data for both models. This indicates that the developed models are capable to simulate temperature profile of steel substrate protected with different type of PFP.

The third studies introduce nanoparticles as fire protection additives in the quest to improve the properties of intumescent coatings protection on steel substrate. The assessment tests relied on the exposure of the material to 116 kW/m^2 heat flux by employing a direct flame from a propane burner. In this part of the work, a comparison of the additions of nanoclay, nanographene and multiwall carbon nanotubes, on their influence on intumescent coating behaviour, were studied. It is found that the addition of halloysite and graphene is able to maintain the substrate temperature below the steel failure temperature (450°C) after 2 hours of testing.

Overall, this study has been able to give a better understanding of various aspect of PFP performance on aluminium and steel through the different trials conducted. Recently established multi-layered laminate have demonstrated positive potential to be further developed as PFP materials especially in application that required lightweight structure. The developed models enable the user to simulate various type of PFP on steel using small-scale propane burner testing to replicate large-scale testing where the results can be a guidance and assessment for further development of the PFP.

Acknowledgements

First and foremost I would like to express my sincere appreciation to my supervisors, Prof. Gibson and Dr. George Kotsikos, for their assistance and guidance throughout this study. Without their constant support, this thesis would have not been possible.

I would also like to acknowledge my sponsors, Universiti Kuala Lumpur MIAT (UniKL MIAT) and Majlis Amanah Rakyat for the opportunity and financial support given to me to undertake this study.

Special thanks to Mr. Kai Yi from the Aerospace Research Institute of Material and Processing Technology for his help with the experiment and modelling during his visit as Visiting Scholar here. To my friends Kak Su, Nisa, Min, Katerina, Maria, Fazi, Kak Anna, Ayad, Asim, Sandra, Pietro, Johannes, Fatma and Hasan thank you for your friendship and also for being there through the ups and downs. My thanks are also extended to all Balai Malaysia Newcastle members, who have made home feel closer in one way or another. I also wish to extend my thanks to all support staff at the School of Mechanical and Systems Engineering for their assistance directly or indirectly during my studies.

Last but not least, I am truly grateful to my parents and siblings for their endless encouragement and support in every step that I have taken. I would not be here if it was not because of their prayers.

Table of Contents

List of Figures

List of Tables

List of Abbreviations and Symbols

Abbreviations	Description
1D	1-dimensional
CFRP	Carbon fibre reinforced polymer
COM_FIRE	Simulation program to run composite in fire
DSC	Differential scanning calorimetry
Glare	Glass laminate aluminium reinforced epoxy
HR10, HR20, HR40	Heating rates of 10°C/min^{-1}, 20°C/min^{-1}, 40°C/min^{-1}
TGA	Thermogravimetric analysis
HRR	Heat release rate
TTI	Time to ignition
THR	Total heat release
MARHE	Maximum average rate of heat emission
ARALL	Aramid fibre aluminium laminate
CARALL	Carbon fibre aluminium laminate
LDHs	Layered double hydroxides
CNT	Carbon nanotubes
MLG	Multi-layer graphene
MWNT	Multiwall carbon nano-tubes
FGNP	Functionalized graphene nanoplatelets
AFP	Active fire protection
PFP	Passive fire protection
ATH	Aluminium trihydrate
$Mg(OH)_2$	Magnesium hydroxide
ISO	International Organization for Standardization
LOI	Limiting oxygen index
NES	UK Naval Engineering Standard
CFD	Computational fluid dynamics

Symbols	Description
α	Thermal diffusivity
t_0	Initial time
5XXX/6XXX	Class of aluminium, 5 or 6
A	Pre-exponential rate factor (s-1)
ASTM	American Section of the International Association for Testing Materials
b	Slab half-thickness
Bi	Biot number
C_p	Specific heat of the composite
C_{pg}	Specific heat of the volatiles
e	Absorptivity of the protection surface
E_i	Activation energy (J/mol)
F_0	Fourier number
h	Heat transfer coefficient
h, h_g	Enthalpy of the composite and the volatile
k	Thermal conductivity of the composite in the through thickness direction
m_g	Mass flow if volatile
n_i	Order of the reaction
Q_i	Heat decomposition
R	Universal gas constant (8.314 J/mol.K)
T	Temperature
t	Time
T	Temperature (K)
T_0	Initial uniform temperature of the PFP and substrate
T_1 (K)	Surface temperature/ hot face temperature of the PFP
T_{Fire} (K)	Fire temperature
Tg	Glass transition temperature
x	Distance below the hot surface in the through-thickness direction (m)
X	PFP thickness
ϵ	Emissivity
ρ	Density of the composite (kg/m^3)
σ	Stefan-Boltzmann constant ($Wm^{-2}K^{-4}$)

List of Publications

1. S. Christke, A. G. Gibson, Wan Wan Jusoh, G. Kotsikos. Use of expandable multi-layer metal laminates as fire protection for aluminium and CFRP aerospace structures. 20th International Conference on Composite Materials, Copenhagen, 19-24th July 2015.
2. A. G. Gibson, Wan Wan Jusoh, G. Kotsikos, P. Di Modica, S. Christke, K. Yi, A.P. Mouritz, E. Kandare, RMIT, Australia. Model for the characterisation and design of passive fire protection (PFP) systems for steel structures. Proceedings of the 17th European Conference on Composite Materials (ECCM17). Munich, Germany, June 2016.
3. K. Yi, Wan Wan Jusoh and A. G. Gibson. Thermal modelling of epoxy based intumescent coating in fire protection using passive fire protection (PFP) systems for steel structures.
   Proceedings of the 17th European Conference on Composite Materials (ECCM17). Munich, Germany, June 2016.
4. Wan Wan Jusoh, G. Kotsikos, A. G. Gibson. A propane burner test to characterise the performance of passive fire protection (PFP) formulations. 16th European Meeting on Fire Retardant Polymeric Materials. Manchester July 2017.
5. A.G.Gibson, W.N.B. Wan Jusoh, G.Kotsikos (2018). A propane burner test for passive fire protection (PFP) formulations containing added halloysite, carbon nanotubes and graphene, Polymer Degradation and Stability, 148, pp. 86-94.

Chapter 1. Introduction

Protection against fire has always been a priority in any industry. High public awareness about fire safety has led to a lot of research being conducted in this area over the years. The main purpose of fire protection is to control and eliminate a fire before it could have more serious consequences in terms of money and human life.

Three major sectors where flame retardants are required are transportation, construction and the oil and gas industry. The main hazards during aircraft fires, for example, are heat, smoke, and toxic gases. Life-threatening levels of these hazards are produced by cabin flashover, the time to which is largely governed by the rate of heat release of the materials on fire (Hergenrother *et al.*, 2005; Griffin, 2010; Fogle *et al.*, 2012).

The USA Federal Aviation Administration indicates that the total heat release, heat release rate and smoke emission are the major elements to look out for in a fire. The total heat released within the first two minutes should not exceed 65 kW.min/m^2. During a post-crash fire, the fire should not reach the interior within 4 to 5 minutes after a crash and the material used has to protect passengers from any interference of a post-crash fire (Gaetano, 2010 ; Mróz *et al.*, 2016). Marine regulatory agencies, such as the International Maritime Organization as stated in the High Speed Craft Code and the US Coast Guard, demand that fire protection should be able to protect aluminium from exceeding 230 ℃ during a standard fire resistance test.

Metallic materials like aluminium and steel are among the most commonly used materials for structural frameworks, especially in aerospace, oil and gas and building construction. Both materials offer numerous advantages, but suffer the same disadvantage in fire, where they soften or lose rigidity and compromise the integrity of the structure. Prevention of the structural collapse of a building is paramount to ensure the safe evacuation of people from the building (Duquesne *et al.*, 2004; Jimenez *et al.*, 2006b). Structural survivability depends on the properties of the structural materials in resisting deformation and failure, rather than the prevention of combustion.

The simplest way to overcome the above-mentioned disadvantages of metal frameworks is to protect the metallic material from fire. In general, the main objective of fire protection is to limit and suppress the fire either by mechanical means or chemical reaction and slowing down the heat transfer between the fire and insulated material. A good fire protection will delay the failure time of the protected structure and extend the strength integrity of the burning materials which will provide extra evacuation time.

Generally, the response of combustible materials to fire can be classified into fire reaction and fire resistance.

1.1 Fire Reaction

Fire reaction is the ability of a material to burn or undergo combustion during the early stages of a fire, typically due to ignition and flashover. The fire reaction also illustrates the level of smoke toxicity from combustible materials. Babrauskas and Peacock (1991) reported that the reaction-to-fire is the response of the material upon heating or exposure to fire, which includes the heat release rate, time-to-ignition, flame spread and oxygen index.

1.1.1 Heat Release Rate

The heat release rate is one of the vital fire reaction parameters which indicates the hazard associated with combustible materials. The heat release rate value of composite materials determines the thermal energy released in the process of thermo-chemical decomposition, and especially the flammable gas released during the decomposition of the matrix polymer or organic fibres. The maximum amount of heat released by the material during combustion is specified as the Peak Heat Release Rate (PHRR), which is an important indicator of the temperature and the maximum transmission rate of fire. The PHRR is the maximum amount of heat released by the material during the combustion process and is a critical control for the temperature and the maximum transmission rate of fire.

1.1.2 Time-to-Ignition

Time-to-ignition is the length of time during which flammable materials can resist radiant heat flux before igniting and flaming combustion. Ignition time can be used as a rough measurement or estimation of the fire resistance of a material.

1.1.3 Flame Spread Rate

The flame spread rate is determined as the speed of the flame front moving over the surface of a combustible material. This rate is measured experimentally either in a downward, vertical or inclined direction.

1.1.4 Oxygen Index

The oxygen index is described as the minimum oxygen content required to sustain the flaming combustion of a material. High oxygen index materials are usually used in high-risk applications like internal structures and components, since these can self-extinguish when the fire becomes deprived of oxygen.

1.2 Fire Resistance

Fire resistance is described as the ability of a material to constrain the spread of fire and maintain structural integrity. Three main fire-resistant properties are heat insulation, burn-through resistance and structural integrity.

1.2.1 Heat Insulation

Heat insulation is the resistance of the material preventing heat from flowing through it during a fire. A good heat insulation material like a composite is able to reduce the advance of a fire from one space to another.

1.2.2 Burn-through Resistance

Burn-through resistance is the time needed by the flame to penetrate through the material and develop from the back side. Materials such as composites have better burn-through resistance compared to metal with low melting temperature like aluminium that could melts above 600°C.

1.2.3 Mechanical Integrity

Mechanical integrity is defined as the capability of the structure to retain its mechanical properties such as stiffness, creep resistance and strength upon being exposed to fire and after the fire is extinguished (Mouritz and Gibson, 2006).

1.3 Project Objectives

The thesis is divided into six chapters with the main three chapters focus on thermal behaviour of different types of PFP using aluminium and steel as substrate. The first studies developed a multi-layer laminate consisting of thin metal foils made from aluminium, titanium and stainless steel with 30µm thickness and bonded together using epoxy resin (see figure 1.1). The primary objective of this studies is to determine the thermal properties of multi-layered laminates and the effect of using low and high melting points foils as the front surface of the laminate. Although studies has been conducted by Maljaars and Fellinger (2005), Fogle *et al.* (2012) and Afaghi Khatibi *et al.* (2014) on the properties of aluminium at elevated temperature, fire protection studies using similar methods are very limited in number.

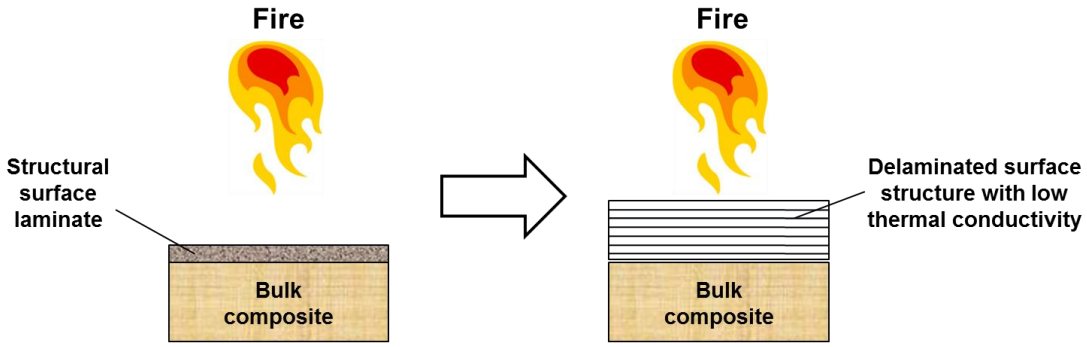

Figure 1. 1 Multilayer protection mechanism

This new approach of insulation uses material which is lighter than that in the conventional flame retardant method. Aluminium 5083, which is chosen as a substrate in this study, is commonly used in marine and other exterior industries due to its low weight and corrosion resistance (Fogle *et al.*, 2012). Although the aluminium 5XXX series has been used extensively in the marine industry, reports on its fire properties are limited.

The second studies evaluate two newly developed models with different rear face conditions (Model I (Insulated Rear Face) and Model II (Uninsulated Rear Face)). The models predict the temperature profile of steel protected with different types of PFP, which are commercial intumescent coating, ceramic wool and a furan microsphere composite. The commercial coating and ceramic wool are commonly found in various industries as steel structural protection, while the furan microsphere is made from a new biodegradable furan resin with microsphere glass fibres which make it an environmental friendly PFP. This composite will have great advantages if it can replace the intumescent coating which decomposes at high temperatures and produces large amounts of smokes and chemical gases during fires. The models developed are expected to be able to simulate the temperature profile of the steel substrate under different type of PFP.

The final studies determine the influence of the addition of nanoparticle halloysite, multiwall carbon nanotube and nanographene on the basic in-house intumescent coating formulations upon exposure to direct flame from a propane burner. This project uses a steel plate as a substrate, as most intumescent coating applications are commercially used as passive fire protection on a steel structure. The changes in the macrostructure and microstructure on each formulation before and after a fire test are determined using a digital camera and Scanning Electron Microstructure (SEM). The influence of the nanoparticles on the steel temperature profile was simulated using Model II (Uninsulated Rear Face) established in the earlier studies in this thesis.

Chapter 2. Literature Review

2.1 Background of Fire

In order for material to ignite, three basic elements need to be available. Fire will occur when fuel, heat and oxygen are present in the right combination. A fuel is any flammable material that could undertake combustion, while heat is the amount of energy needed to ignite the fuel, and oxygen is the oxidising agent. All three elements are interconnected in a chemical chain reaction that sustains and continues the combustion process, until the absence of any basic ignition elements (see figure 2.1 below).

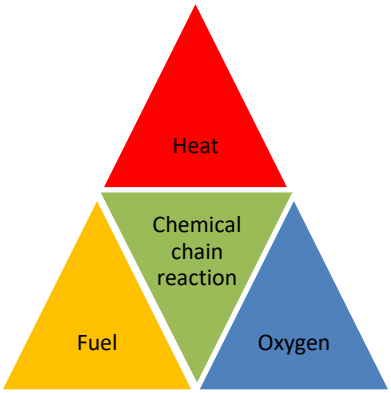

Figure 2.1 Fire tetrahedron representing the connection between the elements of combustion

The stages of fire growth shown in figure 2.2 start with an induction period which involves heating of material prior to flaming ignition. Ignition takes place either spontaneously or is caused by an external source, such as a spark or flame. During ignition, an exothermic reaction increases the temperature, leading to the breakdown of chemical bonds and the production of a volatile substance. Prior to ignition, the internal moisture evaporates, and the volatile gasses produced change the internal structure of the material.

Ignition time is among the important parameters for the thermal resistance of a material. The longer it takes for the material to heat up, ignite and start a fire, the higher its ignition time. The ignition time is reduced with the increase of heat flux. As soon as ignition occurs, the decomposition of material and the amount of combustible gases increase (Xu and Fang, 2013).

Once ignited, combustion is self-sustaining and grows through the process of flame spread. The material will experience pyrolysis and decompose, creating more flammable products. During the combustion period, radiative heat will be transferred to nearby objects or material and the fire will spread. As this process continues, the radiant heat flux will increase and fire could fill up the room with a flammable or explosive fuel-air mixture, which leads to a flashover condition (Hull and Stec, 2009).

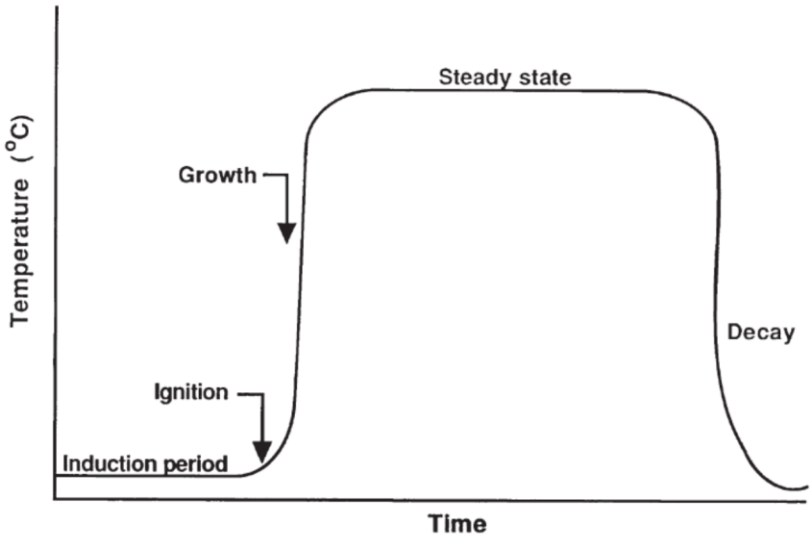

Figure 2.2 Stages in a fire (Hull and Stec, 2009)

Flashover by definition could be a sudden transformation of localised fire, and it is still reasonably easy to extinguish it before moving to the fully developed fire stage with the participation of combustible material (see figure 2.3). Any occupants trapped at this stage will have a small chance of survival (Drysdale, 1999). Many fire scientists agree that the main element of flashover in a fire is the peak heat release rate (PHRR).

PHRR is reached when any one of the following events occurs: (a) the fire becomes ventilation-controlled and combustion proceeds at a steady-state rate; (b) a fire suppression system activates; (c) the decay phase begins (in a fuel-controlled fire) (Bwalya, 2008).

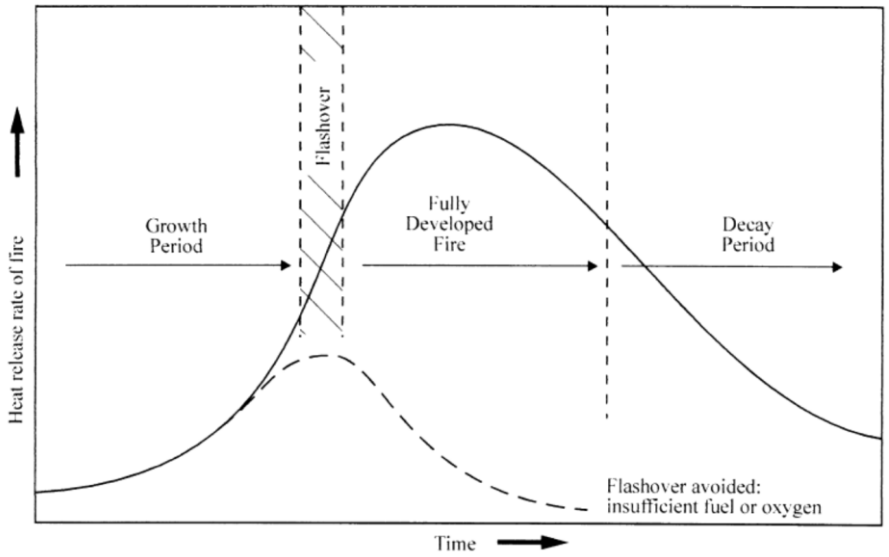

Figure 2.3 Schematic of fire growth within a compartment (Drysdale, 1999)

2.2 Fire Detection System

Fire detection systems could be either manual or automatic systems. Fire detectors can be basically divided into three categories: heat detectors, smoke or gas detectors, or flame detectors. Fire detector applications are summarised in table 2.1 below.

Type	Where to use	Action	Recommended Use	Cost
Heat Detectors				
Fixed temperature	Large open areas, to protect heat-generating equipment	Respond when a predetermined temperature is reached	Use limited to indoor applications	Low
Rate of rise	Large open areas	Responds to a specific temperature rise per minute	Should be used indoors; low false-alarm rate	Low
Rate compensated	Large open areas, to protect heat generating equipment	The detector and its enclosure has to reach a critical temperature. It compensates to spikes.	Should be used indoors, low false-alarm rate.	Low
Smoke Detectors				
Photoelectric	Projected beam type used in open areas, high rack storage, computer rooms and aircraft hangars	Smouldering fires	Must be used indoors	Moderate
Ionization	Offices, computer rooms, combustible materials	Fast-flaming fires	Should be used indoors	Moderate
Flame detectors				
Infrared	Hazardous work, explosive and rocket propellant manufacturing, aircraft hangars	Rapid response to infrared radiation generated by fire	Indoor use, may be affected by heat	High
Ultraviolet	Hazardous work, explosive and rocket propellant manufacturing, aircraft hangars	Rapid response in milliseconds to ultraviolet radiation generated by fire	May be used indoors or out, lenses need cleaning	High

Table 2.1: Summary of fire detector applications (Duncan, 2001)

2.3 Fire Protection

ASTM E119 is one of well-known standard for fire testing which is a widely used standard for walls, partitions and floor or roof systems. The standard is used to determine the response of materials, products or assemblies upon exposure to heat and flame under controlled temperatures as provided by furnace. This method is aim to assess the period for the specimen to retain its structure integrity and exhibit their dependant properties upon the predetermined test exposure. Thermocouples are attached at several locations of the specimen to monitor the heat conduction during the testing. Some countries have their own fire testing standards, as shown in figure 2.4. The assessments made in these countries are quite similar based on the temperature-time curve. Nonetheless, the assessment criteria are marginally different in terms of the size of test specimens, heating methods, temperature-time curve standards, test methods and the performance criteria used (Hung and Chow, 2002).

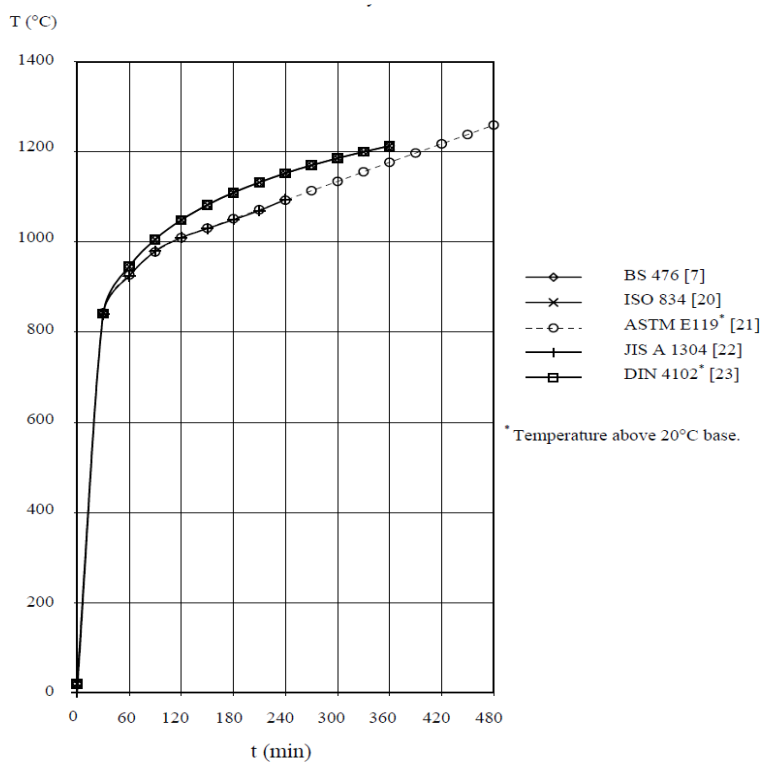

Figure 2.4 Comparison of different standard temperature-time curves (Hung and Chow, 2002)

Basically, fire protection can be divided into two main categories: active and passive fire protection. Both types of protection are meant to provide the safeguarding of structural components by keeping the temperature below a critical temperature and preventing the fire from spreading for a certain period of time (Mróz *et al.*, 2016).

2.4 Active Fire Protection (AFP)

In the event of fire, an AFP system requires some activation response, either mechanically or electronically. Fire alarms, water sprinklers, automatic extinguishing spray systems and smoke exhaust systems are among the widely used in commercial and residential buildings.

A properly installed active fire detector will be able to identify heat or combustion in its early stages and raise an alarm. The most important component in active protection methods is the actuation method. The actuator contains thermal detectors such as sprinklers or automatic fire detectors (see figure 2.5). Choosing the best actuation method depends on the response time and reliability required and also the level of alarm nuisance to be tolerated (Milke, 2016).

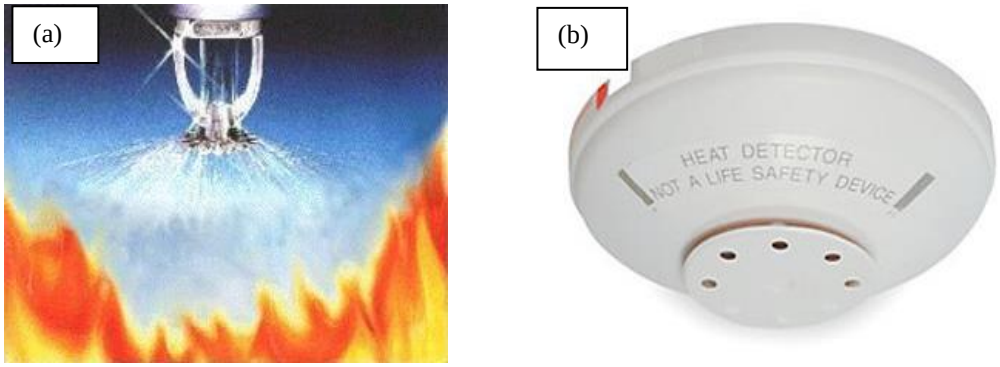

Figure 2.5 Example of active fire protection: (a) water sprinkler; (b) heat detector (www.newark.com)

2.5 Passive Fire Protection (PFP)

Passive fire protection can be described as a stand-alone protection system that could provide thermal protection without any need for external activation. PFP systems will become active spontaneously in the presence of fire.

PFP will reduce and slow down the development of fire as soon as it is exposed to it, but the protection depends on the thermo-physical and thermo-mechanical properties of the protected structure and the changes in the PFP materials during exposure to fire (Gomez-Mares *et al.*, 2012b; Milke, 2016). PFP systems can be divided into several groups, such as thermal insulation barriers, sprays, intumescent boards and seals.

2.5.1 Thermal Insulation Barrier

Mineral wool, which is sometimes known as rock wool, is among the oldest types of non-combustible insulation material. This mineral wool will not burn but melts beyond 1000°C and is commonly found in residential and industrial buildings, piping and also furnace industries. Kaowool from the words kaolin and wool, is one of the synthetic mineral wools. that consists of different lengths and diameters of amorphous fibres. Expanded perlite, shale, clay, slate and vermiculite are also non-combustible mineral materials which may be considered as aggregates for fireproofing (see figure 2.6) with high thermal insulation to give good protection upon exposure to fire (Mróz *et al.*, 2016).

In building construction, cementitious fireproofing materials like vermiculite or clay made from inexpensive raw materials are among the favourites for PFP systems because of its competitive price. Non-combustible materials have been effective and preferred for many years until recently, when the advances in intumescent coating formulations have made these more favourable.

Figure 2.6 Example of fireproofing material sprayed onto steel structure (http://southerninsulationgroup.com/sprayed-fire-resistive-material/)

2.5.2 Concrete and Gypsum

Concrete is a common material found in any basic civil engineering structure and it comes with large amounts of bound water. This water will vaporise due to the heat from exposed surfaces in fires, and it absorbs the heat and thus reduces the temperature in the internal part of a structural member. The low thermal conductivity of concrete will then give adequate evacuation time to occupants (Mróz *et al.*, 2016).

Another type of PFP is gypsum, also known as calcium sulphate dihydrate. Gypsum is a crystalline mineral found in sedimentary rock or it can also be found as synthetic gypsum from coal-fired electrical utilities which have removed the sulphur dioxide from flue gasses.

Upon exposure to heat, water will be released from the crystal lattice of calcium sulphate dihydrate, which together with free moisture, evaporates thus absorbs a significant amount of heat. The dehydration process happens between 80°C and 250°C subject to the heating rate of the gypsum board and its composition (Paulik *et al.*, 1992; Kontogeorgos and Founti, 2012).

2.5.3 Multi-Layered Laminate Protection

Laminated materials, also known as multi-layer composites, are a combination of different materials cohesively bonded together to meet the application requirement. The most common multi-layered materials are known as Fibre Metal Laminated (FML) composites. Among commercially available FML are GLARE (Glass fibre aluminium laminate), ARALL (Aramid fibre aluminium laminate and CARALL (Carbon fibre aluminium laminate).

According to (Sinmazçelik *et al.*, 2011) researchers have also been exploring the potential of using metallic alloys such as magnesium and titanium in FML instead of aluminium alloys. The combination of these high performance alloys will improve the low performance of aluminium alloy thermal properties.

Multi-layer fire retardant materials usually consist of numbers of metallic linings and non-metallic layers. The metallic material generally found is aluminium, steel or titanium while the non-metallic layers will be the adhesive either from thermoset or thermoplastic resin.

The rapid expansion of lightweight structural components has become the main drive of thin metal applications like metallic foils. Metallic foils are widely use in food and electronic packaging industries especially as aluminium foils, where they are used as wraps, bags and electrical appliances and other decorative applications.

Foil materials can usually be found within the range of 10 µm to 250 µm. Foils with thickness below 200 µm are known for their light weight with effective thermal insulator and protection against environmental effects such as air and moisture (Keles and Dundar, 2007; Desgrosseilliers *et al.*, 2013).

However, Lee *et al.* (2013) reported, damage like dissimilar roughness, oxidation or corrosion will have a major effect on the mechanical behaviour of thin metallic foils compared to its bulk materials.

Foils made from titanium based alloys are generally found as honeycomb material in aerospace structures because of their low density and good thermal properties. Titanium foils are used on wing and fuselage skins and as a noise damping in jet turbines.

Burianek and Spearing (2000) and Kim and Ramulu (2007) investigated the prospect of using titanium foils as facesheets of polymer matrix composite in high temperature applications, such as airframes and combustion engines. It is believed that the use of titanium foils with high durability are able to protect the polymer matrix composite from environmental effects like oxidation and moisture, as well as providing impact resistance and bearing properties (Burianek and Spearing, 2000; Kim and Ramulu, 2007).

The use of stainless steel foils with excellent corrosion resistance, high weldabilities and high strength also become popular due to the downsizing of electrical and medical devices.

Nevertheless, a study on insulated aluminium using laminated foils as fire protection is relatively new. A recent studies conducted by Christke *et al.* (2016) has successfully indicated good potential for the use of aluminium foils as passive fire protection on aluminium substrate. The aluminium multi-layer laminate is able to show a similar temperature reduction to that provided by superwool and intumescent coatings.

2.5.4 Intumescent Coating

Intumescent coatings are among the most well-known types of passive fire protection materials for steel in built infrastructure and offshore applications. Intumescent coating is easy to apply to any surface and does not change any of the properties of the substrate. The application of intumescent coatings in various industries can be traced back to the 1980s.

Intumescent coatings are designed to perform under severe conditions and maintain the integrity of steel between 1 and 3 hours when the temperature of the surroundings is in excess of 1100 ^{o}C such as in the oil and gas industry (Jimenez *et al.*, 2006b).

Intumescent coating can be either water based, solvent based or epoxy based. The coating will begin to melt and expand between 200 °C to 250 °C. Simultaneously, chemical reactions are initiated which release inert gases with a reduction in thermal conductivity.

Intumescent materials start to expand above a critical temperature, producing an expanded carbonaceous char which protects the underlying substrate by slowing down the rate of heat transfer from the fire. The reaction leads to the expansion or foaming of the coating, sometimes up to several times of its original thickness, to form a protective carbonaceous char that acts as an insulative barrier between the fire and the substrate (Jimenez *et al.*, 2006b).

The expansion of the intumescent structure into an insulative barrier has been represented by Duquesne *et al.* (2004) as in figure 2.7 below, where the expansion process is described as a slow diffusion of gases within the structure.

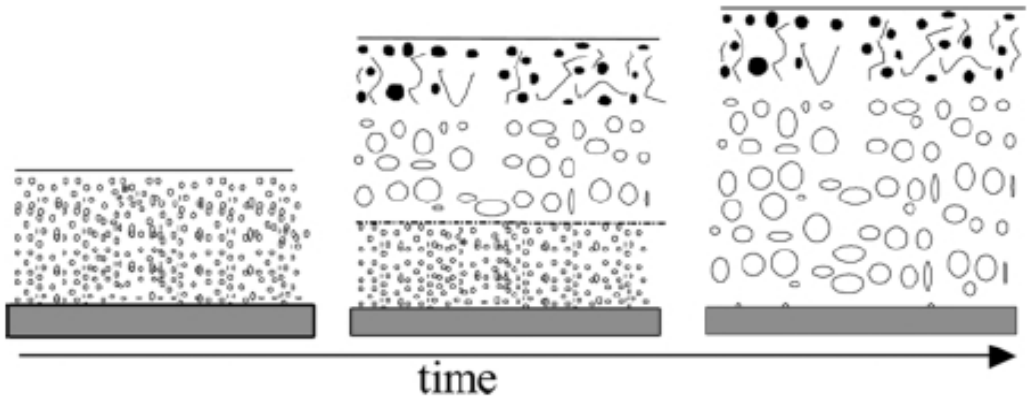

Figure 2. 7 Intumescence process involving the diffusion of gases to form an insulative barrier (Duquesne *et al.*, 2004)

In pioneering work, Camino *et al*., (1984); (1989) explained that the process of pyrolysis turning polymers into volatile flammable products is prevented by the presence of a protective char limiting the transmission of heat and oxygen. The formulation of the coating has to be optimized in terms of chemical and physical properties in order to form an effective protective char (Camino *et al.*, 1984; 1989).

Generally three active ingredients are used: an acid source, which is normally ammonium polyphosphate or a mineral acid; an 'carbonifics' source such as char-forming polymers or polyols and a 'spumific' or blowing agent such as melamine that promotes the production and the foaming of gases (Camino *et al.*, 1984; 1989; Jimenez *et al.*, 2006b), along with the presence of a binder and the addition of various fillers to improve fire retardancy performance.

The mechanism of intumescence usually starts with the acid breaking down to yield a mineral acid, which then takes part in the dehydration of a carbonization agent to yield the carbon char. Finally, the blowing agent decomposes to yield gaseous products. The latter cause the char to swell, and hence provide an insulating multi-cellular protective layer (Jimenez *et al.*, 2006b).

The production of char from the organic polymer and intumescent additives in the liquid phase lead to physical combination, chemical interaction and the development of char-bonded structures, according to Horrocks *et al.* (1996). If the chemical properties are compatible, any flame retardant additives and char formation polymer will combine and bond with intumescent additives.

Intumescent coatings generally experience four stages of physical and chemical changes when exposed to fire, according to (Griffin, 2010) as displayed in figure 2.8. In this study, the coating used is a epoxy-based material with inorganic filler component which are glass fibres and zinc borate particles. The first stage is when the polymer matrix melts depending on whether the polymeric binder is thermoplastic or thermoset. In the second stage, constituents of the coating decompose, producing gas which expands and cause the matrix foams. In the third stage, the polymeric component is converted into an inert and porous carbonaceous char, along with further gas evolution. Finally, the char itself undergoes degradation.

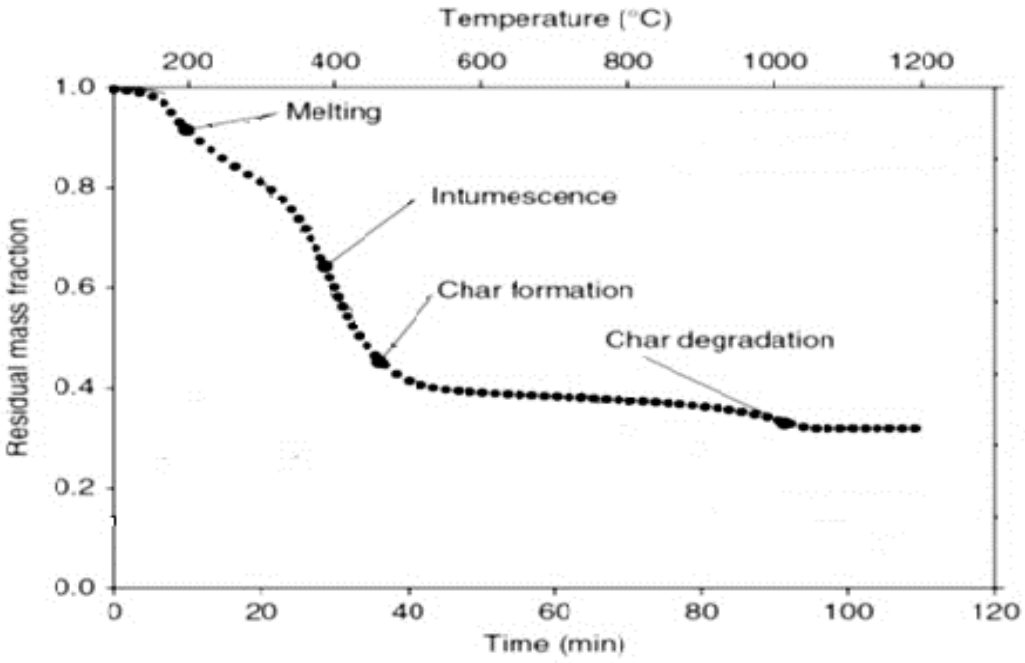

Figure 2. 8 TGA/DSC plots of intumescent coatings heated under nitrogen with indications of four stages of physical and chemical changes (Griffin, 2010)

An effective intumescent shield must be mechanically stable to facilitate the internal gas pressure and it must be able to swell to stop heat transfer to the substrate as the temperature increases (Bodzay *et al.*, 2011). At the same time it must remain attached to the substrate that it is intended to protect. These elements of microstructure and the expansion of the char are crucial in order to give excellent heat insulating properties (Lecouvet *et al.*, 2013a).

Intumescent coatings are of course susceptible to ultraviolet and other elements of environmental exposure factors that will reduce their fire protection capability during fire. In particular, key components of intumescent systems may leach out over time, reducing effectiveness. As described by Wang *et al.* (2010) the continuous loss of hydrophilic elements as ageing increases reduces the final expansion and increases the thermal conductivity of the substrate.

Much research has focussed on enhancing the flame retardancy of epoxy and other resins through combinations with various flame retardant additives. These have included halogenated elements which been exceptionally effective. However, these ingredients produce toxic and corrosive gasses during combustion (Liu *et al.*, 2014) and are also highlighted as key elements in global warming.

2.5.5 Fire Retardant Fillers

An organic polymer is the fuel alongside oxygen and heat in a composite material fire triangle. Quenching the fire by cooling can be achieved by the use of additives that can absorb a portion of the total heat and reduce the temperature until the burning material will no longer release enough volatile vapour to maintain the combustible mixture.

Fire retardant fillers have been estimated to present about 500, 000 tonnes or about 40 % of the total fire retardant additive market by weight. Endothermic decomposition of the fillers produces inert gasses such as water or carbon dioxide (Hornsby, 2007).

The two major metal hydroxides used as fire retardant fillers are aluminium trihydrate (ATH) and magnesium hydroxide ($Mg(OH)_2$. Both fillers can be found naturally and synthetically. It is understood that the aluminium hydroxide ($Al(OH)_3$) and magnesium hydroxide ($Mg(OH)_2$) in polymeric materials have a triple function as filler, flame retardant and smoke suppressant (Liang, 2013).

ATH is used in inert mineral fillers that will decompose at around 300 ^oC to form a protective, non-flammable layer on the material surface and produce water. ATH decomposes according to the following reaction:

$$2Al(OH)_{3(s)} \longrightarrow Al_2O_{3(s)} + 3H_2O_{(g)} \qquad [2.1]$$

Normally, ATH is added at around 60 wt.% by mass to make it effective as a fire retardant filler. This high loading affects the mechanical properties of the composite and it has always been a limitation of metal hydroxides (Hull *et al.*, 2011).

Magnesium hydroxide is the second most common fire retardant filler and decomposes around 300 ^oC, compared to ATH but is more expensive. Magnesium hydroxide has similar properties to ATH, and will release water during breakdown to magnesium oxide (Formosa *et al.*, 2011; Hull *et al.*, 2011):

$$Mg(OH)_2 \longrightarrow MgO + H_2O \qquad [2.2]$$

The breakdown of magnesium hydroxide starts at about 300^oC and is an endothermic reaction. Magnesium hydroxide seems to offer high levels of fire retardancy and does not produce smoke or corrosive fumes (Hornsby, 2007).

The greater decomposition of $Mg(OH)_2$ compared to ATH allows the former to be used in polymers with higher processing temperatures close to 200 ^oC, such as polyamides and polyesters (Formosa *et al.*, 2011).

2.5.6 Nanomaterial Fire Retardant Fillers

Commonly found nanomaterials in flame retardant materials are like silicates, carbonaceous nanomaterial, and inorganic hydroxides (Alongi *et al.*, 2015). Studies have also been conducted on carbon based flame retardant additives, such as multiwall nanotubes, functionalized graphene, black carbon and extended graphite (Laachachi *et al.*, 2015).

Reports also show improvements in fire retardants using layered double hydroxides (LDHs), polyhedral oligomeric silsequioxanes (POSS) (Du *et al.*, 2009), lamellar nanoclay with Polyamide-6 (PA6) (Gilman *et al.*, 2000) and halloysite nanoclay (Lecouvet *et al.*, 2013a). Nanomaterials disintegrate during combustion and form a carbonaceous structure on the surface which acts as a barrier to heat and mass transport which protects the polymer underneath from the heat source (Wang and Wilkie, 2006).

Carbon Nanotube (CNT)

Kashiwagi *et al.* (2005b) and Du and Fang (2011) have reported that carbon nanotubes (CNTs) can provide combustible polymer material with flame retardant properties from the cluttering of CNTs.

Dittrich *et al.* (2013) studied the effects of spherical carbon black (CB), tubular multiwall carbon nano-tubes (MCNT), expanded graphite (EG) and semi-commercial thin multi-layer graphene (MLG). The research revealed that MLG shows promising results compared to spherical particles and tubes, due to the rise in the onset temperature of polypropylene decomposition and changes in the rheological behaviour of polymer melt (Dittrich *et al.*, 2013).

Improvements in fire retardancy depend on the development of the network structure of CNTs to create a layer of thermal shield from the flame. The addition of CNTs as low as 0.5 wt.% to 7 wt.% has been proven to be effective in improving a flame retardancy (Kashiwagi *et al.*, 2005a; Kashiwagi *et al.*, 2005b; Rahatekar *et al.*, 2010; Dittrich *et al.*, 2013).

The addition of CNT form a thermal shield protects the matrix and creates a skeleton frame that increases char strength. However, according to Du and Fang (2011) entanglement between the CNTs at the degradation temperature will lead to a fragile char and weaken fire protection.

Ding *et al.* (2016), on the other hand, reported that MCNTs increase the initial decomposition temperature and influence the thermal barrier by preventing heat transfer and diffusion.

Isitman and Kaynak (2010) reported that there is a relatively small enhancement by the addition of clays (3 wt.%) and CNT (1 wt.%) in terms of weight fraction, with increments of 1.5% of the LOI test results. This was attributed to the migration of nanoparticles in the direction of the flaming surface, thus protecting the polymer.

Nanoclays

The advantages of nanoclay and nanotubes in promoting a protective layer during combustion manages to control heat and mass transfer has attracted a lot of attention in recent years (Isitman and Kaynak, 2010). Several studies have reported that the addition of nanoclay in polymer matrices is able to decrease its heat release rate of the polymer (Gilman *et al.*, 2000; Lecouvet *et al.*, 2013a; Kahraman *et al.*, 2015).

Nanoclays improve a polymer's barrier properties by creating a shield that prevents the movement of gas molecules through the polymer matrix when heated and separates the polymer base from the thermal energy.

Beyond a certain amount of nanoclay (~3 wt.%), its cross-linked network will prevent inert gas from escaping and increase melting phase viscosity, which leads to the reduction of char thickness and poor flame retardancy (Lecouvet *et al.*, 2013a).

Nanoclay has a layered structure and is a hydrous aluminium silicate with metal oxides and organic material elements. Depending on the structural and physical properties, it can be categorized into a few classes such as, for example, halloysite, montmorillonite, kaolinite and bentonite (Shan *et al.*, 2015; Nazir *et al.*, 2016).

Kashiwagi *et al.* (2004) reported that peak heat release was reduced by 40 % with only 0.1 wt.% addition of nanoclay . In a study on silica-based polymer nanocomposite, it was also found that the addition of silica gel to the low-molecular-weight poly(methyl methacrylate) leads to the formation of silica near the sample surface during combustion and reduces heat release rate by around 50% compared to a pure sample (Kashiwagi *et al.*, 2002).

Lecouvet *et al.* (2013a) reported the effects of the addition of nanohalloysite in intumescent polypropylene nanocomposites in cone calorimetry tests at 50 kW/m^2. It was found that the addition of 3 wt.% of nanohalloysite gives the maximum efficiency in reducing the second peak of heat release rate (HRR) values from 206 kW/m^2 at 530s for intumescent coating formulation without nanohalloysite to 145 kW/m^2 at 740 s for intumescent coating formulation with nanohalloysite.

The combination of halloysite in intumescent formulations creates stronger char strength. The char develops good structural integrity with even void size and no cracking with increasing clay content. A cross-sectional view of the char reveals a “pillar” like structure linking the bottom and cellular foamed layer (Lu and Wilkie, 2010), as shown in figure 2.9.

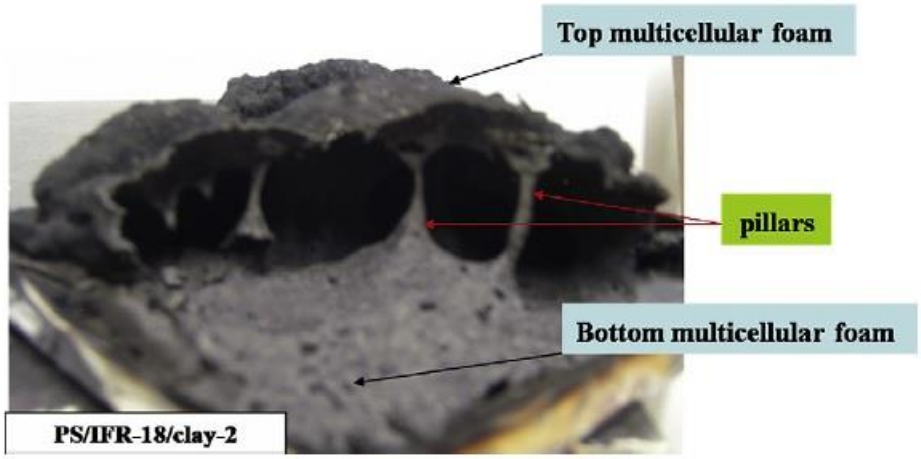

Figure 2. 9 Image of char residue from intumescent flame retardant composite with additives after cone calorimetry tests (Lu and Wilkie, 2010)

This structure exhibits good mechanical strength at high temperatures and against the internal pressure generated by degradation products. This will therefore avoid feeding the gas phase, which means a lower flame intensity of the fire (Lecouvet *et al.*, 2013a).

Gilman *et al.* (2000) has reported that the addition of nanoclay montmorillonite in polymeric matrices manages to reduce the peak HRR up to 50-70%. Montmorillonite is a smectite clay with poor bonds between the cation and water molecules and layer silicate. Montmorillonite particles can help to reduce the flammability of polymeric materials to prevent a strong boiling process in the course of combustion. If the amount of clay is less than 3%, there is an obvious reduction in PHRR due to radical trapping by the iron present in the clay, as reported by Zhu *et al.* (2001).

Nanographene

The broad potential of graphene use in the fields of nanocomposites, nanoelectronic, batteries or super-capacitors has generated great interest among researchers.

Graphene is more preferable as a nanofiller compared to carbon nanotubes in terms of manufacturing cost and the tube entanglement which is commonly found with carbon nanotubes. Graphene platelets have a high surface area, high mechanical strength and good chemical stability (Zaman *et al.*, 2011; Liu *et al.*, 2014).

A study was conducted by Guo *et al.* (2011) on the flame retardant properties of graphene, graphite oxide and functionalized graphite oxide in epoxy-based composites. The TGA results for samples with graphite addition showed that graphene promotes higher amounts of remaining char and reduces derivative thermogravimetry peaks.

The authors also concluded that the graphene and functionalized graphite samples increased the thermal stability and flame retardancy of epoxy-based composites. The TG-FTIR spectrum of the gas phase display combustion at low temperatures but lower amounts of gas were released at higher temperatures, which could be due to the effect of the layered structure of graphite (Guo *et al.*, 2011).

It has been reported by Liu *et al.* (2014) that char development is promoted with the increase of graphene content and improved the thermal degradation and stability of epoxy resin at high temperature (400-430°C). The addition of 4.7 wt.% graphene increased the char residue by up to 5.8%.

In previous work by Mohammadi *et al.* (2015), the addition of 2 % Functionalized Graphene Nanoplatelets (FGNP) to IFR formulations enhanced the fire retardancy of the coating and extended the time to failure. The presence of FGNP strengthens the char structure and its adhesion to the steel compared to IFR formulations without FGNP where the char becomes detached from the substrate.

A rise in maximum degradation temperature in TGA data for IFR-FGNP is associated with the strong interfacial bond between FGNP and the epoxy which increases the activation energy of thermal degradation by blocking the thermal motion of the polymer chains.

This view is supported by Yuan *et al.* (2014) and Liu *et al.* (2014) who proposed that the spread of graphene with a specific structure in the matrix forms a barrier against combustible gas and heat, acting as a heat sink by preventing heat build-up and also eliminating radicals formed in the thermal degradation process. The high surface ratio of graphene prevents a pathway for gas molecules to diffuse and slow down the heat transfer.

The addition of graphene increases the thermal conductivity of the composite, as has been reported previously by various researchers (Chatterjee *et al.*, 2012; Liu *et al.*, 2014). This, however is compensated for the addition of more than 1wt.% of graphene which promotes more char residue and therefore improves the thermal barrier effect that exceeds the effect of thermal conductivity by reducing the PHRR (Liu *et al.*, 2014).

Studies by Zhang *et al.* (2010) and Mhike *et al.* (2014) both have found that flake graphite was able to prolong the time to ignition (TTI) in polyethylene.

2.6 Epoxy Resin

Epoxy is a thermosetting resin widely used for surface coating, adhesives, semiconductors, and as filler or fibre-reinforced composites in aerospace, automotive and marine vessels because of its low cost, easy processing, good mechanical properties and environmental stability.

The resin curing process is usually 150-180 °C involving cross-linking reactions between the monomers when an initiator is added to activate the polymerization process to create a chain molecule. This organic based polymer unfortunately, is one of the sources contributing to the fire. The volume of heat released from the fire depends on the quantity of flammable volatiles produced from the breakdown of polymer matrix during a fire.

At an adequate temperature roughly around 380 to 450 °C with the presence of oxygen, epoxy will undergo a series of chemical reaction mechanisms of polymer decomposition. Gibson *et al.*, (2001) reported a gradual decomposition of the resin phase which subsequently produces liquid and gaseous products once going in the fire.

Chain scission is the dominant reaction in the decomposition of the polymer. The rising temperatures lead to a breaking of the polymer chains into monomeric, oligomeric and materials of low molecular weight. This process produces different kinds of reactions such as volatile gas, char and soot particles in the air. These volatiles consist of various gas, which can flammable, such as carbon monoxide and methane, and non-flammable like carbon dioxide and water (Mouritz and Gibson, 2006).

In the course of fire, resin reaches the glass transition temperature for thermosetting and softening for thermoplastic. This phase transition makes the resin begin to reduce its mechanical strength which significantly affects the structural load (Gibson *et al.*, 2006; Gibson *et al.*, 2011)

Polymer reinforced fibre composite using organic materials such as epoxy as matrix has shown possibility for use in applications that would be exposed to fire. It is able to resist the high temperature through low fundamental thermal conductivity and also from the endothermic resin decomposition process when an adequately thick section is used

2.7 Biodegradable Resin

Phenolic resin is one of the conventional thermoset resins such as epoxies, vinyl esters, and unsaturated polyesters that are commonly used in protective interior varnishes, electrical insulator layers and anticorrosion coatings for metals. It is well-known for its exceptional chemical and thermal resistance and is produced from phenol and formaldehyde (Biedermann and Grob, 2006; Rivero *et al.*, 2014). Formaldehyde is highly toxic and its volatility can be released during usage, manufacturing, storage and deposition stage of any production process containing residual formaldehyde (Rivero *et al.*, 2014).

In recent years, a lot of attention has been paid to producing products from renewable resources that are sustainable and eco-friendly. The growth of sensitivity towards the environment among policymakers has been the driver for the development of environmentally friendly polymer-based products that are mostly based on hydrocarbon sources (Rivero *et al.*, 2014; Kandola *et al.*, 2015; Monti *et al.*, 2015).

Researchers have successfully produced vegetable oil, linseed oil and soybean oil as base materials for resin and hardeners (Gupta *et al.*, 2011; Bertomeu *et al.*, 2012; Gandini and Lacerda, 2015). Campaner *et al.* (2009) have developed the Cardanol-based novolac resin curing agent for diglycidyl ether of bisphenol A epoxy resin made from cardanol cashew nut shell liquid.

Although the toxicity of renewable resources is lower than that of hydrocarbon-based resin, the flammability of the new resins must be able to provide as effective fire protection as conventional resin, but without contamination by formaldehyde emissions (Kandola *et al.*, 2015; Monti *et al.*, 2015).

Specifically for phenolic resin, few studies on furan resin have demonstrated positive results when replacing phenolic resin in terms of thermal properties and reaction to fire, as reported by Rivero *et al.* (2011), Kandola *et al.* (2015) and Monti *et al.* (2015).

Furan resin made from agricultural residues containing pentoses through furfural alcohol polymerisation has shown positive results when replacing phenolic resin in terms of thermal properties and reaction to fire.

There are only a few available publications on furan thermal degradation and its charring mechanism. According to Monti *et al.* (2015), the possible formation of a heat resistant structure in the char is due to aromatisation by the dehydration of crosslinking structure in furan resin. Monti *et al.* (2015) also reported that the comprehensive breakdown of the organic structure to organic volatile does not contribute to heating, but instead changes it to a stable char.

2.8 Fire Testing

2.8.1 Cone Calorimeter

Cone calorimeter has been used extensively for research and development in fire retardant materials. A cone calorimeter test is usually conducted according to ISO 5660 and ASTM E 1354. Cone calorimeter is a forced combustion test which principle of measurement is based on the amount of heat release during combustion which is linked to the amount of oxygen used during combustion. Heat release rate is the main contribution of fire spread and growth. The time and magnitude of the heat release is crucial in estimating the rate of fire growth. This bench scale fire testing using 100 mm x 100 mm sample plate under forced-flaming conditions.

The burning environment of the cone calorimeter is capable of producing a representation of actual well-ventilated fire conditions where the heat flux could reach 100 kW/m^2. Cone calorimeter provide constant heat flux on the sample surface causing the phase transition and formation of pyrolysis within the sample where the decomposition occurs. The ignition of the material will occur when the surface temperature exceeds the decomposition temperature in pyrolysis formation zone (Schartel *et al.*, 2005). Tests using the cone calorimeter can be conducted in a horizontal or vertical direction, as shown in figure 2.10.

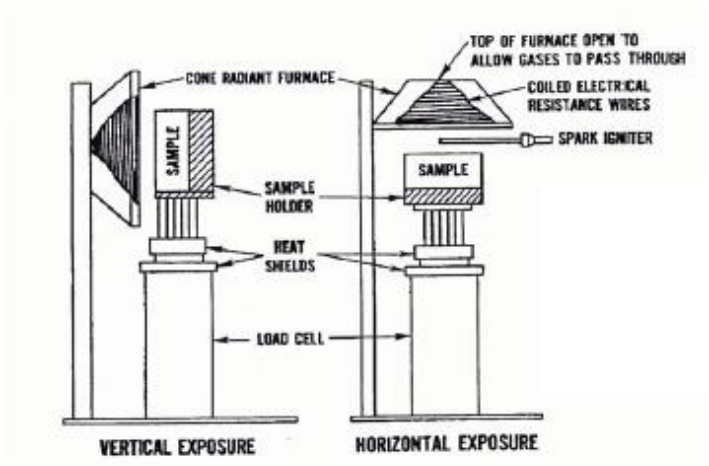

Figure 2. 10 Schematic of cone calorimeter sample in vertical and horizontal directions (Greene).

In a horizontal orientation, the convective heat transfer is almost negligible. The flame spread in this orientation is much slower because of the initial heating by conduction and the downward radiation (Hull and Kandola, 2008). The vertical test flame spread is more rapid and able to replicate a real fire in the vertical direction. The effect of ply degradation on composite materials can also be determined through this orientation (Mouritz and Gibson, 2006).

Babrauskas (1992) reported that during a horizontal direction test at 25 and 100 kW/m^2, about 2 % peak variation was detected on the sample surface, whereas the peak variation is increased to 7 % in a vertical direction test.

The accuracy of the main data collected from the cone calorimeter is vital since it will become the input for the modelling and approximation of large scale fires. Fire properties such as HRR, mass loss, smoke production and char yields are measured, and with an additional gas analyser, the range of results will be improved (Schartel *et al.*, 2005; Lindholm *et al.*, 2012).

2.8.3 Limiting Oxygen Index

The limiting oxygen index (LOI) is defined as the minimum amount of oxygen needed to sustain flaming combustion, and it can be considered as a measure of the ease of self-extinguishment of a burning material. The LOI is widely used to determine the fire performance of composites, although the correlation between the index value and heat release rate for example, may not be clear (Weil *et al.*, 1992).

The LOI test is conducted in a rig with a vertical chimney 450 or 500 mm in height with an internal diameter of 75 or 100 mm (see figure 2.11). The chimney is made from heat-resistant glass, which allows observation of the burning. Tests are usually run at room temperature, but it is also possible to test at higher temperatures by heating the chimney. Oxygen and nitrogen are supplied at the base of the chimney that flow through a layer of glass beads that could provide even mix before entering the main chimney.

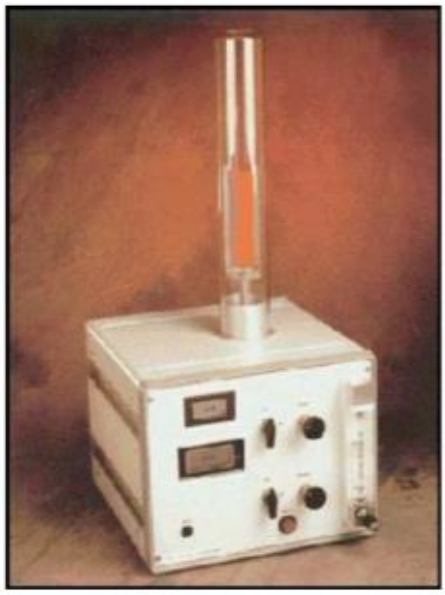

Figure 2. 11 Example of limiting oxygen index apparatus

During an LOI test, samples are exposed to an ignition flame atmosphere with different oxygen levels. The results will determine the minimum oxygen the sample needs to burn with a candle-like flame.

The LOI method was established in numerous test standards, such as the ASTM D2863, ISO 4589-2 and NES 714. However, the oxygen index value can vary with changes in temperature, resulting in changing relative flammability rankings of some materials (Mouritz and Gibson, 2006).

2.8.4 Jet Fire Test

Jet fire testing is among the important risk assessment tests for the safety of pipelines, gas pressure vessels and other components that could potentially produce a high-pressure flame.

According to standard jet fire test ISO 22899-1:2007, the test consists of simulation of thermal and mechanical loads produced from high-flammable gas pressure. During the test, the jet flame is aimed at the test piece and the burn-through time and temperature rise in the case of are evaluated. A large jet fire test, able to produce a 20 meter long horizontal flame form a natural gas onto the test sample. The sample is exposed to 300 kW/m^2 heat flux with high gas pressure of ~50 ms^{-1}. The sample is exposed to the flame until the rear-face reaches a certain temperature and the burn-through resistance of the material is determined (Mouritz and Gibson, 2006).

European Accident Database reported that, most jet fire incidents involve liquefied petroleum gas (LPG), either during transportation or processing. Mishandling of LPG is the main contributor to incidents which lead to serious impacts (Gómez-Mares *et al.*, 2008).

2.8.5 Furnace Test

The certification of fire resistance in large composites such as ships, buildings and offshore platforms is usually tested using a furnace. Most furnace tests expose a panel to controlled temperature-time conditions. The temperature of the sample in the furnace test is monitored using a thermocouple attached to the surface either exposed or unexposed to the flame. The test sample fire resistance is usually defined by the time taken for unexposed panels not to exhibit surface temperature of 160°C or for a hot spot to reach 180°C.

Commonly, temperature-time heating curves are divided into cellulosic and hydrocarbon fires. According to the ASTM 119, within 5 minutes of cellulosic fire testing the flame temperature will reach 500 °C and increase as the time is extended. A cellulosic fire is normally fuel by the combustion of timber or fabrics. Hydrocarbon fires, on the other hand, are fuelled by oil and gas and the flame temperature could reach 1000 °C within 5 minutes or even sooner. Figure 2.12 shows common temperature-time heating curves used in furnace testing.

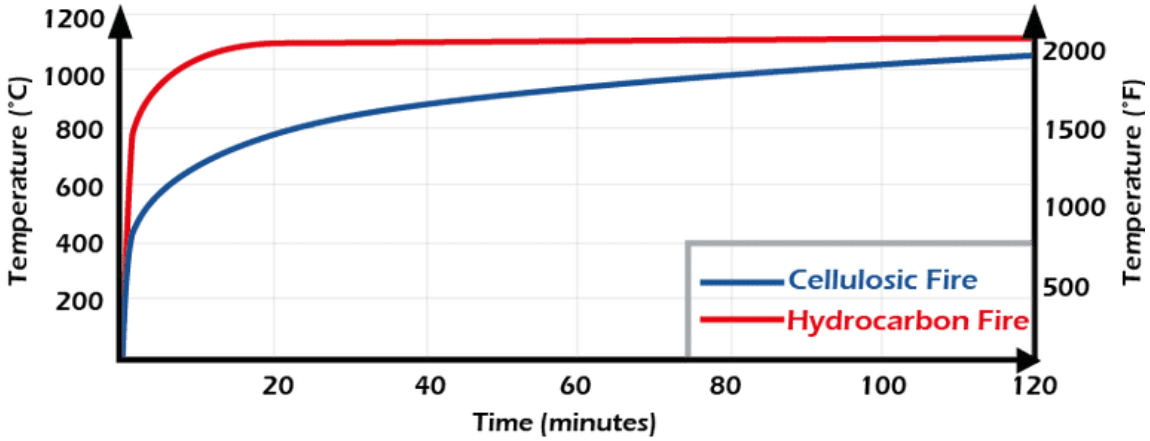

Figure 2. 12 Standard fire curves for cellulosic and hydrocarbon fire (http://interdam.com/a0-a60-h0-h60-h120-fire-ratings/)

2.9 Aluminium In Fire

Recently application of aluminium in offshore platforms, marine industries, transportation and bridges (see figure 2. 13) has increased due to the versatility of aluminium alloys that come with durable, lightweight and good corrosion resistance, which is desirable compared to steel.

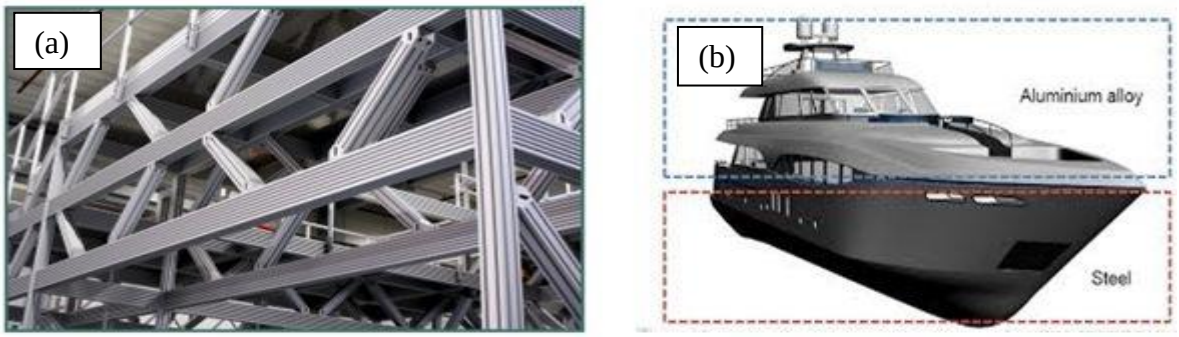

Figure 2. 13 stable aluminium frames and working platforms (b) lightweight aluminium alloy widely used as ships structures (www.rk-rose-krieger.com)

There are different classes of aluminium depending on its alloying elements. Series 2XXX and 7XXX, usually found in the aerospace industry contains more chromium, while series 5XXX and 6XXX are generally used as structural material for the marine industry.

Aluminium alloy is known to have a high thermal conductivity that is between 100 to 250 W/m.K at room temperature, subject to the type of alloys as indicated in figure 2.14 (Maljaars *et al.* (2005)). At room temperature, the specific heat (Cp) is ~900 J/kg℃ while at 500 ℃ it is around 1100 J/kg℃. The density of aluminium is ~ 2700 kg/m^3 and uncoated aluminium emissivity ε_{al} varies from 0.03 to 0.31 while for coated aluminium either with paint, insulation or soot is generalized at 0.7 (EN 1999-1-2, (2007).

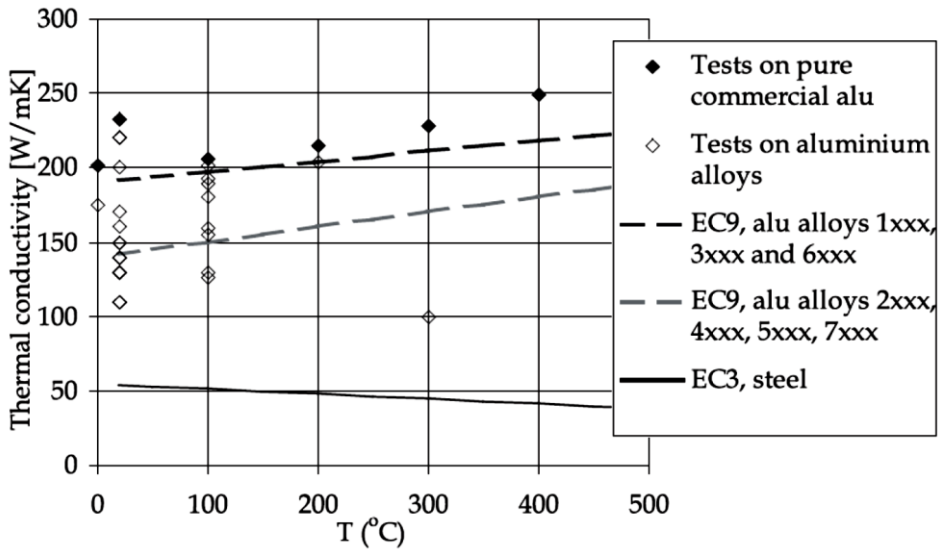

Figure 2. 14 Thermal conductivity of aluminium alloys and of steel at elevated temperature (Maljaars *et al.*, 2005)

The high thermal conductivity of aluminium has raised concerns, particularly regarding the fire safety of aluminium where the mechanical properties start to degrade at 150 ℃ with 50 % yield strength reduction at around 275 ℃ (Langhelle and Amdahl, 2001).

The mechanical strength of aluminium rapidly decreases with the rising of temperature. The low softening temperature of aluminium (150 ℃) has become the motivation for many researchers to develop models to predict the failure time and temperature of aluminium. These researches have mainly focused on the aluminium response under the load while being subjected to one-sided heating (Suzuki *et al.*, 2005; Kandare *et al.*, 2010b; Maljaars *et al.*, 2010; Fogle *et al.*, 2012; Afaghi Khatibi *et al.*, 2014).

Maljaars *et al*. (2010), conclude in his research, that insulation for aluminium structures needs to have a low density, low thermal conductivity and be flexible to meet the large thermal-creep deformations of aluminium. The insulation also needs to be cohesive with the structure and does not promote corrosion.

According to the International Maritime Organization (IMO) in the High Speed Craft Code and US Coast Guard, during the standard fire resistance test, the insulation should be able to provide necessary protection to prevent the aluminium temperature from exceeding 230 ℃ (IMO, 1998). In Eurocode 9: Part 1-2 recommends the failure temperature to be 170 ℃ for aluminium structure design in fire (BS, 2009).

2.9.1 Aluminium Under Tensile Load in Fire

The degradation of aluminium strength and stiffness at elevated temperature is more significant than steel as reported by Maljaars *et* al. (2005) in figure 2.15 even though the aluminium and steel are in the same dimensions.

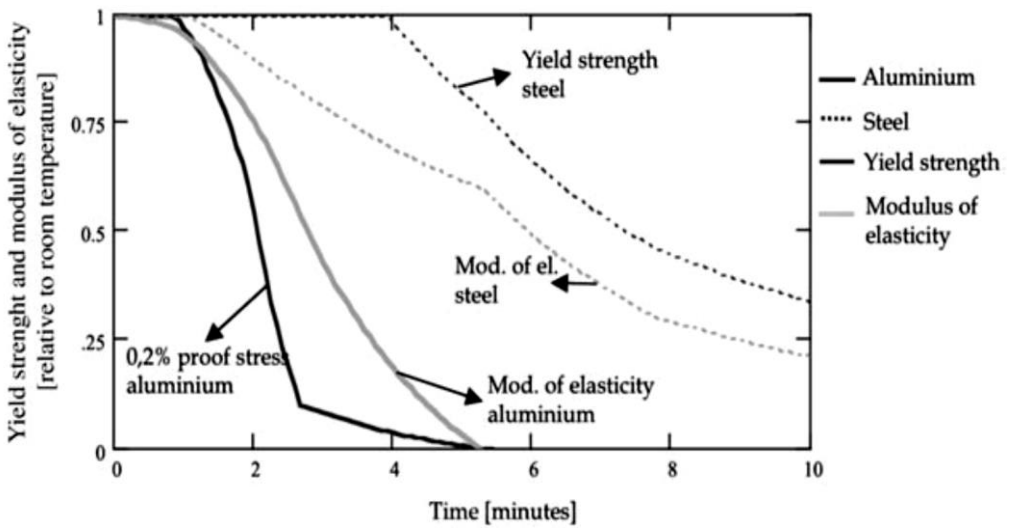

Figure 2. 15 Mechanical properties of steel and aluminium square hollow section 50 x 50 x 2 mm exposed to a constant elevated temperature (Maljaars *et al.*, 2005).

Fire testing underload is a more reliable method for assessing the structural integrity during fire than without loading (Fogle *et al.*, 2012). Afaghi Khatibi *et al*., (2014) describe upon exposure to the heat flux, the plate initially expands due to thermal expansion of aluminium.

After a specific time (which is dependent on the applied tensile stress and heat flux), the width of the plate reaches maximum value due to expansion and then begins to progressively contract. This contraction thin the plate especially in the middle part. A basic visualization in figure 2.16 shows the tensile-loaded plate in one-sided heat flux.

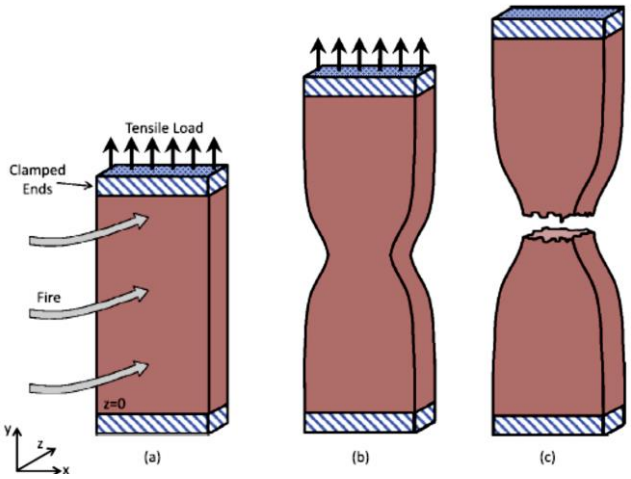

Figure 2. 16 Representation of the thermal mechanical modelling condition of aluminium plate heated from one-side by fire while loaded in tension (a) before the plastic necking phase (b) during necking and (c) after final failure (Afaghi-Khatibi *et al.*, 2014)

Aluminium strength reduces at around 150-250 °C due to dislocation recovery and precipitate growth. The strength continues to decrease as the temperature increases to 250-350 °C due to recrystallization during the annealing temperature (Gupta *et al.*, 2001b; Vandermeer and Hansen, 2008; Summers *et al.*, 2014). This has been also supported by various researchers who found that the aluminium starts to lose it strength at 150 °C and at around 350 °C, 50 % of the strength is reduced (Kandare *et al.*, 2010a; Afaghi Khatibi *et al.*, 2014; Christke *et al.*, 2016).

2.9.2 Aluminium Under Compression Test

Aluminium is vulnerable to buckling failures due to its low ratio of stiffness over strength. Although the buckling failure for aluminium is quite similar to steel design, failures in aluminium happen earlier than those in steel.

Maljaars *et al.* (2009) reported that the failure temperature of 5XXX and 6XXX series aluminium under compression at elevated temperature are within 170 to 350 °C (Maljaars *et al.*, 2009a; Maljaars *et al.*, 2009b). Fogle *et al.* (2012), reported that the failure temperature for the aluminium plates that were tested at different heat flux lies between 100 to 480 °C depending upon the applied stress (10 % to 85 % of the room temperature Euler buckling load) and the type of the aluminium.

Assessing the structural integrity on structural load is more predictable in a fire resistance test with load compared to without load because of the relationship between the applied stress and the failure temperature (Fogle *et al.*, 2012).

2.10 Carbon Fibre Reinforced Plastic (CFRP) in Fire

The growing use of carbon fibre reinforced plastic (CFRP) in the transportation industry, such as aerospace and marine applications, has raised the issue of fire safety of the structures. Upon exposure to fire, heat flux will be transferred through the CFRP. Once the hot surface region reaches about 200-300 °C, the pyrolysis process will begin, and epoxy matrix starts to crack, producing volatile gasses and char formation on exposed regions.

The entire organic material in this region has changed to char. The formations of these char could act as thermal barriers protecting the heat from transferring further into the laminate. Under the char region is the decomposition area where the partially decomposed resin heated lower than the char formation temperature. In the next region, the delamination cracks between the plies and matrix can be found.

The rear face region will remain unaffected if the heat transfer is not enough to create delamination or softening of the matrix. If the heat exposure is prolonged, the composite temperature will continue to rise and the pyrolysis will take place on the unexposed region and eventually the composite will burn out (see figure 2.17) (Davies *et al.*, 2006; Mouritz and Gibson, 2006; Mouritz *et al.*, 2006; Quang Dao *et al.*, 2013).

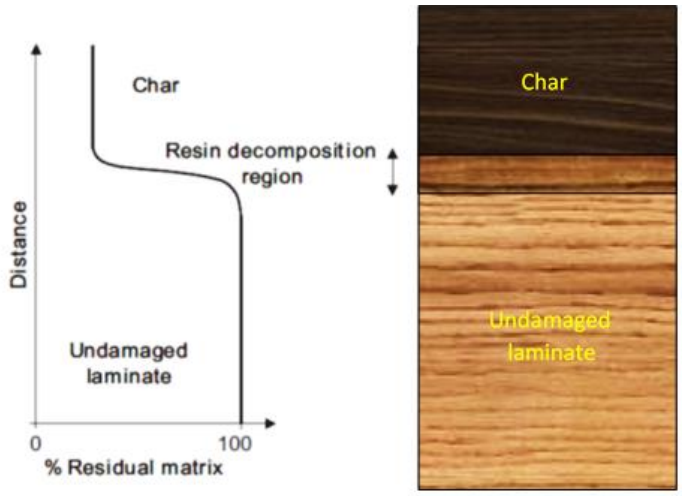

Figure 2. 17 Schematic of resin degradation through laminate, with resin decomposition zone and residual char with example composite cross-section exposed to a heat flux of 50 kW/m^2 (Mouritz and Gibson, 2006)

After exposure to fire, delamination and cracking of plies and matrix is usually observed on composite layers. This is due to the fact that internal pressure built-up within the material from the volatile gas production or the vaporization of trapped moisture. The volatile out-gassing prevents the air from penetrating into the composite. This happen above the glass transition temperature of most polymers (Mouritz and Gibson, 2006; Feih *et al.*, 2007)

Chapter 3. Multi-layered Laminate Protection on Aluminium

This chapter outlines the study conducted on the newly developed multi-layer laminates. This new type of PFP will be lighter than conventional PFP such as intumescent coatings. The multi-layer laminates made of aluminium, titanium and stainless steel foils insulating aluminium plate. These foils and aluminium plate are bonded together using hand-lay-up technique using an epoxy resin. In this study, aluminium 5083 is use as a substrate, and commonly found in marine industries due to its low weight and high corrosion resistance. The thermal and physical properties of multi-layer laminate samples were characterised and evaluated upon exposure to constant heat flux. This new approach of insulation is lighter than conventional flame retardant material like intumescent coating.

3.1 Multi-Layered Laminate Material Background

In this study, aluminium foils will be the main part of the multi-layered laminate. Compared to other type of foils, aluminium foil is the most used foil in everyday applications and also known for its light weight, good corrosion resistance, and barrier against moisture and oxygen. Although there are many advantages of aluminium, the low melting temperature (~660 °C) of aluminium limits its application in elevated temperatures.

This leads to the fabrication of another two foil laminates with higher melting temperatures to improve their fire protection but made from lightweight material. Titanium and stainless steel foils are selected as the front layer followed with layers of aluminium foils at the back. Versatility of both foils in any applications and melting temperatures of 1660 °C and 1400 °C laminate makes it favourable than other metallic foils. Basic physical properties of materials used in this study are tabulated in table 3.1 below.

	Density (kgm^{-3})	T_{melt} (°C)	T_{decomp} (°C)	Conductivity ($Wm^{-1}K^{-1}$)	Heat Capacity ($Jkg^{-1}K^{-1}$)
Epoxy resin	1160	-	300-350	0.18-0.2	800-1200
Aluminium	2700-2750	660	-	204	910
Titanium	4500	1660	-	19-23	540
Stainless Steel	7480-8000	1400	-	12-45	490-530

Table 3. 1 Material physical properties

The 30 µm micron thickness foils used in this study are in the same thickness as foil tape which is generally found as ducting, joining dissimilar materials like glass fibre or rockwool and heat reflection in the electronics industry. Commercially, 20 to 50 µm thickness foils are considered as medium gauge foil.

3.2 Multi-layered Sample Preparation

Each sample consists of 20 layers of foils in three different configurations as shown in figure 3.1 (a) below. A non-fire retardant epoxy resin RS-L135 with RS-H137 hardener from PRF Composite Materials which was used to bond the foils and plates together in this study.

Foil laminates were prepared by the hand layup method using a hand brush and roll onto an aluminium plate using a rolling pin and a sponge roller (see figure 3.1 (b)). Samples were cured at room temperature for 24 hours then post cured at 50 ℃ for 15 hours. All tests used an aluminium plate as substrate except for fire without load test which used both aluminium plate and carbon fibre laminate. This aluminium plate is among low strength aluminium that is normally found in marine applications because of its lightweight and corrosion resistance.

As received foils are in 300 mm widths which are later cut into particular sizes depending upon their specific test. The 30 µm thickness of foils are from Aluminium foils (North East Laboratory Supplies), Titanium foils (William Gregor Ltd) and Stainless Steel SN3034 from Hollinbrow Precision Products.

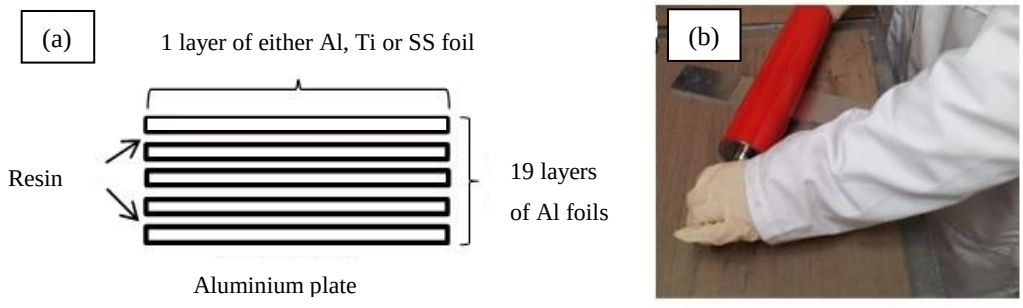

Figure 3. 1 (a) sample configuration with 20 layers of foils. The top layer is interchangeable between Al, Ti or SS foils (b) laminating foils using a rolling pin on substrate

3.3 Thermogravimetric Analysis

Thermogravimetric Analysis (TGA) was conducted on the cured epoxy resin and hardener mixture using PerkinElmer STA3000. The thermal analysis result indicates degradation of the resin upon heating, where the polymer went through physical changes breaking the polymer chain and reducing the mass.

Samples between 8 to 10 mg were examined under inert nitrogen environments to prevent oxidation and burning. The endothermic reaction breaking the chemical bond and evaporate the volatile contents (Laoutid *et al.*, 2009; Monti *et al.*, 2015).

TGA measured the decomposition of resin (mass loss) with the increasing temperature, from room temperature up to 900 ^{o}C. Three different heating rates, 10 °C/min, 20 °C/min and 40 °C/min were conducted in a nitrogen atmosphere.

As observed in figure 3.2, it can be seen that as the heating rate increased, the onset of decomposition curve shifted to a higher temperature due to its thermal kinetics. The first disintegration stage of thermal degradation started between 342 to 373℃ which was about 5% of mass loss is observed due to the evaporation of volatile content.

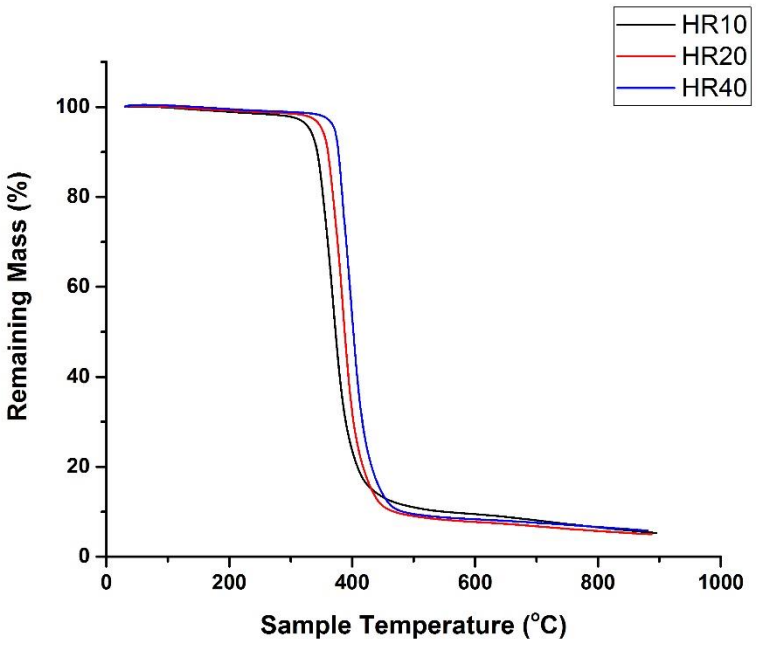

Figure 3. 2 TGA results of PRF resin at different heating rates (10 ℃/min, 20 ℃/min and 40 ℃/min) in a nitrogen gas environment

Significant depolymerisation of the polymer chain in the second stage 350-476 ℃ contributed to more than 80 % of mass loss. In order to determine the maximum decomposition rate, a derivative of *dw/dT* was calculated as shown in figure 3.3 below. At the end of the decomposition about 5-6 wt.% black char is observed around the crucible wall. Glass transition temperature as given by the manufacture is between 78 to 82 ℃.

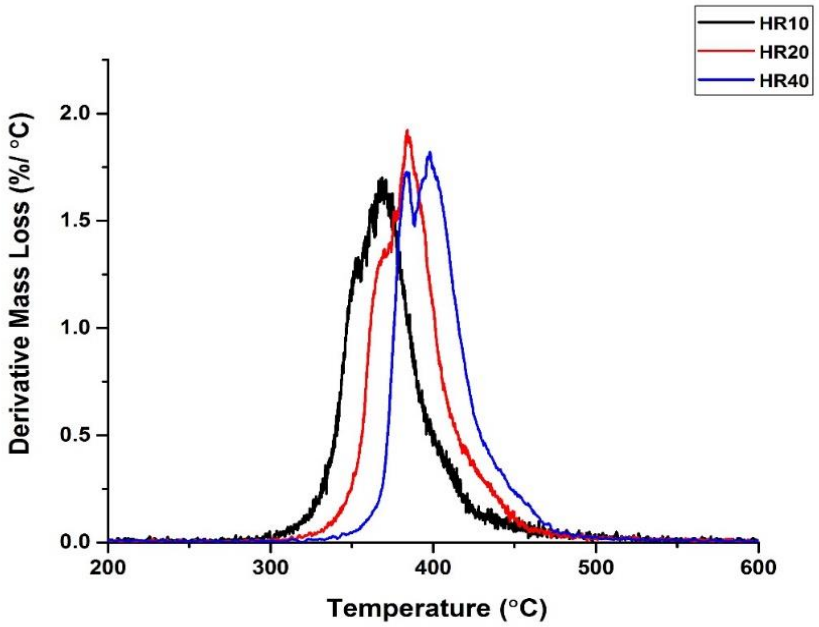

Figure 3. 3 Resin derivative of mass loss from TGA at different heating rates (10℃/min, 20℃/min and 40℃/min) in a nitrogen gas environment

3.4 Propane Burner Calibration Test

All small-scale fire tests were conducted throughout this study using a 60 mm diameter Bullfinch burner at a distance of 350 mm from the hot face of the sample (see figure 3.4). Extensive work has been done by (Browne, 2006) in calibrating the propane burner using a copper block heat flux meter which is compliant with ISO 2685: 1998 (Aircraft: Environment test procedure for airborne equipment. Resistance to fire in designated fire zones). The calibrated propane burner is capable of producing a constant heat flux up to 200 kW/m^2.

A simpler approach uses propane burner calibration performed at a different gas pressure with a constant distance between the burner and the hot face. A ceramic board sized 150 cm^2 was used as a calibration sample with two type-K thermocouple at 1cm away from the hot face. It is secured with kaowool ceramic fibre around the steel frame to minimize the heat conduction through the frame.

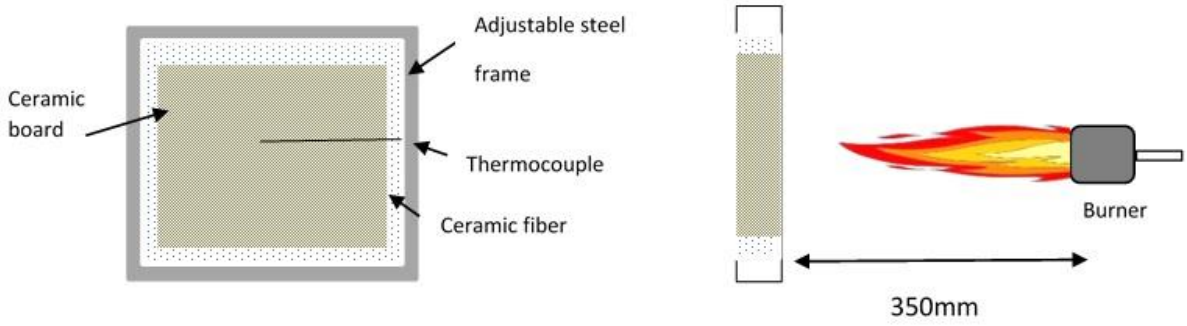

Figure 3. 4 Propane burner fire calibration test set-up for various heat flux (a) front view (b) side view

The Stefan-Boltzman law describes the total energy emitted per unit time by a unit area of black body as:

$$q_b = \sigma . T^4 \qquad [3.1]$$

where

q_b : Energy emitted per unit time by a unit area of black body surface (W/m^2)

σ : Stefan Boltzman constant ($5.67 \times 10^{-8} W/m^2K^4$)

T : Temperature of the black surface

It is assumed that the ceramic board is a grey surface which does not absorb all energy. Simple modifications of the black body law, the Stefan-Boltzman law can be modified into by including the emissivity value (ε). Based on previous studies conducted by Browne (2006) and the emissivity was determined as 0.90.

$$q_b = \varepsilon . \sigma . T^4 \qquad [3.2]$$

Figure 3.5 corresponds to the propane burner calibration test at different gas pressures. Average readings from the two type-K thermocouples were used in the calculation and data show a consistent increment of heat flux as the gas pressure increased. At low gas pressure 0.1 and 0.2 bar, the gas flows were slightly unstable.

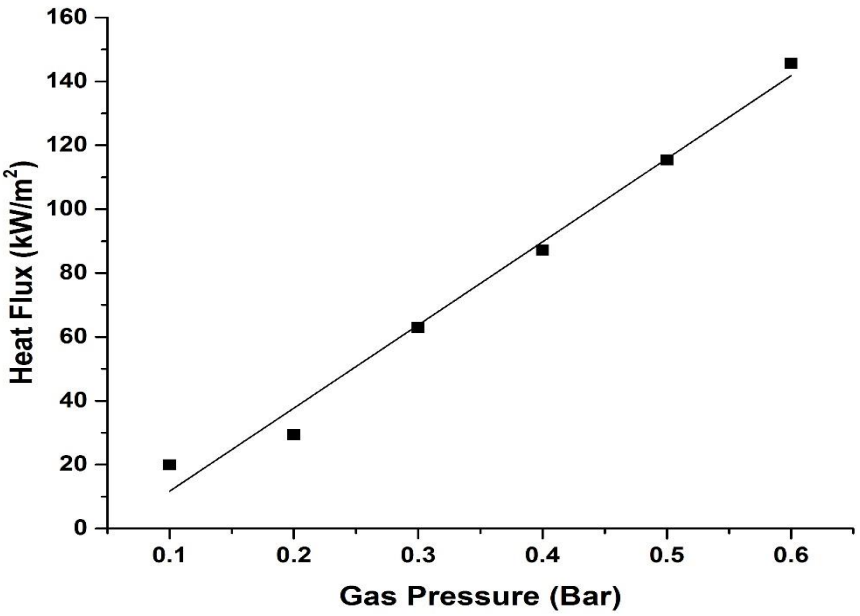

Figure 3. 5 Heat flux from the propane burner calibration curve at different gas pressures

3.5 Fire Test Without Load

The propane gas was regulated to give low and high heat flux of 35 kW/m^2 (500°C) and 116 kW/m^2 (1000°C) with the sample secured on a steel frame using kaowool ceramic fibre. This ceramic fibre is also acting as insulation to the 100 mm square test samples to prevent heat dissipation escaping and reduce the heat conduction between the frame and sample.

The rear face of the sample is left open to the air. Type-K thermocouple is attached halfway through the back of the aluminium plate and another thermocouple is positioned about 1cm in front of the hot face to monitor the flame temperature. These thermocouples are linked to a data logger acquisition brand IO.Tech DAQ Shuttle 55 that is connected to a computer. A similar set-up of thermocouples was applied to all tests.

3.5.1 Fire Test Without Load at High Heat Flux

Testing was conducted on two specimens for each sample until the substrate temperature reached 250 ºC which is considered as the failure temperature of aluminium. Below 100 ºC of substrate temperature, all three laminates (see figure 3.6) give quite similar protection which is contributed by the pyrolysis reaction that is mainly from resin degradation, decomposition of gases and volatile movement.

With further exposure to the heat flux, the aluminium foils started to soften and finally melted and became torn up because of the low melting point of the aluminium (600 ºC) as shown in figure 3.7. Fire test was stopped at around 250 ºC, as aluminium loses its strength between 200 to 250 ºC. Ti/Al takes the longest time to reach 250 ºC because of its high specific heat (528 J/kg℃) which means it needs more energy to increase its temperature by 1 ºC, followed by stainless steel and aluminium.

The substrate temperature profile indicated that Al /Al reached the failure temperature faster than Ti/Al and SS/Al. The broken foil layers had become a passage for the heat to transfer to the substrate, subsequently exposing more heat to transfer to the substrate. Since the melting point of Ti and SS foils is higher than the flame exposed, both samples managed to remain intact without any blistering on the surface.

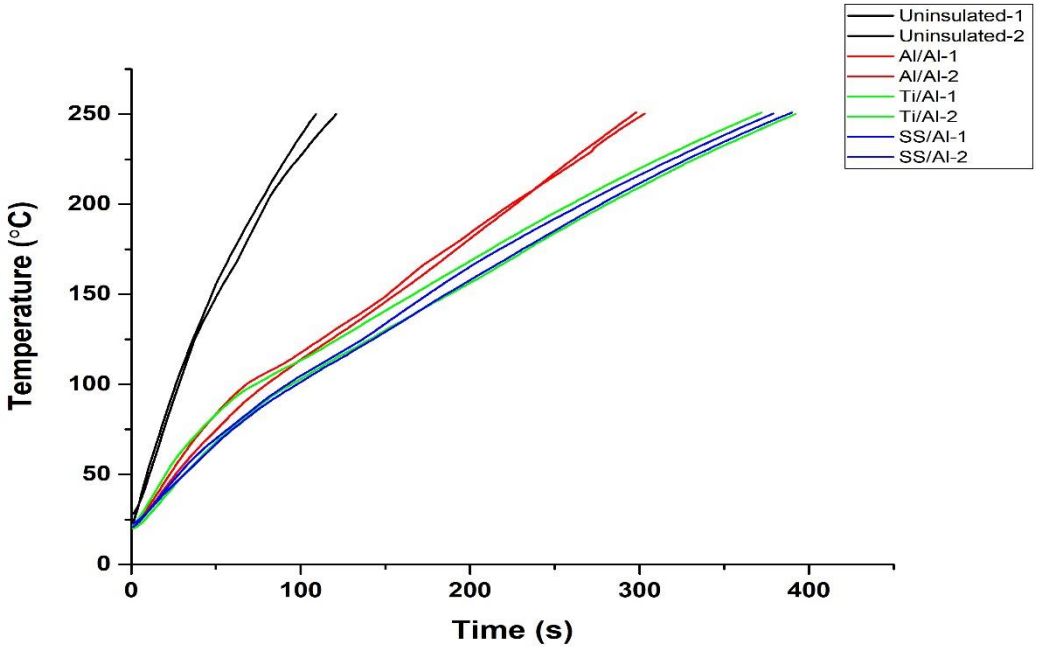

Figure 3. 6 Rear face temperature profile of aluminium substrate with and without different metal laminate protection at a constant heat flux of 116 kW/m^2. Testing was stopped once the temperature reached 250 ^{o}C

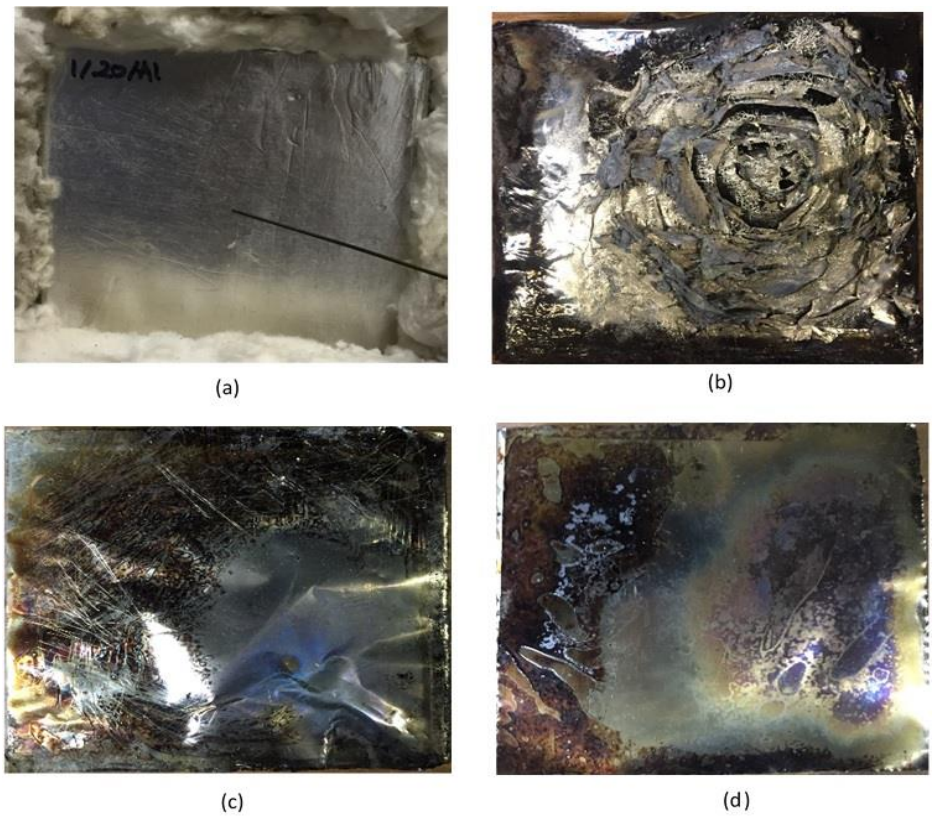

Figure 3. 7 (a) image of metal laminate Al/Al sample before fire testing in a metal frame with ceramic wool insulation. (b), (c) and (d) images of Al/Al, Ti/Al and SS/Al samples after 116 kW/m^2 heat flux exposure.

More than 50% temperature reduction as shown in figure 3.8 obtained on the protected samples against the unprotected sample. This is calculated by taking the average time of failure (115s) of the two unprotected specimens against the average protected samples at that particular time.

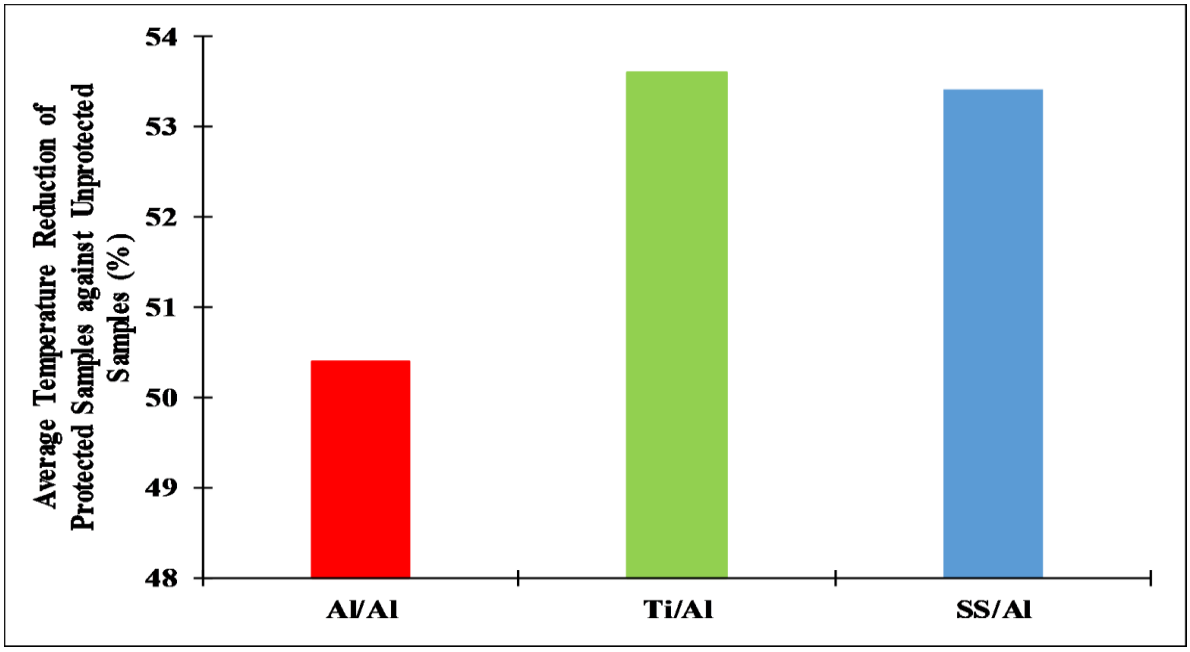

Figure 3. 8 Average aluminium substrate temperature reduction with multi-layered laminate protection against unprotected substrate exposed at 116 kW/m^2 at 115s of testing.

3.5.2 Fire Test Without Load at Low Heat Flux

The multi-layered laminate performance was also tested at lower heat flux (35 kW/m^2) on aluminium substrate and on carbon fibre laminate. In both cases, similar temperature profiles and physical changes were observed on the aluminium substrate. The low heat flux exposure extended the protection up to 30mins compared to 7mins at 116 kW/m^2.

It is observed in figure 3.9 below that it took five times longer for aluminium samples exposed at lower heat flux to reach the failure temperature (250 ^{o}C) compared to when they were exposed to higher heat flux. This rule applied to either uncoated or coated samples. There was a big gap (18 mins) between time to failure of uncoated samples at 35 kW/m^2 with Al/Al samples. This shows that at a lower heat flux, the effect of heat radiation on the front face is not severe on the low melting points and high thermal conductivity of aluminium foils which allows the laminate to slowly degrade, hence significantly protecting the substrate.

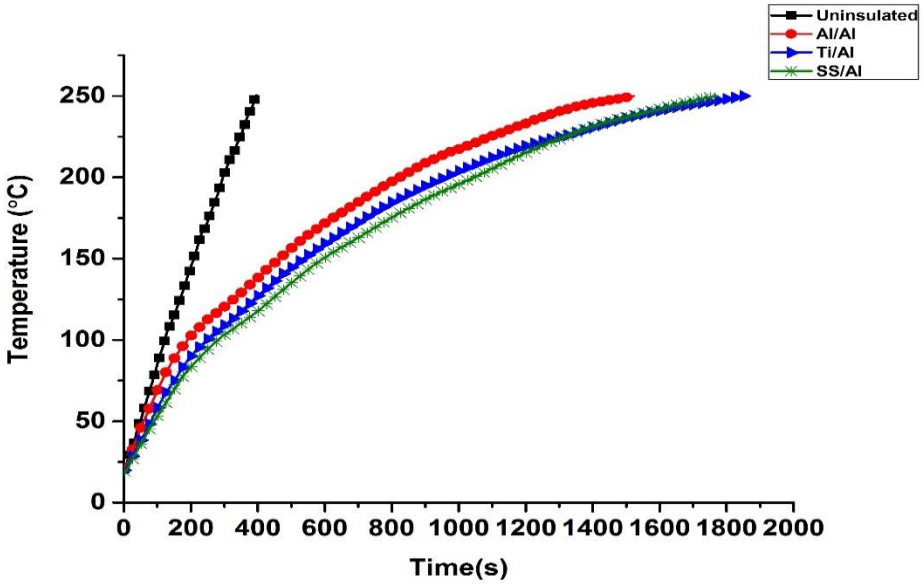

Figure 3. 9 Rear face temperature profile of aluminium substrate with and without different metal laminate protection at a constant heat flux of 35 kW/m^2. This result is a representation of one of the two tested specimens of each sample. Testing was stopped once the temperature

In the case of Ti/Al and SS/Al samples, the high melting points and low thermal conductivity of Ti and SS as a front face were able to give about 300s time lag to reach the failure temperature compared to Al/Al at a low heat flux. At a higher heat flux, less time lag difference (70-90s) is observed because of the high thermal radiant exposure, minimizing the effect of lower thermal conductivity material as a front face (see figure 3.10).

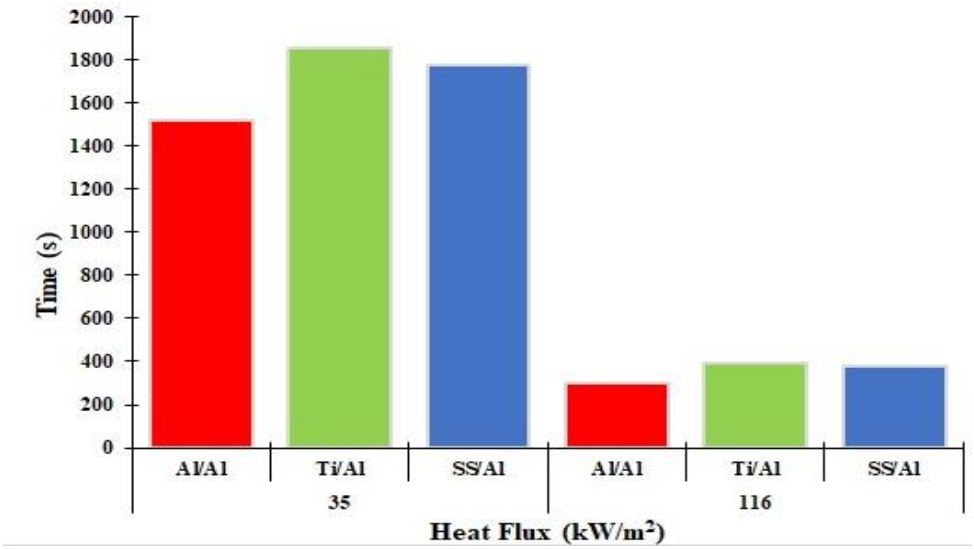

Figure 3. 10 Effect of 35 kW/m^2 and 116 kW/m^2 heat flux on time to failure (250 °C) of aluminium substrate with and without protection. The bar chart represents the average value of time to failure from two specimens for each sample.

In order to evaluate the multi-layered laminate protection on combustible material, the aluminium substrate was replaced with a CFRP. The test was stopped once the CFRP rear face temperature reached 160 ^{o}C to prevent the burn-through during testing. It is also noted that common epoxies have glass transition temperature between 100 to 150 ^{o}C where the mechanical properties begin to degrade (Kandare *et al.*, 2014).

Initial thermal transient in carbon substrate was longer compared to the aluminium substrate due to the lower thermal conductivity of the carbon (see figure 3.11 below). The presence of more combustible material (epoxy) and carbonaceous char in the composite laminate decreased the heat conduction within the pyrolysis zone, thus lowering the combustion intensity at the initial stage. The multi-layered laminate was able to reduce the heat up to 60 % at 100 s of testing in this case (see figure 3.12).

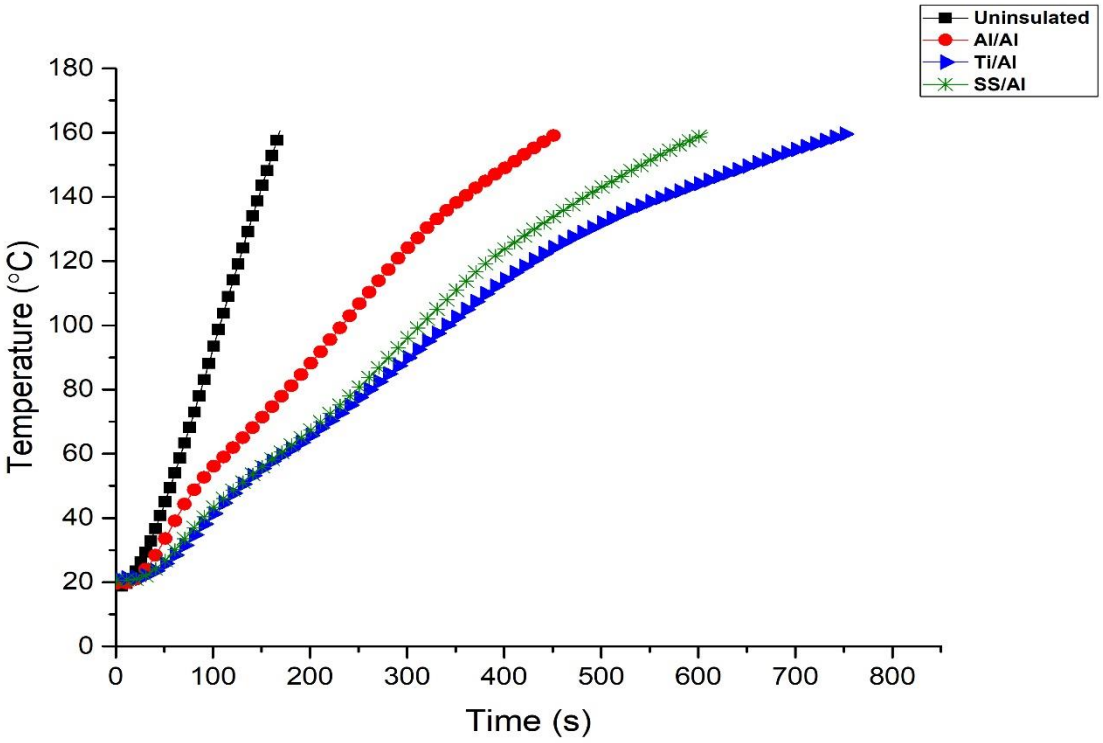

Figure 3. 11 Rear face temperature profile of CFRP substrate with and without different metal laminate protection at a constant heat flux of 35 kW/m^2. Testing was stopped once the temperature reached 160 ^{o}C.

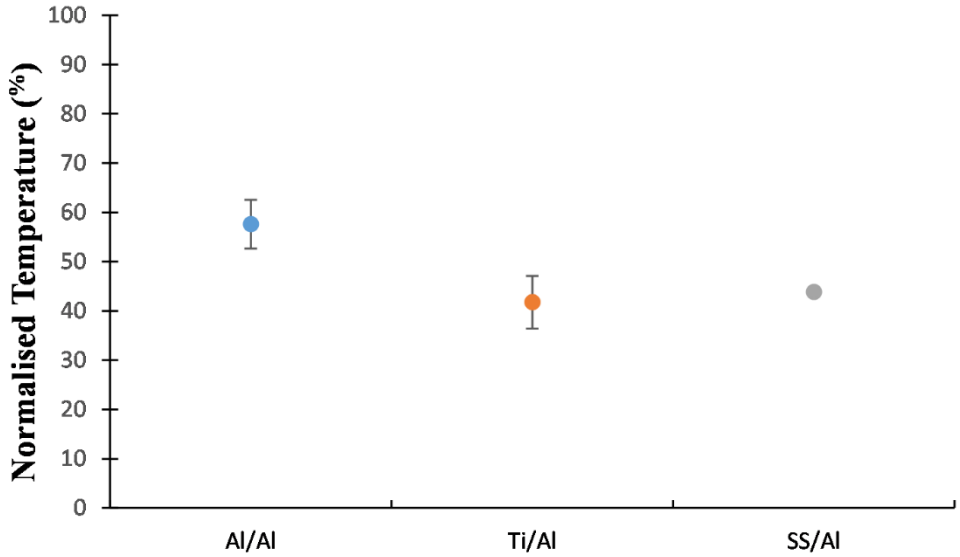

Figure 3. 12 Carbon fiber reinforced polymer (CFRP) substrate temperature reduction with multi-layered laminate protection against unprotected substrate exposed at 35 kW/m^2 at 100s of testing.

Typically, in a fire incident, the front skin of the composite will start softening between 60 to 150 ^{o}C. The degradation of composite matrix will lead to debonding and delamination between the fibres-matrix. The interfacial debonding is due to the different thermal expansion coefficient between fibres and epoxy that create interfacial cracking (Gibson *et al.*, 2010; Kandare *et al.*, 2014; Grigoriou and Mouritz, 2016).

The debonding and delamination in the carbon laminate is clearly observed in an unprotected sample, shown in figure 3.13 below. McManus and Springer, (1992) reported that the composite undergoes chemical reactions generating vapour and volatiles at elevated temperatures. The vapours will fill up the gap between layers during the heating and delaminate the composite (McManus and Springer, 1992).

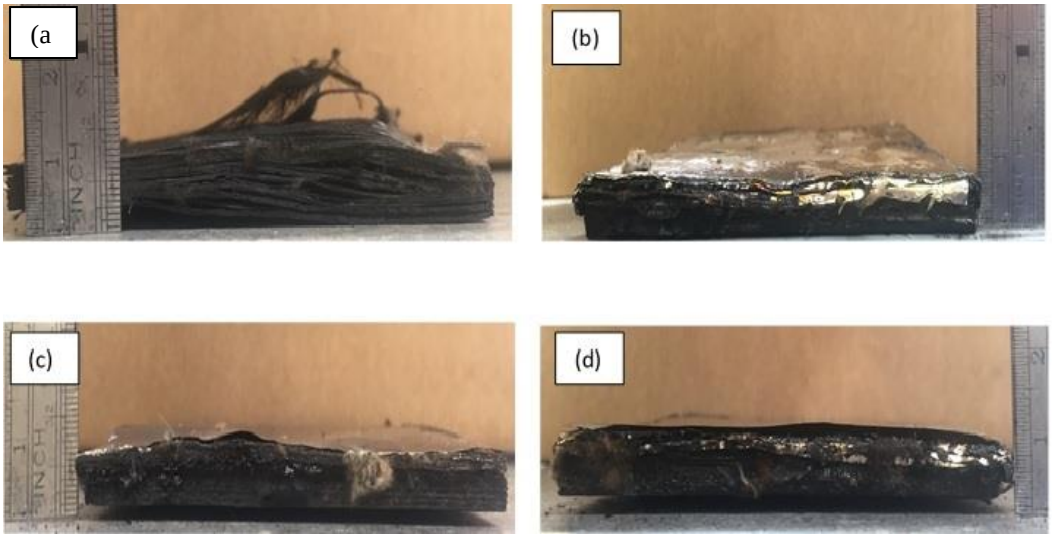

Figure 3. 13 Delamination and debonding of CFRP after exposure to a constant heat flux of 35 kW/m^2 (a) unprotected CFRP; protected CRFP using (b) Al/Al (c) Ti/Al (d) SS/Al

3.6 Fire Under Load Test

Insulated and uninsulated plates were put under tensile and compression load while being subjected to a constant heat flux using a propane burner to simulate an actual fire. The burner is positioned at 350 mm in front of the sample to give a one-sided heat flux similar to a fire test without load testing set up. Mechanical tests were conducted on a Universal Testing Machine (UTM) 50 tons (W&T Avery Ltd). The testing set up consists of a loading frame, hydraulic pressure system, burner assembly and data acquisition logger. Both tests conducted with similar setting up of propane burner as previous tests but conducted in a larger room compared hence affecting the values of the constant heat flux applied.

3.6.1 Fire Under Tensile Load

Tensile test samples were prepared using 300 mm x 50 mm x 10 mm aluminium plates with the laminate size 120 mm x 50 mm bonded in the middle of the plate. Before the fire test began, tensile test was performed on the unprotected aluminium plate at room temperature to determine its yield strength.

The plate was pulled until it is broken, and it was observed that the plate yields at 150 kN thus the test was stopped. Samples were later put under a constant load of 75 kN which is about 50% of the yield load. Before the fire ignited, the load was introduced to the sample and maintained until the test was finished. The mid-section of the plate was exposed to heat flux of 112 kW/m^2 supplied by a propane burner.

The top and bottom of the unprotected area of the sample were wrapped using a ceramic blanket with thickness of 25 mm and density 64 kg/m^3 and secured with wire. Both sides of the plate were covered with Cemtherm ceramic board to prevent the sample's backface from being exposed to the fire. A layer of steel foil was used to cover the adhesive between the ceramic board and the aluminium plate. Figure 3.14, displays the tensile sample.

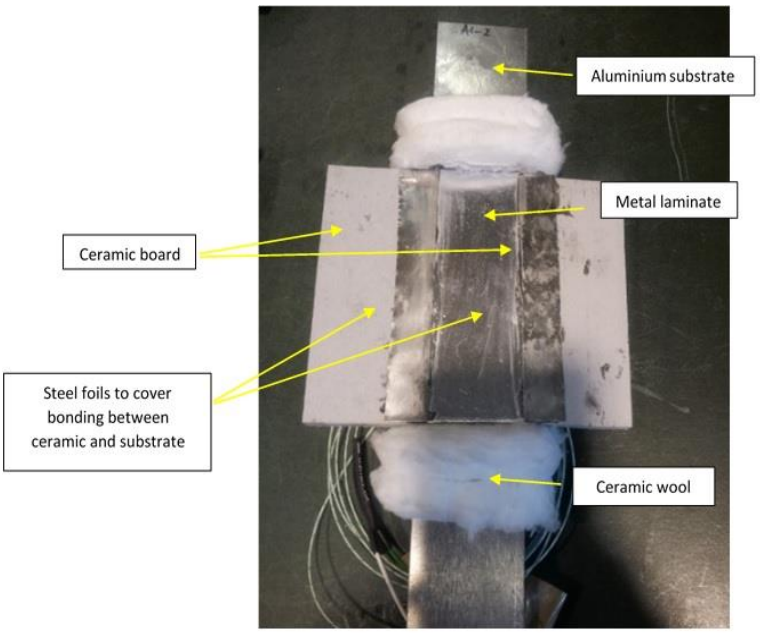

Figure 3. 14 (a) Image of fire test under tensile load sample attached with ceramic board on both sides of the plate with a layer of steel foil to cover the adhesive line from direct contact from fire.

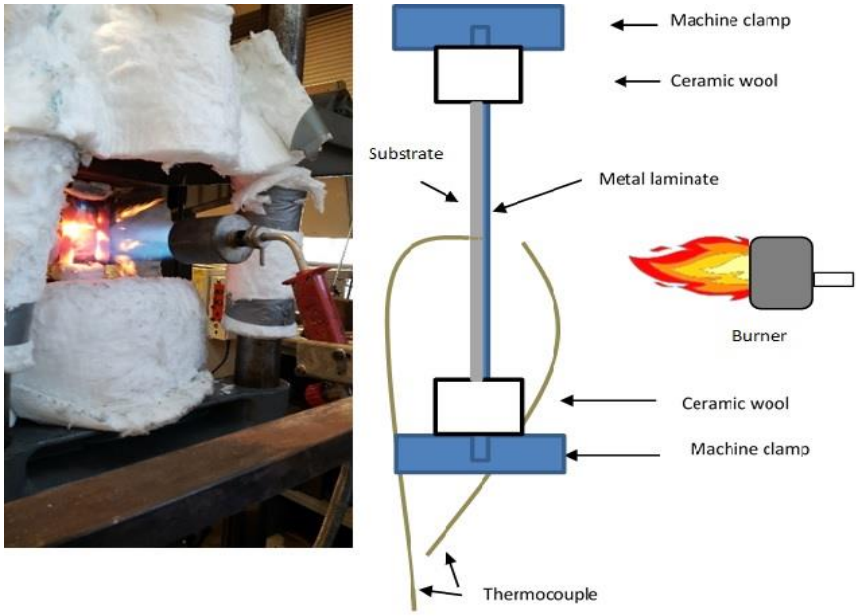

(a) (b)

Figure 3. 15 (a) ceramic wool covering the UTM machine from fire during 112 kW/m^2 heat flux exposure (b) diagram of fire under tensile load testing set-up on UTM

Type K thermocouples are placed at the back surface of the plates and in front of the exposed surface to record the fire temperature. Crosshead and the load frame columns of the UTM are also covered with a ceramic blanket to avoid overheating (see figure 3.15 (a) and (b)).

The effectiveness of the multi-layered laminate as a PFP is evaluated based on the time-to-failure and failure temperature of the aluminium plate during fire under tensile load testing.

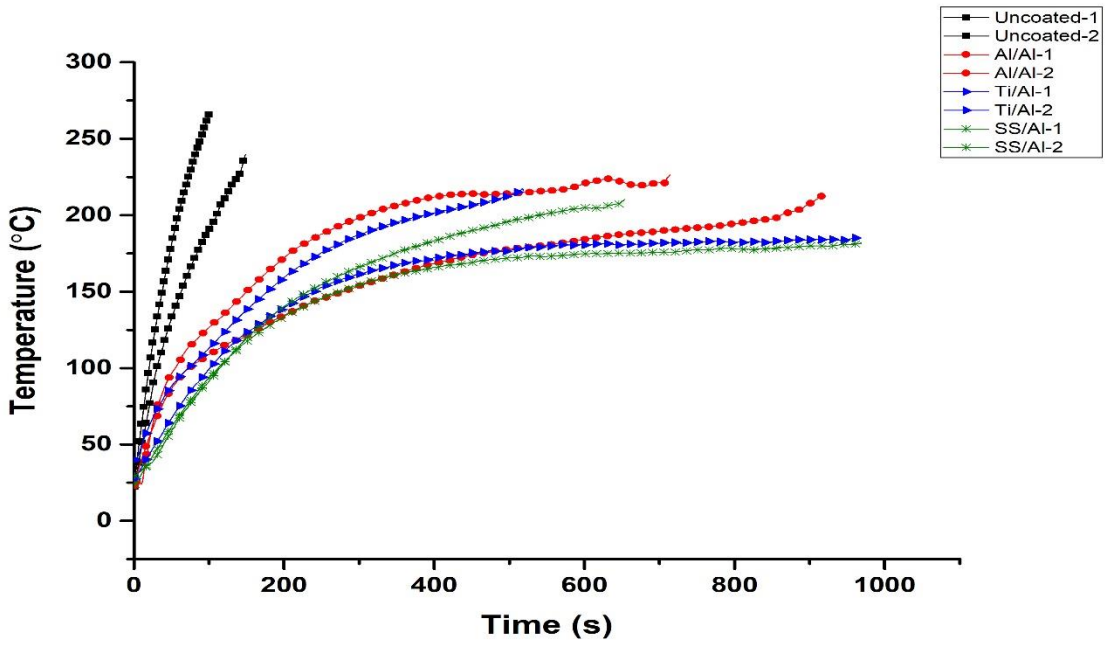

Figure 3. 16 Rear face temperature profile of aluminium substrate protected with and without different multi-layered laminate protection at a constant heat flux of 112 kW/m^2. Testing was conducted under constant load (75 kN) until the sample failed.

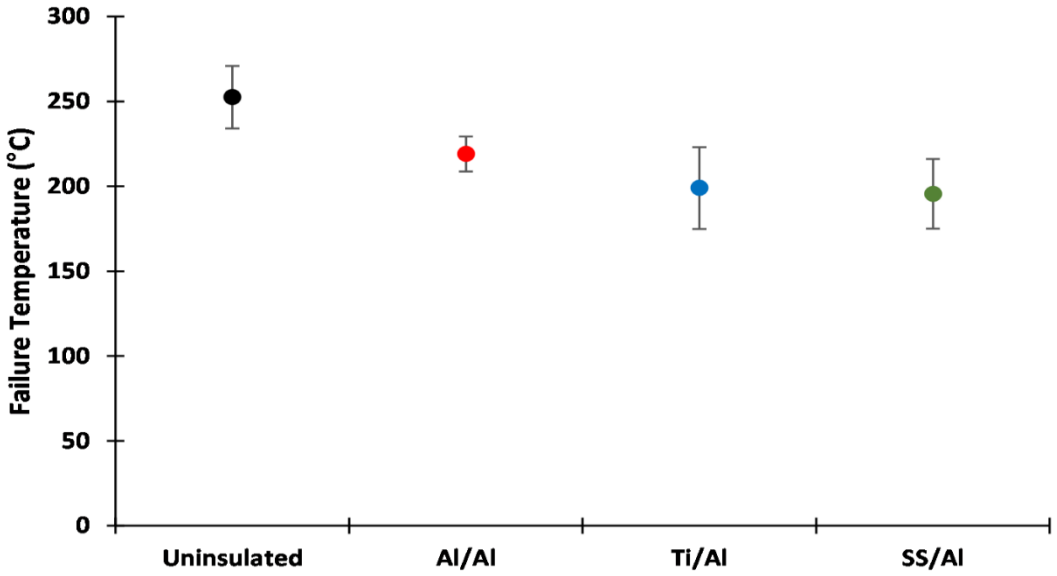

Figure 3. 17 Average failure temperature of aluminium substrate protected with and without different multi-layered laminate protection at a constant heat flux of 112 kW/m^2 and 75 kN load

Data tabulated in figure 3.16 above shows that the failure temperature for all uninsulated and insulated samples were between 181 to 266 ℃ which is around the recrystallization temperature (200 ℃) of aluminium. At recrystallization temperature, the strength of aluminium significantly reduced to 50 % of its yield strength. The time to failure between the specimens varies few minutes due to the machine limitation that need manual operation by two persons. The load cell need to be adjusted manually as soon as the fire ignited by different individuals but unfortunately the timing is difficult to control.

Despite the failure time being close within the insulated sample, Al/Al failed at a higher temperature than Ti/Al and SS/Al (see figure 3.17). The higher failure temperature of Al/Al sample could possibly indicate that the rate of heat transfer or thermal diffusivity through Al/Al from the hot face to the cold face is faster than other insulated samples which consequently increased the failure temperature of Al/Al compare to Ti/Al and SS/Al at a comparable failure time. In general, thermal diffusivity is the thermal conductivity divided by density and specific heat capacity at constant pressure. As reported from previous experiments, it is shown that the low melting point of aluminium as front face of Al/Al is allow more heat transferred compared to other insulated samples.

Softening onset temperature of aluminium alloys is above 120-150 ℃ where the Young's Modulus starts to reduce and significantly decrease the stiffness (Faggiano *et al.*, 2004; Grigoriou and Mouritz, 2016) which leads to the aluminium substrate experiencing necking and the laminate detaching from the aluminium surface as shown in figure 3.18.

Figure 3. 18 Necking on the aluminium substrate after exposure at a constant heat flux of 112 kW/m^2 and 75 kN load

3.6.2 Fire Under Compression Load

The effect of compressive stress with one sided heat flux was studied in this section. Figure 3.19 below, is the diagram of a fire under compression load set-up where the sample was positioned on the loading stage facing the burner with a constant heat flux of 85 kW/m^2. A room temperature compression test was conducted prior to the fire test to confirm the buckling load. The load was kept as 75 kN (50% from buckling load) throughout the testing. Clamps that exposed to fire are covered with a thick ceramic blanket similar to the tensile testing discussed earlier.

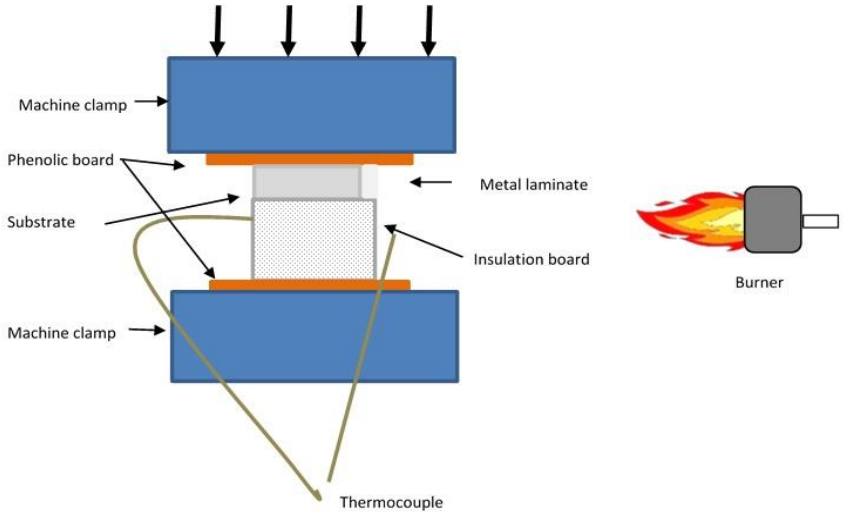

Figure 3. 19 Diagram of fire under compression load testing set-up on the UTM with constant 85 kW/m^2 heat flux

The compression test was done on a sample with a dimension of 50 mm x 50 mm x 10 mm (figure 3.20 (a)). 40 mm^2 Sindanyao insulation boards are fixed on both sides to protect the rear face from fire. The top and bottom of the sample is attached to phenolic board from Tufnal board to produce fixed-fixed end conditions on the sample. All plates were tested parallel to the rolling direction of the plate as well as the direction of the thermocouple which was drilled halfway through.

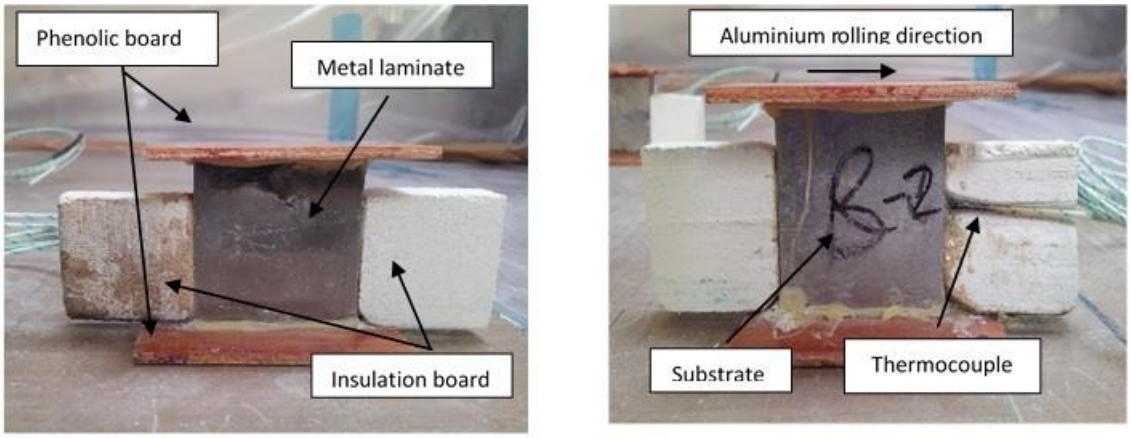

(a) (b)

Figure 3. 20 Image of front face of fire test under compression load sample (a) phenolic board on the top and bottom of the sample to create fixed-fixed end conditions. Insulation board bonded on both sides (b) thermocouple drilled in the aluminium rolling direction

Time to failure and temperature at failure are provided in figure 3.21. The applied load is 50 % of the buckling load value which is 140 kN (280 MPa) at room temperature. As expected, time to failure of the insulated sample is longer than the uninsulated sample.

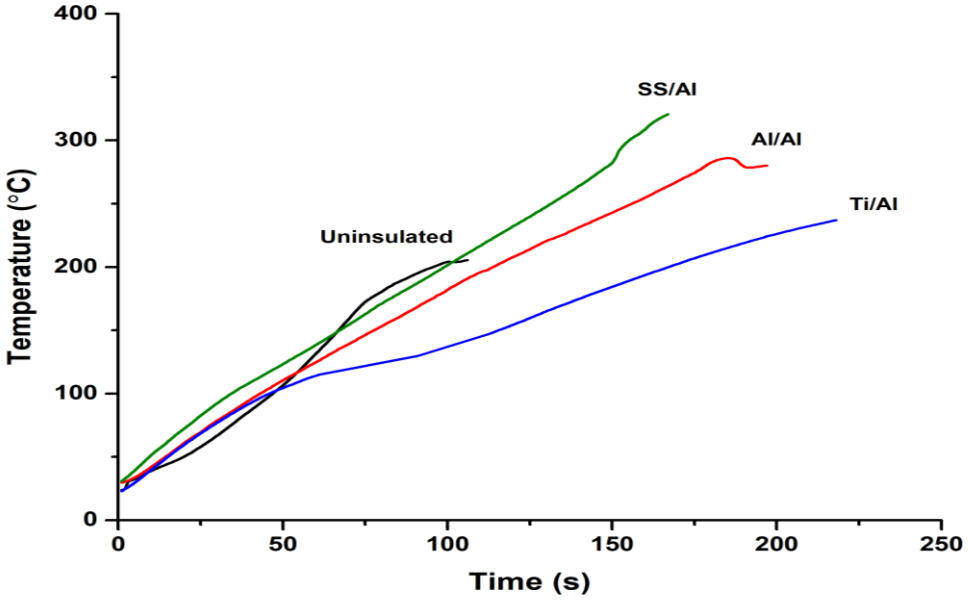

Figure 3. 21 Representation of one out of two specimens' rear face temperature profile of aluminium substrate with and without different metal laminate protection under 50 % of buckling load at a constant heat flux of 85 kW/m^2 Testing was conducted until the sample failed

Al/Al, Ti/Al and SS/Al failed at temperatures above 250 ^{o}C with Ti/Al giving the longest protection. Despite the different types of metal laminate used on the substrate, the time to failure and the failure temperature are quite close to each other and show a similar trend. This is supported by Suzuki *et al.*, (2005) who discovered the critical failure temperature for aluminium in compression stress is between 250 to 450 ^{o}C depending on the type of aluminium alloy, stress applied and slenderness ratio.

One of possible explanation of similar failure properties within the insulated sample is that compression force during the testing might have detached the metal laminate from the substrate. This has allowed the heat to transfer to the substrate through the gap within the debonded layers of foils and the substrate, which happens approximately around the same period for all the insulated samples. Figure 3.22 show the buckling effect of tested sample on insulated and uninsulated sample.

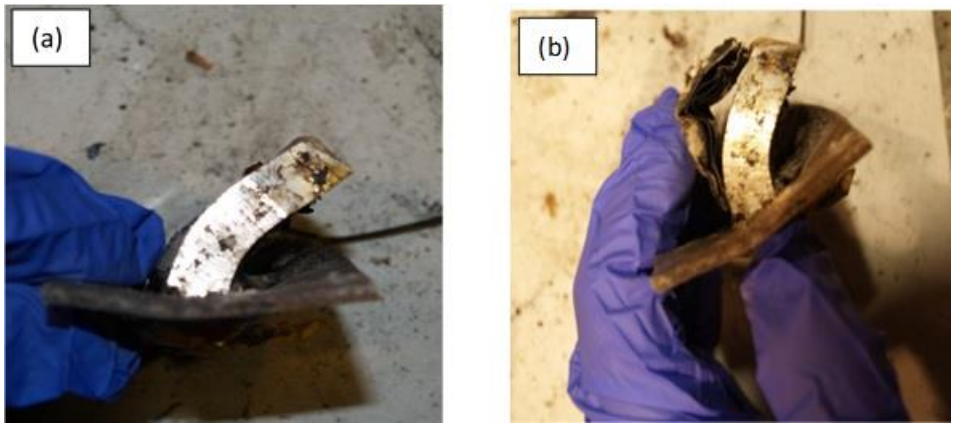

Figure 3. 22 Image of buckling effect on tested samples (a) with and (b) without the insulation after compression test under 50 % of buckling load with constant heat flux exposure at 85 kW/m^2

3.7 Cone Calorimeter Testing

A cone calorimeter test was conducted to determine the multi-layered laminate fire protection ability under horizontal radiant heat flux. The test was conducted on multi-layered laminate using aluminium plate and CFRP as a substrate using a cone calorimeter from Fire Testing Technology (FTT) which tested according to ISO 5660. All samples are 100 x 100 mm and are mounted in a steel sample holder.

In normal practice of cone calorimeter testing, it is used to measure the heat release rate based on calorimetry of oxygen consumption. The heat output collected are mainly from the combustible materials sample that consumed oxygen during combustion. In the case of testing on aluminium plate substrate, very little data can be gathered from the test since the multi-layered laminate and the aluminium substrate mostly consist of non-combustible materials. The purpose of testing the aluminium substrate alone is to test the samples under constant heat flux with different setting up and compare it to previous tests.

For the aluminium substrate testing, a type-K thermocouple was placed at the bottom of the substrate with the tip of the thermocouple inserted halfway through the 10mm thickness aluminium to measure the rear face temperature profile (see figure 3.23). The thermocouple was not attached to 5.30 mm thickness CFRP samples as it is a combustible material and data collected from the cone calorimeter will be used as findings.

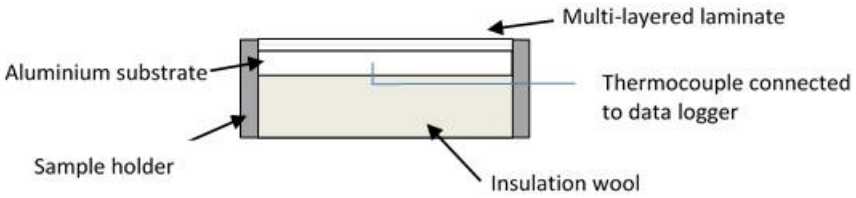

Figure 3. 23 Schematic diagram of cone calorimeter test on multi-layered laminate on aluminium substrate connected with type-K thermocouple to measure the rear face temperature

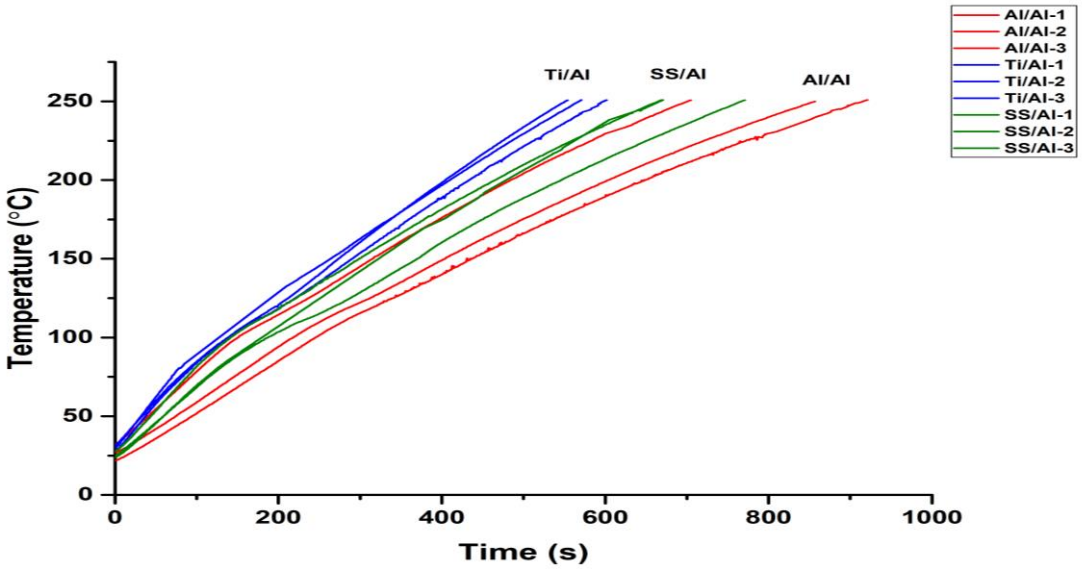

Figure 3. 24 Temperature profile of aluminium substrate protected with different multi-layered laminate exposed to 50 kW/m^2 until rear face temperature reached 250 ^{o}C

The temperature profile of the protected aluminium substrate in figure 3.24 shows quite interesting findings. The rear face temperature of the substrate disclosed that the sample protected with Ti/Al reached the failure temperature of aluminium (250 ^{o}C) faster than any of the other samples, which is opposite from previous fire testing results.

Swelling of the laminate was observed during the testing with only a small flame spotted at the edge of the sample holder that went out after a few seconds. The swelling was distinctive in this test because of the sample holder constriction on the sample edges. The laminate surface was also noticed to be bubbling, especially on Al/Al once the rear face temperature reached around 110 ^{o}C.

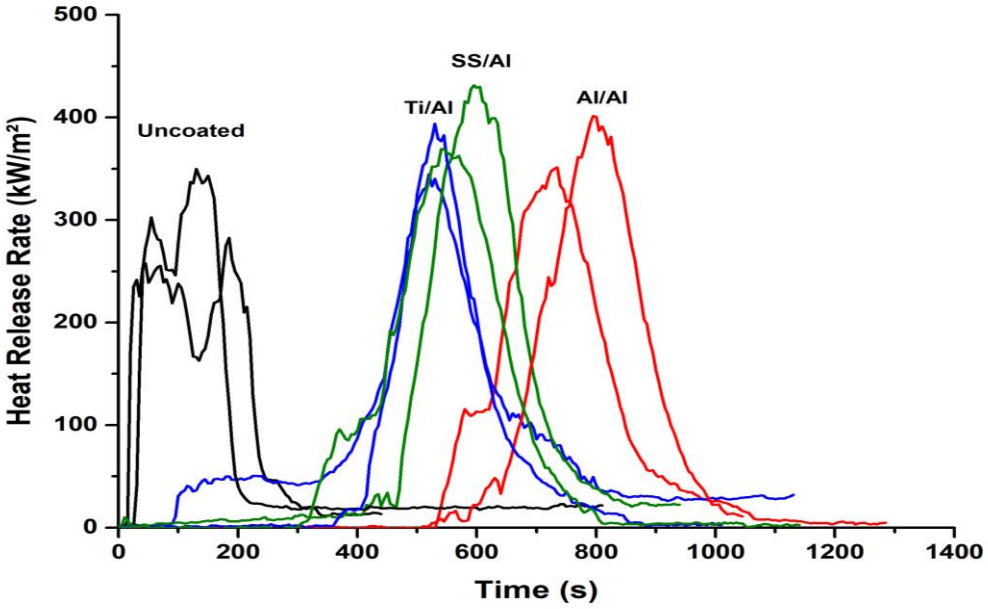

Figure 3. 25 Heat release rate (HRR) of unprotected and protected CFRP at 70 kW/m² on the cone calorimeter test

The cone calorimeter test on combustible substrate as shown in figure 3.25 also indicated that Ti/Al reached peak HRR faster than other samples which as supported by the non-combustible substrate temperature profile. The swelling and bubbling was detected everytime before the sample ignited on the laminate surface which was obvious when using CFRP as a substrate.

From table 3.2, the multi-layered laminate managed to reduce the maximum average rate of heat emission (MARHE) at least up to 50 % of the unprotected CFRP even though the value of HRR produced by each sample was not significantly different.

	TTI (s)	Peak HRR (kWm^{-2})	Mean HRR (kW/m^{-2})	THR (MJm^{-2})	MARHE (kW/m^2)	Mass Lost (%)
Unprotected CFRP-1	20	283	118	52	207	33
Unprotected CFRP-2	15	350	70	55	237	26
Al/Al + CFRP-1	449	351	57	74	76	30
Al/Al + CFRP-2	538	401	72	76	77	56
Ti/Al + CFRP-1	300	345	81	91	107	30
Ti/Al + CFRP-2	365	394	96	62	85	27
SS/Al + CFRP-1	418	431	87	82	102	31
SS/Al + CFRP-2	305	369	71	81	109	35

Table 3. 2 Data collected from cone calorimeter testing on unprotected and protected CFRP at 70 kW/m^2

A larger flame was observed on the combustible material due to the bigger amount of pyrolysis and gas flow within the sample. More pyrolysis reaction will leads to earlier decomposition and ignition time. It is assumed that trapped pyrolysis gases within the laminate layers and the sample holder in Ti/Al and SS/Al is higher than Al/Al in both substrate conditions.

The low thermal conductivity of Ti and SS contribute in reducing the convection heat transfer from pyrolysis and hot gases from escaping through the surface, compared to Al/Al. This findings is opposite from the testings done earlier, regardless of whether on combustible or non-combustible substrate.

Babraukas (2003) reported that air flows is trapped from all sides in horizontal samples with relatively nearly similar surface temperatures, while for vertical samples, a boundary layer is developed with most of the flow being bottom-up. In either vertical or horizontal orientation, the radiative environments are alike except for the convection of the heat (Babrauskas, 2003).

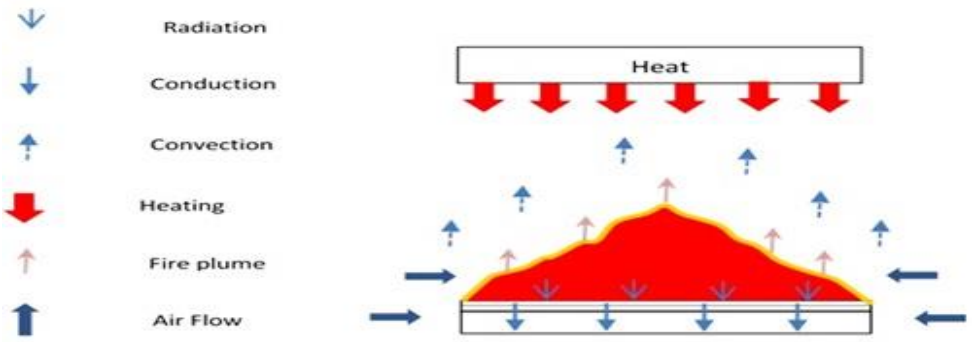

Figure 3. 26 Schematic diagram of main component in heat transfer and air movement during horizontal fire testing (Tsai, 2009)

In his studies on the effect of cone calorimeteter orientation as shown in figure 3.26 below. Tsai (2009) also found that in horizontal orientation, the volume of pyrolysis gases is greater compared to pyrolysis gases flowing upwards and along the surface in the vertical orientation.

3.8 Conclusion

Results from fire test without loading on the unprotected and protected substrate reveal that Ti/Al and SS/Al manage to give better protection than Al/Al to the substrate upon exposure to 35 or 116 kW/m^2 constant heat flux. This is true for both combustible and non-combustible substrates.

The Al/Al sample was found to be broken and blistering during fire test due to the low melting point of aluminium that has become a passage for the heat to transfer to the substrate in comparison to Ti and SS as a front face, which was still properly intact because of the higher melting temperature.

Results obtained from the fire under tensile load test, show the failure temperature of samples are around the recrystallization temperature of aluminium, which is ~200 ^{o}C. This is supported by Gupta *et al*., (2001b), Vandermeer and Hansen (2008) and Summers *et al.*, (2014) in their research that reported the aluminium strength reduced up to 50% around 150-250 ^{o}C due to dislocation recovery.

In the fire under compression load test, the time to failure of insulated samples are quite close to each other with the failure temperature above 250 ^{o}C. Maljaars *et al*. (2009) and Suzuki *et al*. (2005) agreed that the failure for aluminium under compression at elevated temperature lies around 170 to 350 ^{o}C depending on the stress applied. An assumption was made that the compression force has bent the substrate and therefore detached the metal laminate from protecting the substrate. The fact that the samples are similar in size (50 mm x 50 mm) could minimize the effect of different type of multi-layered protection on the compression strength.

Although Ti/Al and SS/Al samples seemed to give a better performance in previous fire tests, this is not the case for cone calorimeter testing. In either combustible or non combustible substrate, the results in cone calorimeter testing reveals that Al/Al is able to reduce the heat transfer to the substrate and extend the time to ignition better than Ti/Al and SS/Al. One of possible explaination of this outcome could be due to the trapped volatile gasses within the specimen due to the encapsulated frame.

It can be concluded that using a high melting foil as a front face for the multi-layered laminate like titanium and stainless steel delay the degradation of the laminate thus extended the protection time on the substrate when dealing with vertical fire.

These results provide important insights about the performance of the multi-layered laminate depending on the set up of testing which affects the heat transfer mode, thermal flows and heat flux direction to the exposed surface. Therefore, these findings help to give a better understanding on multi-layered laminate fire performance in different conditions.

Chapter 4. Different Passive Fire Protection (PFP) Systems for Steel Structures

This chapter will describe the use of a small-scale propane burner test to characterise kaowool which is found in fire blanket, commercial intumescent coating and a new biodegradable composite made from furan resin and glass microsphere. These three different types of PFP materials are mainly apply on pipelines, platforms or storage tanks in oil and gas which is made of steel. In this industry, steel is widely used as a metal structure compared to aluminium due to its higher strength and temperature degradation. For this purpose, the PFP materials are attached to 10 mm thickness steel substrate before exposing it to a constant heat flux of 116 kW/m^2. The results show that, although the three PFP materials reacted differently upon exposure to fire, their temperature-time profiles show similar patterns when simulated using the new Model I and II developed by Gibson *et al.* (2016).

4.1 Introduction to PFP Qualification Testing

According to the Hazard XII European Advances in Process Safety, in order for a PFP system to qualify for commercial use, it needs to be able to satisfy rigorous conditions related to real fire events. The assessment takes into consideration the type of fire and parameters like duration, heat flux, spread of flame, fire temperature and toxicity (Gibson, 1994). A correct qualification of commercial PFP is the foundation of fire safety in buildings, offshore and transportation structure.

Among the main requirements of PFP system approval is the ability to prevent the steel from reaching a critical temperature (450^{o}C). The certification procedure of PFP is divided into cellulosic and hydrocarbon fire exposure. According to BS 476-20:1987, the standard cellulosic fire curve will reach 500°C in 5 minutes and rise to 945°C over time, while a fire from hydrocarbon compounds (oil and gas) with flame temperature can go up to 1000°C within 5 minutes.

The PFP used for offshore facilities is subjected to a hydrocarbon fire test that would require expensive large-scale qualification testing to assess fire resistance in a furnace or exposure to jet fire (see figure 4.1).

Figure 4. 1 Example of commercial jet fire testing in the oil and gas industries (Jotachar JF750)

Commercial PFP is made of various types of materials, including cementitious, intumescent coating, fibre-reinforced composites and ceramic fibres that could consist of organic or non-organic materials.

Inert inorganic-based materials become brittle after exposure to fire and are usually used in permanent installations in large facilities, while organic-based materials exhibit better mechanical properties and plastic behaviour which is more suitable for light structures and is replaceable when damaged (Landucci *et al.*, 2009).

As reported by Gibson *et al.* (2016), other than the 'HP/A' method, there are no commonly accepted design equations that can be used to model the heat transmission of any particular PFP.

In this study, three different PFP materials, which are commercial intumescent coating, furan microspheres and kaowool, are exposed to constant heat flux from a small-scale propane burner. The commercial intumescent coating used in this study is widely used in civil structures and the oil and gas industry on steel structures.

A refractory layer is assumed in PFP so that it could simplify heat conduction through this layer with a near constant heat flux into the metal substrate as described by the term 'lumped parameter'. Details of the kaowool and intumescent coating mechanism and background are reported in Chapter 2 (Literature Review).

4.2 Theory

Gibson *et al*. (2016) reported that heat conduction through PFP can be modelled by considering the initial thermal lag from thermal diffusivity together with initial decomposition for Model I (Insulated Rear Face). This is later followed by a near steady-state period involving only heat conduction through the refractory layer formed for Model II (Uninsulated Rear Face).

The solution involves an effective thermal diffusivity of PFP at the beginning of fire exposure as well as an effective thermal conductivity as associated with later stages of PFP. This approach leads to a simple design equation that can be used to characterise the materials and design of fire protection when using the well-known (HP/A) procedures.

At the beginning of fire exposure, the front face temperature T_1 is considered to be a constant. The heat lost by radiation into the PFP is described by the law of Stefan-Boltzmann radiation, which is expressed as:

$$q = se\left(T_{Fire}^4 - T_1^4\right) \qquad [4.1]$$

where:

σ: Stefan-Boltzmann constant ($Wm^{-2}K^{-4}$),

e: absorptivity of the protection surface

T_{Fire} (K): fire temperature

T_1 (K): surface temperature

4.2.1 Models I (Insulated Rear Face)

Model I is use when the rear face is insulated during the testing. It assumes the unsteady-state heat transfer and non-linear temperature at the beginning of the heat transfer condition, but also a constant temperature difference across the PFP layer while ignoring the temperature rise in the metal substrate. This assumption is applicable only if the temperature increment in the metal substrate is small (T_1-T_0), and errors may result if the substrate temperature increases rapidly; for example, for a material with high thermal conductivity like aluminium.

The accumulated heat flow per unit through the protection at the initial stage of fire exposure is provided by:

$$Q(t) = k(T_1 - T_0)\left(\frac{t}{X} - \frac{X}{\alpha}\left(\frac{1}{6} + \frac{2}{\pi^2}\sum_{n=1}^{\infty}\frac{(-1)^n}{n^2}\, exp\left(-\frac{n^2\pi^2\alpha t}{X^2}\right)\right)\right) \qquad [4.2]$$

where:

T_0: initial uniform temperature of the PFP and substrate

T_1: hot face temperature of the PFP

X: PFP material thickness

Equation 4.2, does not take into account the thermal conductivity of the material. In order to apply the 'lumped parameter' model, the temperature difference through the metal substrate is neglected. The increment in substrate temperature can now be associated with Q(t) by:

$$Q(t) = r_m C_{Pm} b(T - T_0) \qquad [4.3]$$

and so the temperature of the metal is given by:

$$T = T_0 + \frac{k(T_1 - T_0)}{\rho_m C_{Pm} b}\left(\frac{t}{X} - \frac{X}{\alpha}\left(\frac{1}{6} + \frac{2}{\pi^2}\sum_{n=1}^{\infty}\frac{(-1)^n}{n^2}\, exp\left(-\frac{n^2\pi^2\alpha t}{X^2}\right)\right)\right) \qquad [4.4]$$

Initial thermal diffusivity plays a major role in affecting the induction time, which is given by:

$$\alpha = \frac{X^2}{6t_0} \qquad [4.5]$$

$$t_0 = \frac{X^2}{6a} \qquad [4.6]$$

When the sum of the exponential terms in Equation 4.4 becomes close to zero, a linear relationship between substrate temperature and time can be predicted. At this time, the PFP responds as simple resistance to heat transfer, without heat accumulation, as follows:

$$Q(t) = k(T_1 - T_0)\left(\frac{t}{X} - \frac{X}{6\alpha}\right) = \frac{k(T_1 - T_0)(t - t_0)}{X} \qquad [4.7]$$

The thermal conductivity of PFP can then be calculated from the slope of the linear part of the curve. However, in some cases it could be non-linear due to the heating up of the substrate.

4.2.2 Model II (Uninsulated Rear Face)

Model II on the other hand only considers the resistance of PFP against heat transfer into the metal substrate and neglects heat accumulation in the PFP and exothermic or endothermic effects. The initial transient period is ignored in this model with the rear face left open to air.

Heat loss from the rear face of the substrate through convection has substantial effects. The changes in substrate enthalpy are due to the heat conducted through the PFP and the heat loss from the rear face, which gives:

$$\frac{(T_1 - T)k}{X} = \frac{dT}{dt} r_m C_{Pm} b + (T - T_o)h \qquad [4.8]$$

Re-arranging this equation gives:

$$\frac{dT}{T_1 - T} = \frac{k}{X} = \frac{dT}{dt} r_m C_{Pm} b + (T - T_o)h \qquad [4.9]$$

which can in turn be re-arranged to form a differential equation:

$$dT \Big/ \left(-T + \frac{\frac{T_1 k}{X} + T_0 h}{\frac{k}{X} + h} \right) = \left(\frac{\frac{k}{X} + h}{\rho_m C_{Pm} b} \right) dt \qquad [4.10]$$

Integrating this equation and applying the boundary condition that the temperature is T_0 at $t = t_0$, gives the following exponential relationship:

$$T = \frac{\frac{T_1 k}{X} + T_0 h}{\frac{k}{X} + h} + \left(T_0 - \frac{\frac{T_1 k}{X} + T_0 h}{\frac{k}{X} + h} \right) \exp\left(\frac{-\left(\frac{k}{X} + h \right)(t - t_0)}{\rho_m C_{Pm} b} \right) \qquad [4.11]$$

If the rear face heat loss is neglected, this can be simplified to

$$T = T_1 + (T_0 - T_1) exp\left(\frac{-k(t - t_0)}{\rho_m C_{Pm} b X} \right) \qquad [4.12]$$

The fitting involves manipulating three variables, which are induction time, the thermal conductivity of the char and the rear face heat transfer coefficient in Equation 4.11. Figure 4.2 displays the predicted temperature curves for Model I and II.

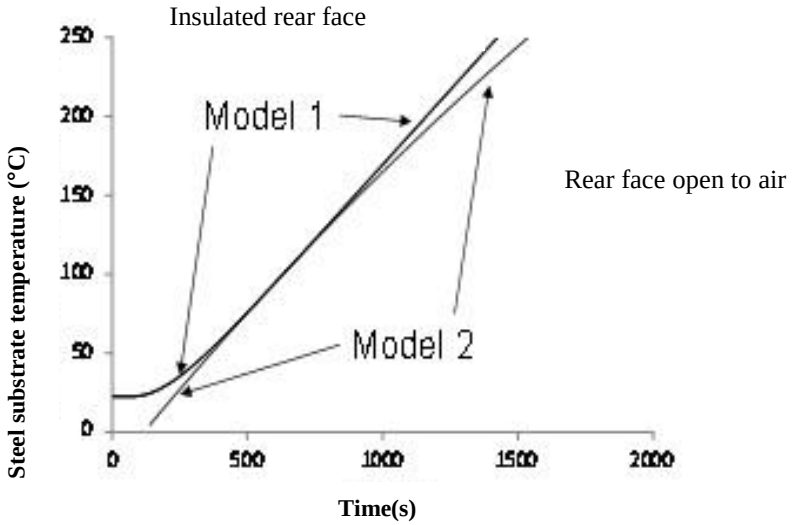

Figure 4. 2 Model I and Model II steel substrate temperature profile curves (with a displaced time axis)

4.3 Sample Preparation

The fire protection performance of three different passive fire materials was tested: a furan based bio-composite made of polyfuryl alcohol (PFA) mixed with glass microspheres, commercially available kaowool ceramic blanket, and intumescent coating. These were exposed to one-sided heat flux at 1000ºC.

Furan microspheres and kaowool samples were secured to 10 mm by 150 mm square steel plates using metal wires (figures 4.3 (a) and (b)) and a thin layer of adhesive, while intumescent coating (figure 4.3 (c)) was cured on 150 mm square steel. All samples were tested at two different thicknesses of 12.5 mm and 25 mm for furan microspheres and kaowool, while the thicknesses of the intumescent coating were 19 mm and 24 mm.

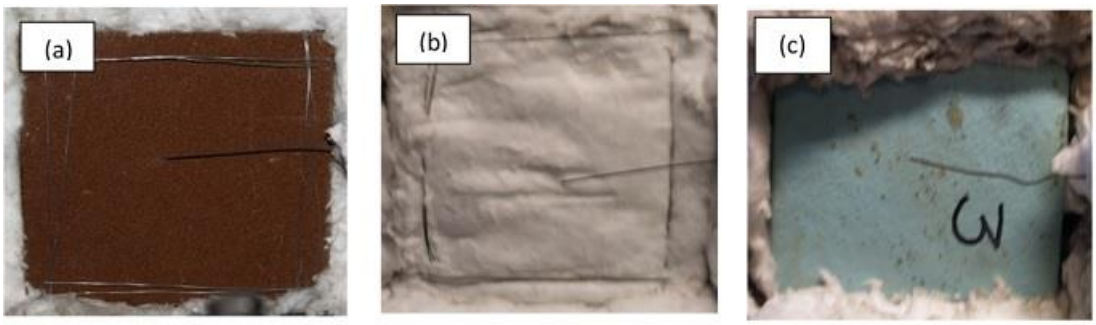

Figure 4. 3 Three types of PFP samples attached to 10mm thick steel, secured with metal wires and ceramic wool around the testing frame: (a) furan microspheres; (b) kaowool; (c) intumescent coating

4.4. Thermogravimetric Analysis (TGA)

In this thermal analysis, the heating rate was set to 10 ℃/min, 20 ℃/min and 40 ℃/min. TGA was not conducted on kaowool due its inert properties and high melting point, so that it would not give much information below temperature of 900ºC.

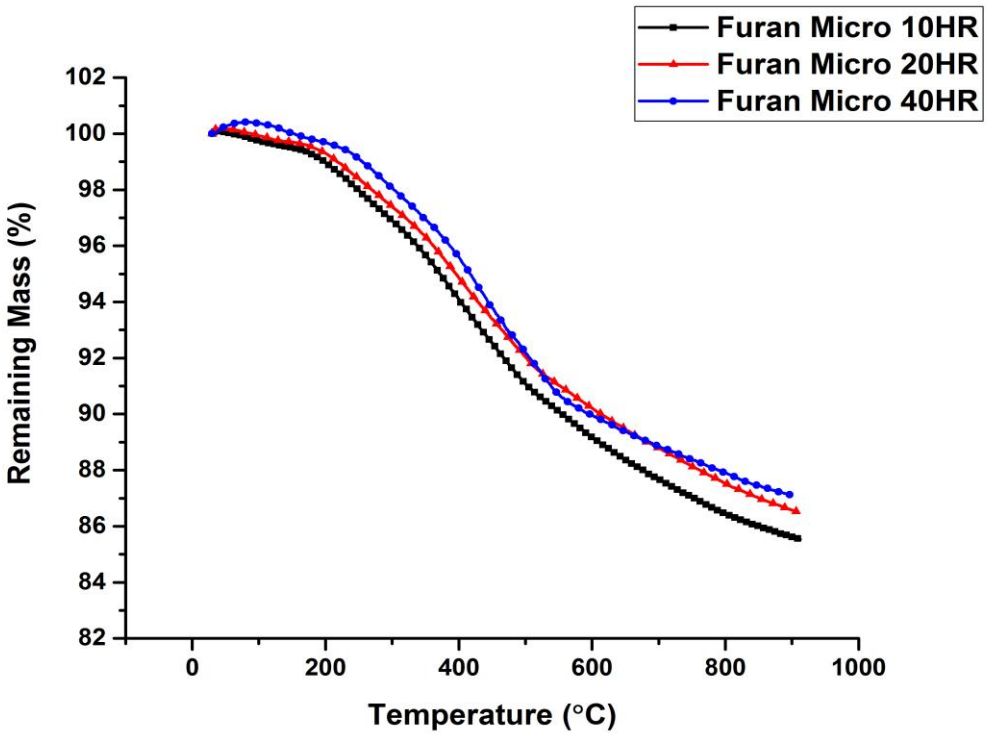

Figure 4. 4 TGA curve for furan microsphere at different heating rates (10 ℃/min, 20 ℃/min and 40 ℃/min) in nitrogen gas atmosphere

The thermogravimetric analysis curves shown in figure 4.4 denote the thermal degradation of furan resin and furan microsphere coating in a nitrogen gas environment.

The two-step reaction curve obtained for furan at the first stage finished about 500 ^{o}C, while the second stage starts at around 600 ^{o}C with the mass remaining at this temperature being 90% for all heating rate. At this stage, oxidation is the main process involved, which will continue until the temperature reaches 900 ^{o}C.

	Onset T of degradation (^{o}C)	**Mass Remaining at 600 ^{o}C (wt%)**	**Final Residue at 900 ^{o}C (%)**
Furan Micro. 10HR	170	90	86
Furan Micro. 20HR	185	90	87
Furan Micro. 40HR	190	90	87

Table 4. 1 Parameters of furan microsphere degradation from TGA

The onset temperature in table 4.1 was estimated using Originlab by seleting the transition point . It is observed that the furan microspheres material has a high final residual weight of more than 85%, with the presence of silica microspheres acting like a heat sink in the composite which inhibits heat diffusion within the epoxy network. The presence of thermally stable silica microspheres with a degradation temperature higher than 900^{o}C leads the bonds between the furan polymer and the silica network to be restructured, which leads to high level of final residues.

According to Guigo *et al.* (2009) and Monti *et al.* (2015), the disintegration of the cross-linked structure evaporate water, releases combustible volatility, leading the material to become more stable material.

Different patterns of thermal degradation curves are found in commercial intumescent coating compared to furan microsphere. This is expected due to the different physical and chemical properties of the PFP system (figure 4.5).

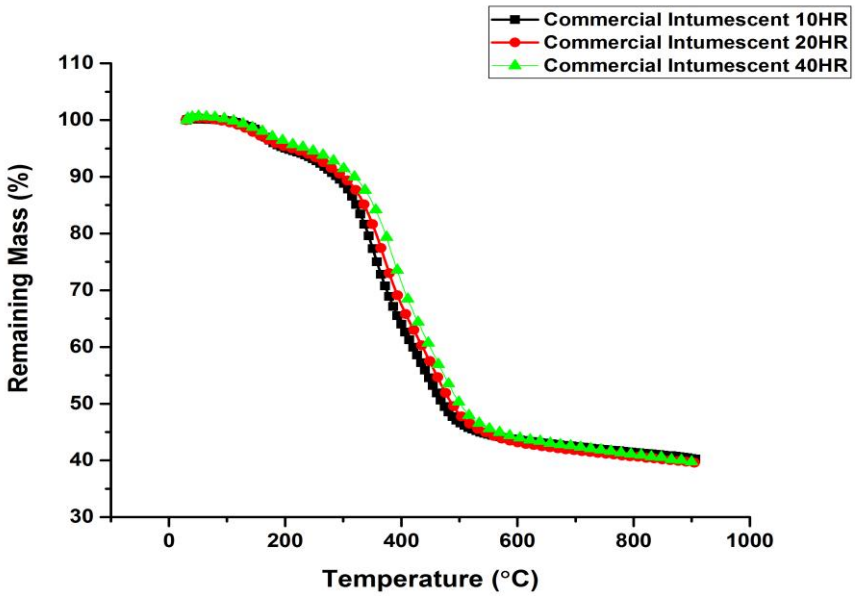

Figure 4. 5 TGA curve for commercial intumescent coating at different heating rates (10 ℃/min, 20 ℃/min and 40 ℃/min) in a nitrogen gas atmosphere

The offset temperatures for the degradation phases of commercial intumescent coating obtained are tabulated in table 4.2.

	Char Formation (°C)	Mass Remaining at 600°C (wt%)	Final Residue (%)
Comm. Intu. 10 HR	492	44	40
Comm. Intu. 20 HR	500	43	40
Comm. Intu. 40 HR	538	44	40

Table 4. 2 Parameters of the degradation of commercial intumescent coating from TGA

According to Griffin (2010), the char formation phase takes place after the coating has degraded and generates gas which is surrounded by molten matrix. At 600^{o}C, it is believed that the coating enters the char deformation phase in which the pyrolysis process creates the inert char structure. The final proportion of the residue of the coating is lower than for furan microsphere at about 40%.

4.5 Fire Testing

A bullfinch burner and propane gas (as mentioned in Chapter 3) were used to provide a heat flux of 116 kWm^{-2} during the fire test, as shown in figure 4.6 (a). The distance between burner and sample was set at 350 mm throughout the test. Heat flux calibration was conducted by placing a calcium silicate board as the sample with a type K thermocouple positioned 1cm away from the board. Once ignited, the gas was allowed to stabilise for a few minutes and the gas pressure corrected in order to obtain ~1000^{o}C.

A type K thermocouple was bonded halfway through the back of the steel to measure the rear face temperature. The ceramic blanket was used to insulate the edges of the samples from the heat flux and also to insulate the rear face for Model I experimental conditions (see figures 4.6 (b) and (c)).

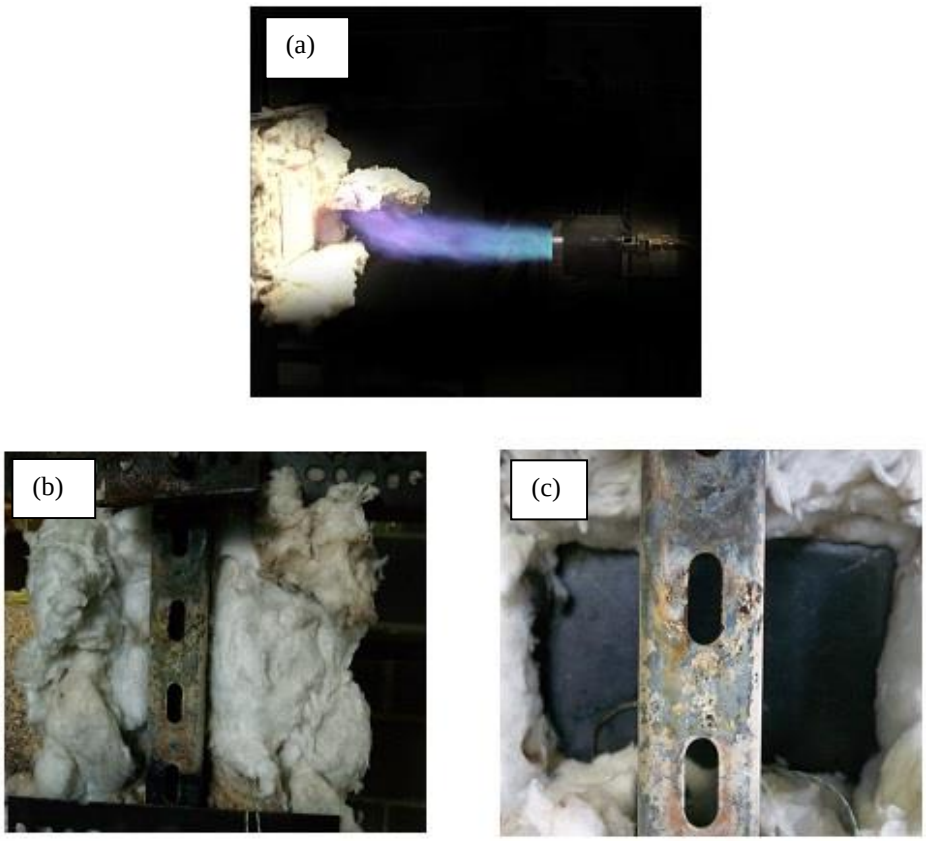

Figure 4. 6 Fire testing set-up: (a) propane burner to provide constant heat flux of 116 kW/m^2; (b) and (c) images of rear faces of uninsulated and insulated samples with ceramic wools

The results obtained from the fire testing of different PFP materials with the rear face open to air are presented below (figure 4.7). All samples were exposed to constant heat flux for up to 1000s. Similar temperature profiles are attained for the insulated rear face as seen in figure 4.8. Based on the temperature profiles, it is observed that the furan microspheres and intumescent coating samples display a longer thermal lag period compared to kaowool at the beginning of the test. The delay in heat transfer in both materials is due to its ability to slowly absorb and transfer the heat.

The results reveal that the furan microsphere managed to slightly reduce the temperature of the steel compared to the intumescent coating in both testing conditions. Almost no smoke was detected during the testing of the furan microspheres compared to the intumescent coatings which produced smoke due to the burning of its organic components. Kaowool with 25 mm thickness gives the lowest rear face temperature among the three PFPs.

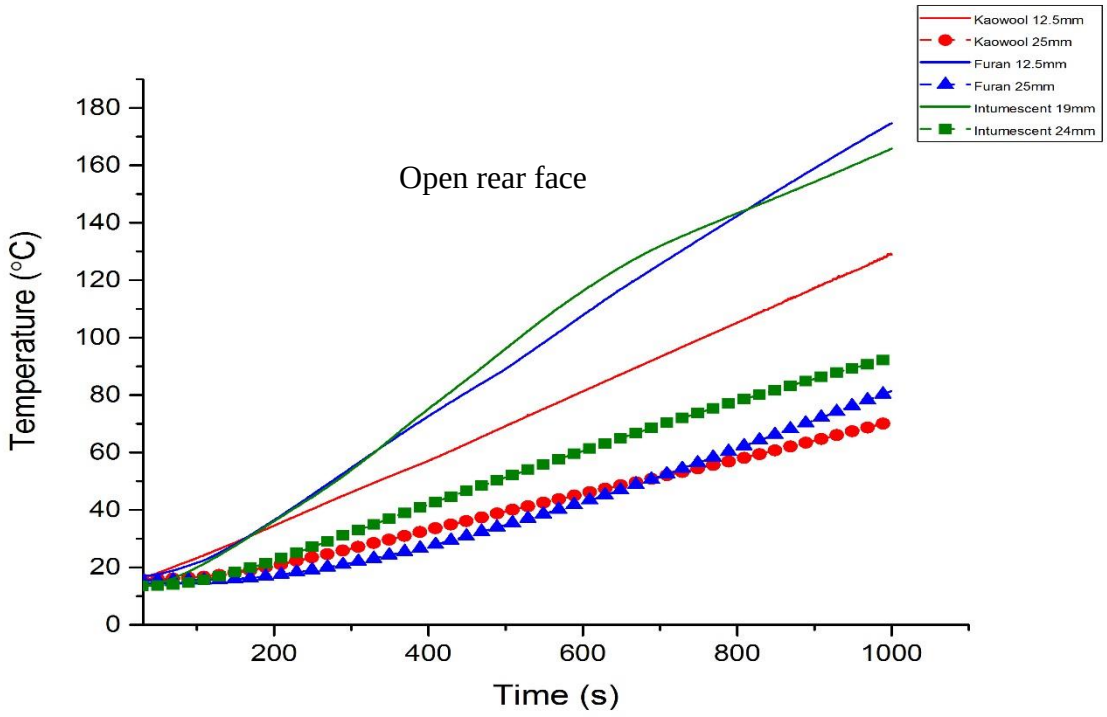

Figure 4. 7 Measured temperature profiles of 10 mm steel substrate with different passive fire protection exposed to 116 kW/m^2 heat flux with Model I experimental conditions (open rear face)

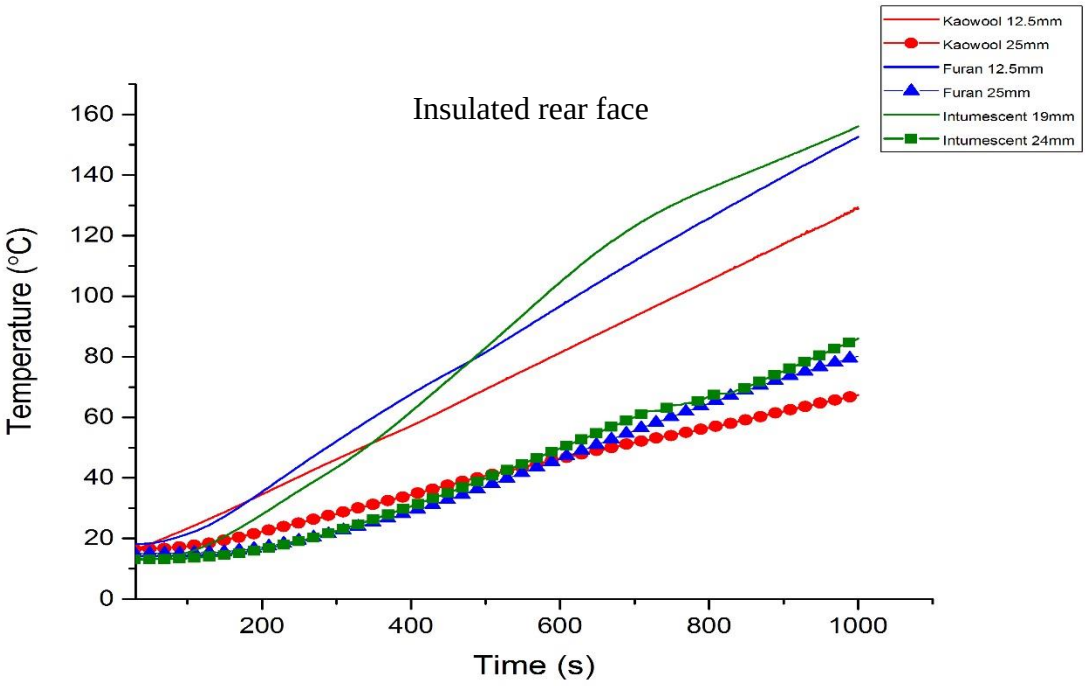

Figure 4. 8 Measured temperature profiles of 10 mm steel substrate with different passive fire protection exposed to 116 kW/m^2 heat flux with Model II experimental conditions (insulated rear face)

No significant physical decomposition is observed in kaowool sample after the test (see figure 4.9). Throughout exposure to fire, it is believed that the air pockets move within the fibrous network (Gibson *et al.*, 2016). From the results, it is clear that kaowool has the lowest thermal conductivity among the PFP materials.

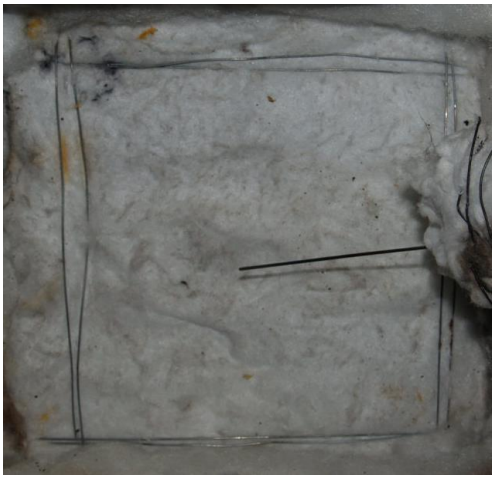

Figure 4. 9 No significant changes in kaowool sample after exposure to 116 kW/m^2 constant heat flux

It is also observed that the furan microsphere 25 mm has a longer thermal initial compared to 25 mm kaowool and 24 mm commercial intumescent coating. As reported in the TGA results, upon reaching 600°C the furan microsphere will start to oxidise and disintegrate, releasing combustible volatile materials. A sharp increase in temperature especially for 25 mm furan microsphere, can be observed from the temperature profile.

Hardly any smoke was observed during the fire testing of furan samples. This is a good sign indicating furan resin's potential for replacing conventional resins such as phenolic resin. Both furan microsphere samples become brittle after the test due to the resin decomposition. This is supported by Monti *et al.* (2015) findings that furan resin becomes fragile due to significant charring. Cracks in the samples detected during the cooling period of are illustrated in figure 4.10. It is assumed that the sample expanded during heating and shrunk as it cooled down. The different level of thermal conductivity between the furan microsphere and steel also contribute to creating thermal stress between the material structures.

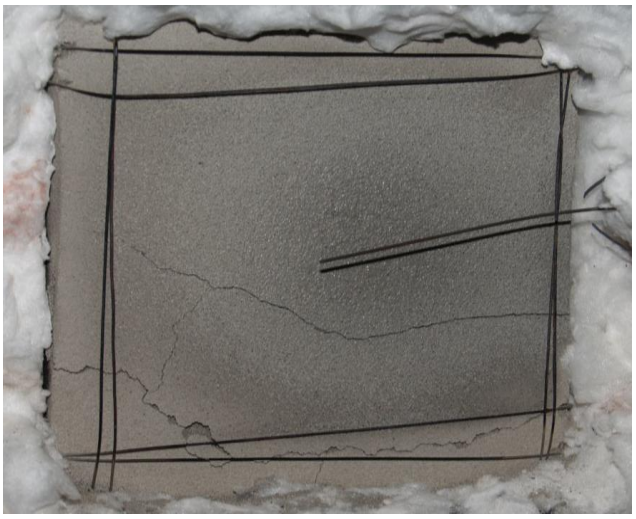

Figure 4. 10 Cracks on furan microsphere after exposure to 116 kW/m^2 constant heat flux

The 19 mm thick commercial intumescent coating expanded to 23 mm (figure 4.11) and the 24 mm thickness of coating expanded to 32 mm. It is noticeable that the intumescence was not fully developed after the test due to time restrictions. Smoke was detected during the testing, especially during the initial ignition period where the pyrolysis reaction and decomposition of the organic intumescent formulation took place. The absence of a good layer of char structure reduces the sample's fire protection efficiency, whilst more heat was conducted through the coatings.

Figure 4.11 19 mm commercial intumescent coating after exposure to 116 kW/m^2 constant heat flux

4.5.1 Simulation Results

It can be seen from figure 4.12 that Model I managed to give a good fit with the experimental curves on both thicknesses of kaowool. This is achieved by using the same thermal constant for both thin and thick PFP.

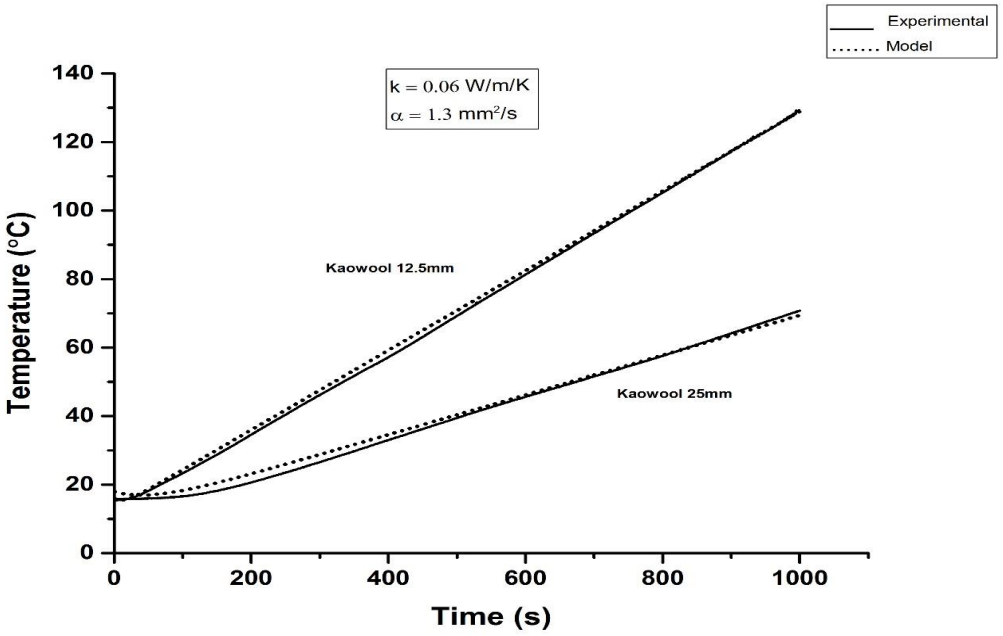

Figure 4. 12 Experimental and Model I simulation on profile for 10 mm steel insulated with kaowool exposed to 116 kW/m^2 constant heat flux

The simulation of Model II for kaowool is achieved by using similar thermal parameters for k and α, but different values of HTC for each thickness, with an induction time of 60 s for 12.5 mm and 100 s for 25 mm (see figure 4.13).

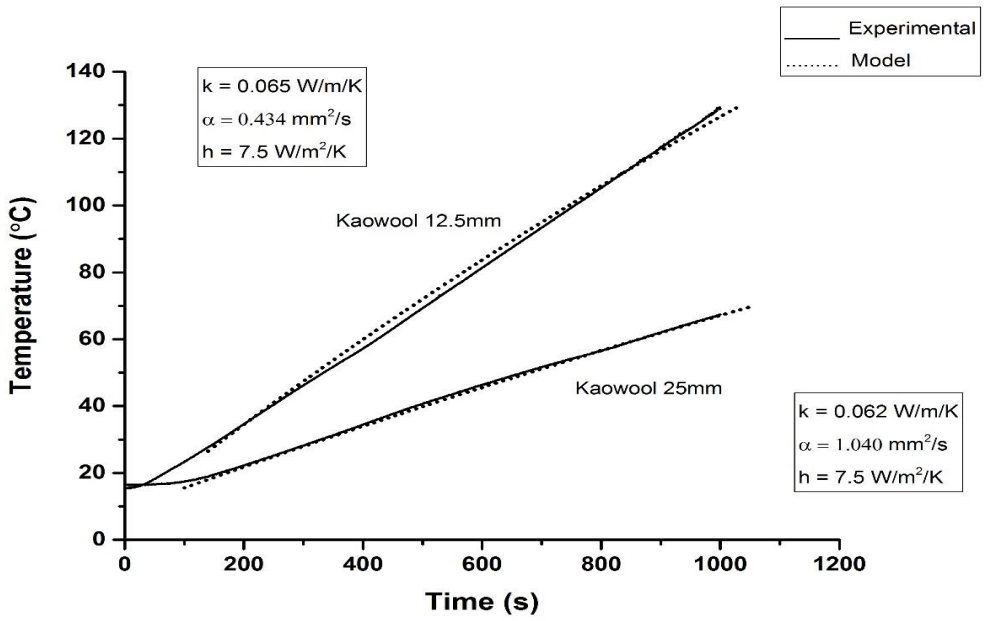

Figure 4. 13 Experimental and Model II simulation on profile for 10 mm steel insulated with kaowool exposed to 116 kW/m^2 constant heat flux

The furan microsphere Model I simulation (see figure 4.14) shows a good fit between the experiment and model curves. From the sample temperature profile slope calculations, it has a higher thermal conductivity compared to kaowool. Both thicknesses exhibit the same thermal parameters of thermal conductivity and thermal diffusivity.

The simulation of furan microsphere requires higher thermal parameters compared to the thicker sample for Model II. A higher value of HTC is needed for the thinner sample because of the higher convective heat transfer as shown in figure 4.15. The induction times for furan microsphere 12.5 mm and 25 mm thick are 90 s and 220 s respectively.

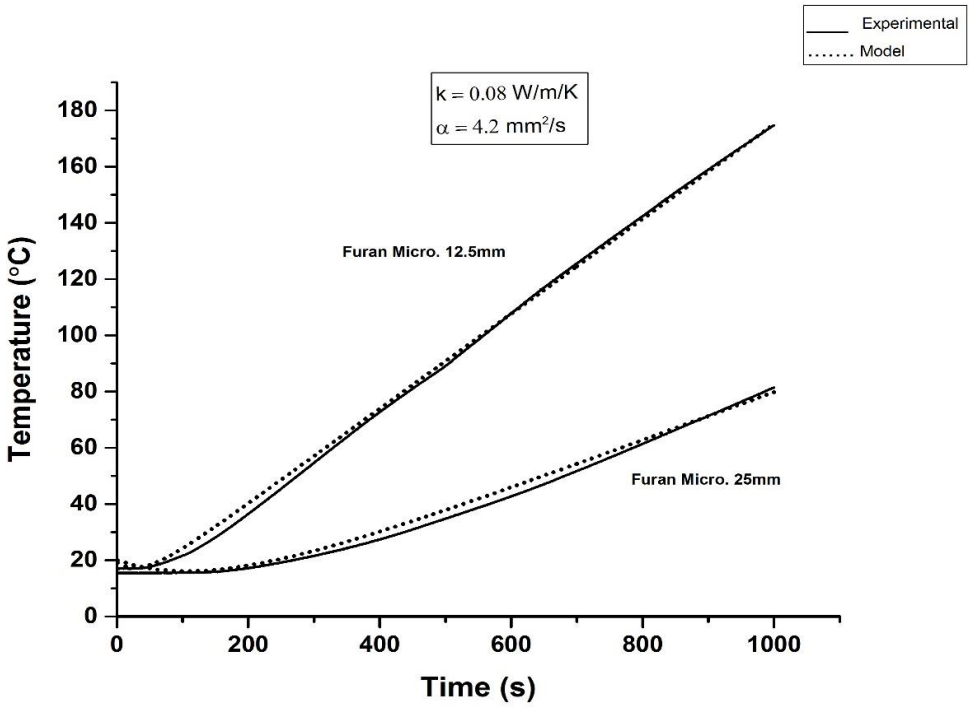

Figure 4. 14 Experimental and Model I simulation of temperature profile for 10mm steel insulated with furan microsphere exposed to 116 kW/m^2 constant heat flux

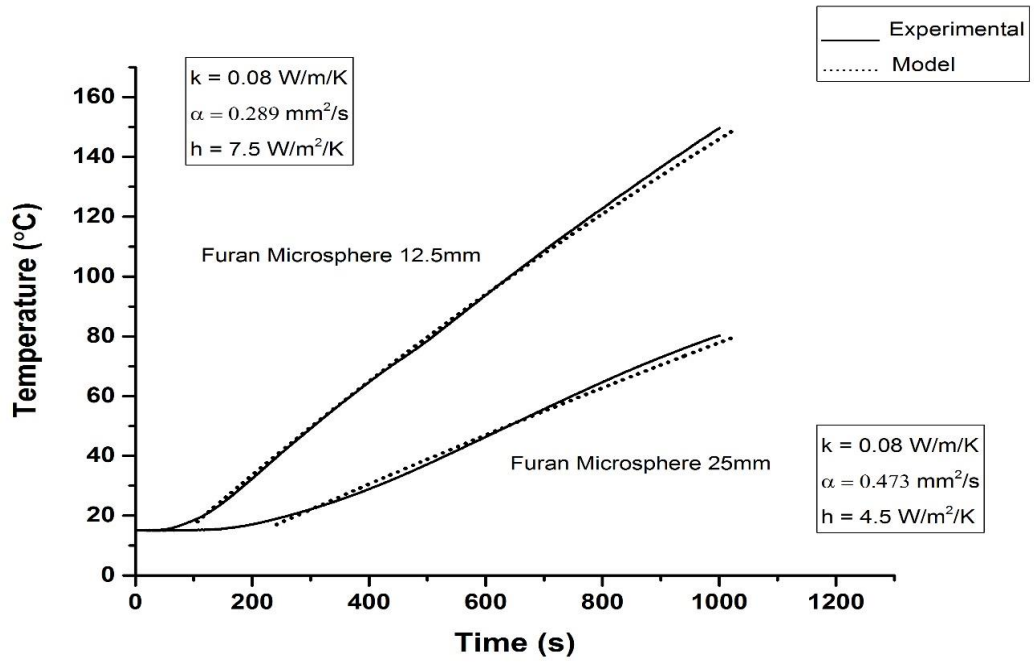

Figure 4.15 Experimental and Model II simulation of temperature profile for 10mm steel insulated with furan microsphere exposed to 116 kW/m^2 constant heat flux

The experimental curves for both intumescent coating samples show a fairly good fit. The induction time for each sample is 175s and 220s for 19 mm and 24 mm thicknesses respectively. Between 100 to 140°C, the 19 mm sample shows a peak which could be due to an exothermic reaction from the melting intumescent constituents that leads to a higher temperature and the beginning of the formation of the char structure (see figure 4.16).

In the case of the 24 mm intumescent coating, the experimental curve does not show an obvious exothermic curve reaction within the 1000s, and the simulated curve gives a good fit throughout the temperature profile as shown in figure 4.17. Lower thermal conductivity and thermal diffusivity is needed for thicker samples. Since the coating is thicker, this sample presumably needs more time in order to undergo the full physical and chemical reactions.

The thickness used for both simulations is based on the initial thickness of each sample. Mesquita *et al.* (2009) also assumed that the intumescent coating is a single homogenous layer in order to derive the effective thermal conductivity and thermal resistance.

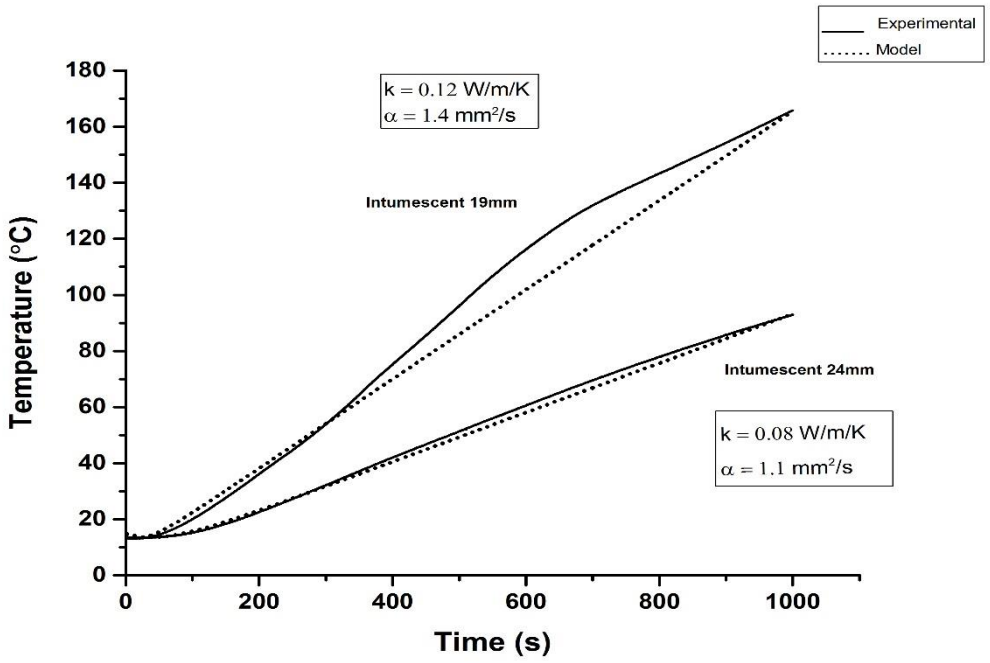

Figure 4.16 Experimental and Model I simulation of temperature profile for 10 mm steel insulated with intumescent coating exposed to 116 kW/m^2 constant heat flux

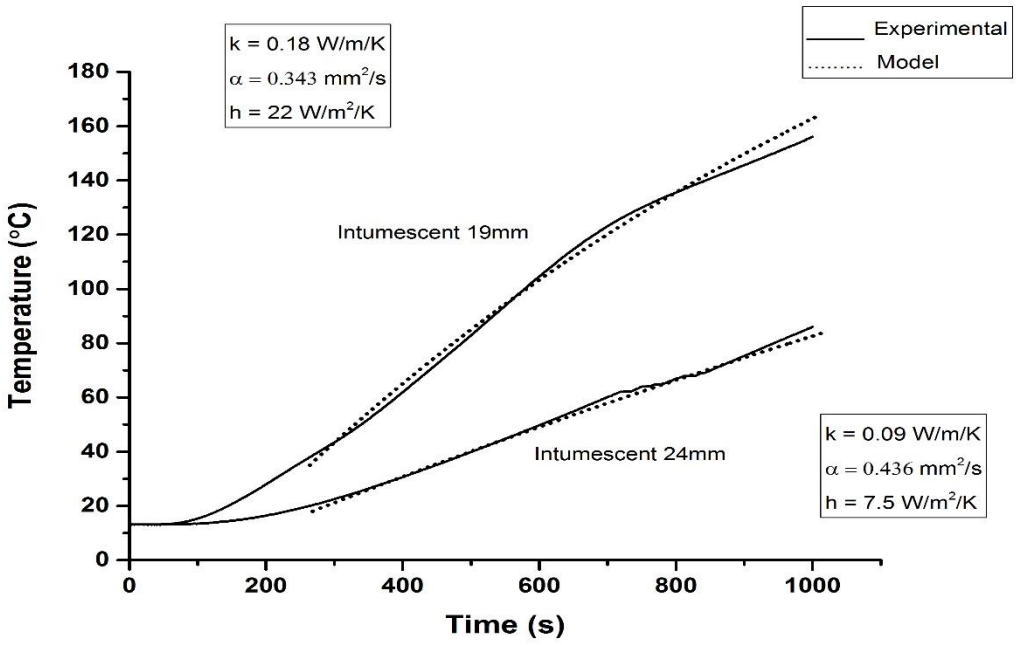

Figure 4.17 Experimental and Model II simulation of temperature profile for 10 mm steel insulated with commercial intumescent coating exposed to 116 kW/m^2 constant heat flux

4.6 Conclusion

The presence of silica microspheres in the furan resin created a thermally stable structure that leads to high final residue in TGA. The fire test results indicate that the furan resin microsphere has a good thermal stability and potential for being used as a PFP material as well as replacing phenolic composites. Nevertheless, further improvement needs to be made to strengthen the fragile char structure of the furan microsphere. It is also observed that no obvious smoke was detected during the furan microspheres fire testing compared to intumescent coatings.

The simulation results also show fairly good fits between experimental and simulation results using Model I and Model II (with thermal lag adjustment) especially for furan microsphere and kaowool samples, which gives a good indication that these models will work for different types of PFP. In the case of intumescent coating, some parts of the 19 mm sample temperature curve were not properly fitted to the model, which is believed to be due to the expansion of the coating which changes the thickness of the sample itself, since the thickness used in the simulation is based on the initial thickness of the sample.

Chapter 5. Intumescent Coating with Nanomaterials Protection on Steel

This chapter will focus on improving the basic formulations of intumescent coatings with the addition of nanomaterials. There have been several studies which focus on introducing nanomaterials as additives in the quest to improve the properties of intumescent coatings, but none of these employed a direct flame from a propane burner in a 1000 °C assessment test. The set-up used here is a small-scale test as experiments described by Gibson *et al.*, (2016) to replicate the jet-fire testing that is often used in the certification of commercial intumescent coatings for offshore structures. In this part of the project, a straightforward comparison is made between nanoclay, nanographene and multiwall carbon nanotubes and their influence on intumescent coating behaviour. The temperature profile of the steel substrate upon exposure to constant heat flux was simulated using the Model II (Uninsulated Rear Face) as in previous chapter.

5.1 Nanomaterial in Intumescent Coating

To achieve a good quality of intumescent coating, a significant proportion of intumescent flame retardant (IFR) additives are needed. High loadings of flame retardant additives often reach between 40 to 65 wt.% and this may have the effect of increasing the material's cost and density, as well as reducing its flexibility and adhesion strength. The possibilities offered by the use of nano-materials as additives is that they may both improve the intumescence process as well as improve the strength and performance of the intumesced material at much lower loadings compared to conventional IFR additives.

It is reported that the addition of flame retardant additives to intumescent systems able to change the chemical reactions within the system (Bourbigot *et al.*, 2000) as well as its physical properties (Bourbigot *et al.*, 2009) upon exposure to heat flux whilst improving the fire protection performance (Alongi *et al.*, 2015).

There have been several investigations involving the incorporation of nanomaterials into IFR formulations to provide improvement in thermal and flammability behaviour. The primary advantage of using nanomaterials as additives to IFRs is their ability to suppress the heat release at low loading without any additional fire retardant additives (Gérard *et al.*, 2012; Alongi *et al.*, 2015)

Each nanomaterial provides different chemical characteristics and physical properties, such as self-passivation, and resistance to oxidation and ablation. It is not proven whether or not nanomaterials produce toxic burning gases, as they do not contain any halogenated elements and are used in low concentrations. Commercially, they can be found in automotive parts, lightweight engineering constructions, coatings and flame retardants (Dittrich *et al.*, 2013; Shan *et al.*, 2015).

Carbonaceous char as mentioned above, plays an important role as a barrier to mass transport, preventing the escape of volatile content and boosting the viscosity of molten polymer through the growth of a network structure between the epoxy-additives or additives-additives. It can also control flame development by prohibiting the dripping and emission of gases (Liu *et al.*, 2014).

5.2 Intumescent Modelling

An intumescent coating has a complex thermal degradation mechanism due to the mixture of various constituents with different properties and applications.

Currently available intumescence models take into account the kinetic parameters during thermal degradation, complex chemical reactions, and thermal and transport phenomena (Lyon, 1998; Mesquita *et al.*, 2009; Griffin, 2010; Staggs *et al.*, 2012; Gibson *et al.*, 2016). These models assume one-dimensional heat conduction, separate thermal properties between temperature and space, and constant heat flux (Moghtaderi *et al.*, 1997; Mesquita *et al.*, 2009).

Heat transfer through the intumescent coating is governed by its thermal conductivity and density. These key parameters influence the expansion during thermal degradation (Gomez-Mares *et al.*, 2012a).

In the present study, the temperature profile of coated steel was modelled based on Model II established by Gibson *et al.* (2016) which was discussed earlier in Chapter 4 of this thesis. The model assumes a thermal lag at the beginning of the test. As reported by Wan Jusoh *et al.* (2017), the heat conducted through the intumescent coating balances the rear face convective loss as follows:

$$\frac{(T_1 - T)k}{X} = \frac{dT}{dt} r_m C_{Pm} b + (T - T_o) h \qquad [5.1]$$

where:

T : steel temperature
T_1 : hot face temperature
T_0 : initial temperature (room temperature)
X : intumecesnt coating thickness
b : metal susbtrate thickness
ρ_m : steel density
Cp_m : steel specific heat
k : char thermal conductivity;
h : rear face heat transfer coefficient
t : time

Integrating the above equation and applying the boundary condition [$T - T_0$ at $t = t_0$] to take into consideration the thermal lag at the beginning of the test gives:

$$T = \frac{\frac{T_1 k}{X} + T_0 h}{\frac{k}{X} + h} + \left(T_0 - \frac{\frac{T_1 k}{X} + T_0 h}{\frac{k}{X} + h} \right) \exp\left(\frac{-\left(\frac{k}{X} + h \right)(t - t_0)}{\rho_m C_{Pm} b} \right) \qquad [5.2]$$

5.3 Coating Preparation

Intumescent coatings were prepared using a non-fired retardant epoxy resin, RS-L135, and hardener RS-H137 supplied by PRF Composite Materials, United Kingdom, mixed with three main intumescent coating additives: Exolit AP 422 which is a fine grain Ammonium polyphosphate (APP), by Clariant Produkte, Deutshland, Melamine (M2659 Aldrich); and Pentaerythritol (P4755) powders supplied by Sigma-Aldrich, United Kingdom.

The intumescent coating (IC) was later mixed with the addition of XGnP graphene (Graphene), halloysite nanoclay (Clay) and multiwall carbon nanotube (MCNT) each at 0.5 wt%. In this trial, a halloysite clay (two-layered aluminosilicate) with mostly hollow tubular structures was used. The average surface area of these particles is 64 m^2/g with 30-70 nm (diameter) x 1-3 µm (length). Figure 5.1 shows a Transmission Electron Microscope (TEM) image of the nanoclay, as provided by the manufacturer Sigma Aldrich, United Kingdom.

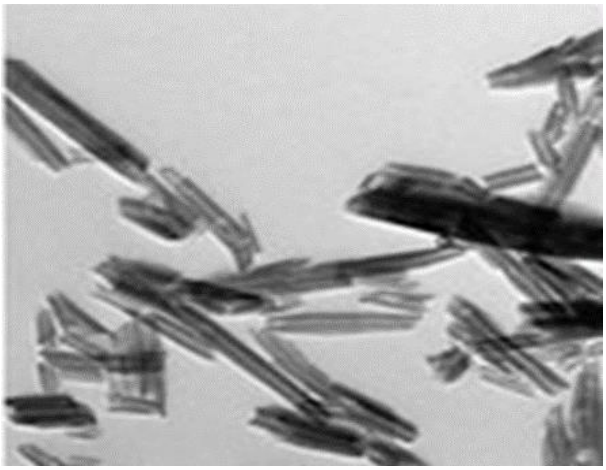

Figure 5. 1 Image of TEM micrograph of halloysite in hollow tubular structures (Sigma Aldrich)

The Grade C graphene nanoplatelets used in this study were supplied by XG Sciences, Inc. (United States of America) with an average width of 1 to 50 µm and surface area of 500 m^2/g, which consist of short stacks of graphene sheets having a platelet shape as shown in figure 5.2 below.

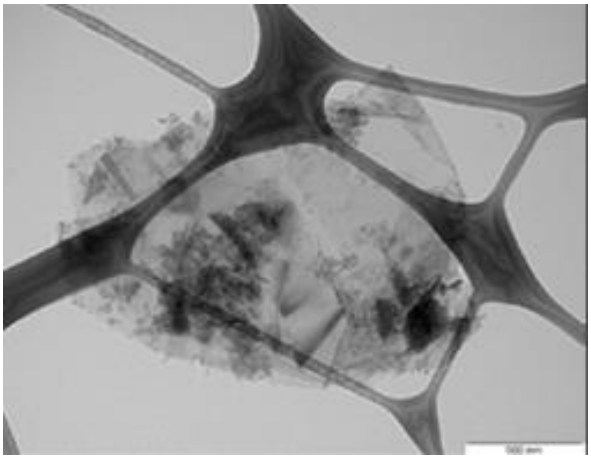

Figure 5. 2 Image of TEM micrograph of graphene sheets in platelet shape (XG Sciences, Inc.)

The carbon nanotubes NC7000 (MCNT) used in this study were supplied by Nanocyl, Belgium. This industrial multiwall carbon nanotube (see figure 5.3) can be found in transportation, electronics and sports good products. It offers good processing ability, high electrical conductivity and black tinting. Its average diameter is $9.5x10^{-9}$ m with an average length of 1.5µm. The surface area measured through Brunauer–Emmett–Teller is 250-300 m^2/g.

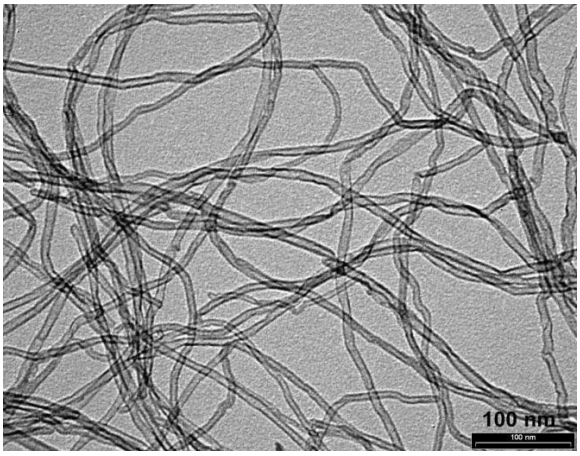

Figure 5. 3 Image of TEM micrograph of Multiwall Carbon Nanotubes strand (Nanocyl)

The coating preparation procedures for the nanomaterials were similar. Pure resin was hand-mixed with the nanomaterials and subjected to sonication at 100% amplitude using a UP200S Ultrasonic Processor from Hielscher for 3 minutes, and then manually stirred using a spatula before further sonication for 3 minutes. The process was repeated for 3 cycles to improve the dispersion of the nanomaterials.

The main additive powders (2:1:1; APP:Melamine:Pentaerythritol) were later hand-mixed into the resin mixture when it had cooled down. Once the mixture was uniformly blended, hardener was added at the end of the process and stirred using a Klarstein mechanical stirrer.

The substrate used in this study was a 100 mm x 100 mm x 10 mm steel plate which was roughly ground, cleaned and degreased using acetone and dried before the application of the coating. Coated steel was left to dry for 24 hours at room temperature. The dry coating thickness was on average 5 mm ($\pm$ 1 mm).

5.4 Thermogravimetric Analysis

The exothermic reactions of the intumescent coatings were evaluated using Thermal Gravimetric Analysis (TGA) conducted with a Perkin Elmer STA 6000, Simultaneous Thermal Analyser. Samples of around 10mg were tested in an inert nitrogen environment (40 ml/min) to prevent oxidation and burning.

A heating rate of 20 ºC/min was used on all samples to determine the mass loss or resin degradation of the material. Primary mass loss was expected due to the decomposition of the resin matrix. The thermal analysis measured the mass loss of the material with increasing temperature from 30 ºC up to 900 ºC.

The influence of the nanomaterials on the resin degradation process is represented in the curves below. Figure 5.4 displays the changes in thermal stability of the original IC and the IC with nanomaterial fillers. The thermal degradation curves exhibit similar behaviour for coatings with or without nanomaterials. Coatings decomposed in a two-step degradation process, unlike the pure resin (without intumescent additives) that decomposed in a one-step degradation (insert graph).

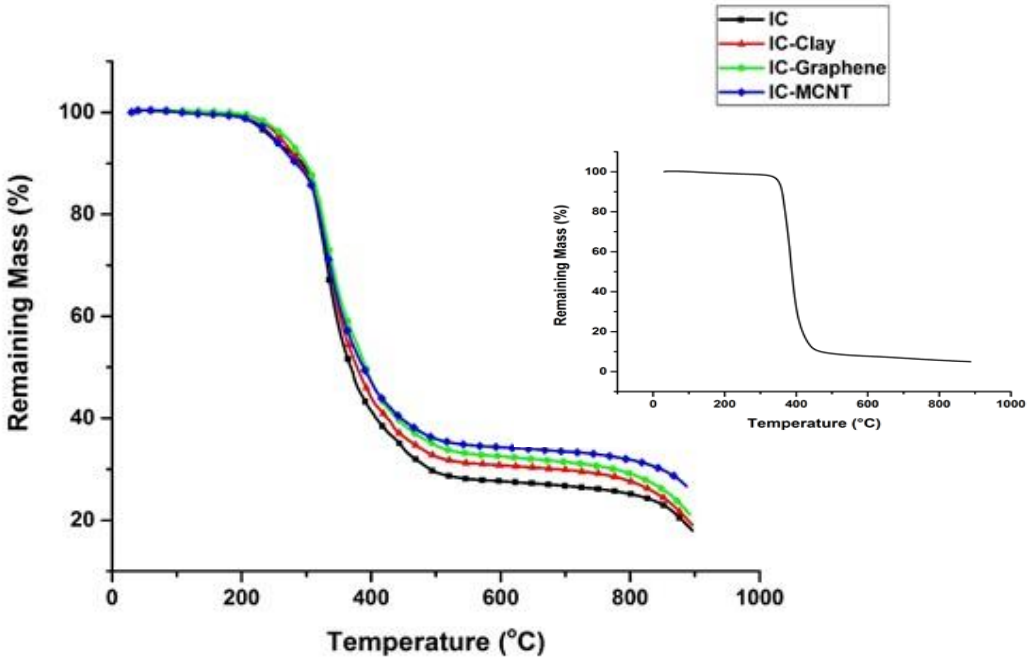

Figure 5. 4 Two-step thermogravimetry analysis curves for samples with and without addition of nanomaterials at 20 ºC/min heating rate. Pure resin shows a one-step curve as in the inset graph.

	T_{10} (°C)	T_{50} (°C)	Final Residue (%)
IC	294	369	18
IC-Clay	290	378	19
IC-Graphene	299	392	21
IC-MCNT	284	385	27

Table 5. 1 Mass loss data during thermal analysis test

The curves do not show significant changes in degradation temperature with the addition of nanomaterials at 10% (T_{10}) of mass loss as shown in table 5.1. As with any other intumescent coating reactions, it is initiated with the evaporation of volatile content and water molecules.

The first stage is between 270 °C and 350 °C, where ammonia and water were released from APP producing polyphosphoric acid that contributed to the weight loss. The evaporation of water molecules during thermal decomposition is a result of removing the secondary alcohol groups and the development of unsaturated structures with cross-linked polyaromatic carbonaceous residue (Liu *et al.*, 2014).

According to Camino and Luda (1998) and Jimenez *et al.* (2006b), PER decomposition occurs between 220 °C and 340 °C, while APP and MEL begin to degrade at 270 °C and 300-370 °C respectively.

The effects of the nanomaterials are observed at 50 % of weight loss due to the intumescence process that started around 300 °C. The onset temperature (**T_{50}**) at this stage shifted up to higher temperature with the addition of nanomaterials, which demonstrates the improvement in thermal stability of the coatings. Carbonization elements start to decompose after 350 °C according to Camino and Luda (1998) and Lecouvet *et al.* (2013a).

According to Griffin (2010), there are four main degradation phases which take place during intumescent coating combustion, which are melting, intumescence, char formation and char degradation. In order to determine the onset temperature of each phase, Originlab software was used for char formation and deformation of the offset temperatures obtained are tabulated in table 5.2 below.

	Char Formation (°C)	Char Deformation (°C)
IC	404	832
IC-Clay	445	837
IC-Graphene	443	838
IC-MCNT	439	834

Table 5. 2 Estimation of onset temperature of degradation phases

It is observed that the onset temperatures for coatings with nanomaterials took place above the onset degradation temperatures of IC alone. According to Lecouvet *et al.* (2013b), the additional investigation of IFR with the presence of halloysite clay shows better thermal stabilization with traces of water released around 100 °C. Then, as the temperature increases to 250 °C, the evaporation of water between the aluminosilicate sheets decomposes the clay.

Marchal *et al.* (1994) reported, that the reaction between 350-430 °C correlates with the chemical reaction between polyphosphoric acid and carbon-rich combinations to produce the phosphor-carbonaceous phase.

Char formation begins around 400 °C as a result of chemical reactions between the nanomaterials and IFR constituents. Above 480 °C the phosphor-carbonaceous structure starts to decompose and degrade. The onset temperatures for char formation and char deformation in IC-Clay and IC-Graphene coatings is quite close, indicating their similar thermal stability properties.

Further char formation developed from the carbonization process leads to an increment in the final residue of the coating with the addition of nanomaterials. From the data, IC-MCNT produced the most carbonaceous char with the highest remaining char of 27 %, followed by graphene at 21 %, clay 19 % and the original at 18 %. It should be noted that the carbonization process was promoted in carbon based nanomaterials like graphene and MCNT compared to other coatings mixture.

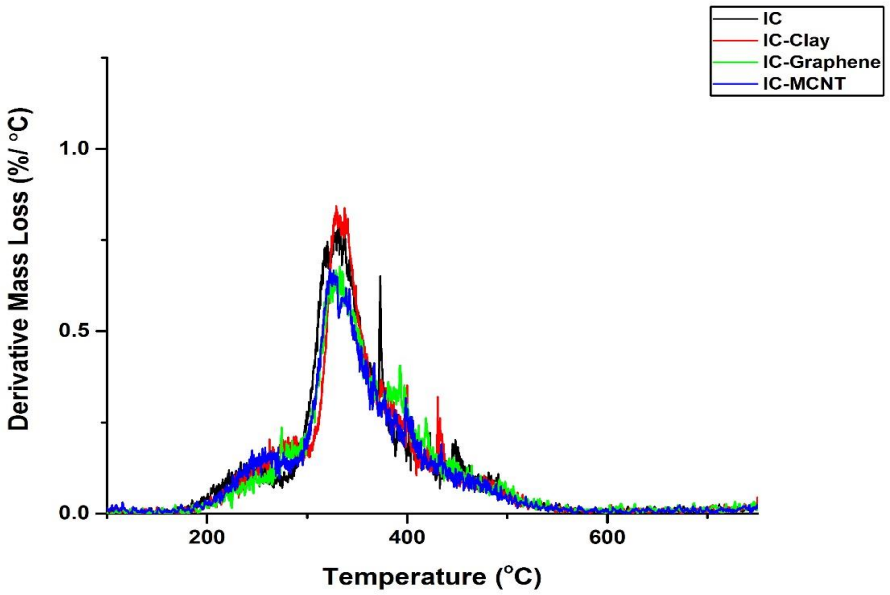

Figure 5. 5 Derivative mass loss curves from thermogravimetric analysis for samples with and without the addition of nanomaterials at 20 ºC/min heating rate

The decomposition rates for the coatings tested are presented in figure 5.5. Initial decomposition started above 200 °C and reached the maximum rate between 320-332 °C. The highest decomposition rate was observed in IC-Clay at 0.8 (%/°C) at 329 °C, while the lowest was IC-MCNT with 0.7 (%/°C) at 333 °C. Beyond 550 °C, the decomposition process slowed down in all coatings.

Different amounts of residual char were obtained depending on the addition of nanomaterials. Jimenez *et al.* (2006a) reported that the decomposition rate significantly slows between 600-800 °C. Based on this TGA test, it can be concluded that MCNT demonstrated the best thermal stability compared to the other nanomaterials because of more char residue than other nanomaterials.

5.5 Fire Test

Samples were placed on a metal test frame with all the sides thermally insulated with a ceramic blanket, leaving the rear face open to air. A Bullfinch propane burner was placed 350 mm away from the front of the sample to provide a constant heat flux of 116 kW/m^2 in tests as per previous testing. The propane burner provides one-sided heating to the sample and simulates actual fire conditions, as shown in figure 5.6.

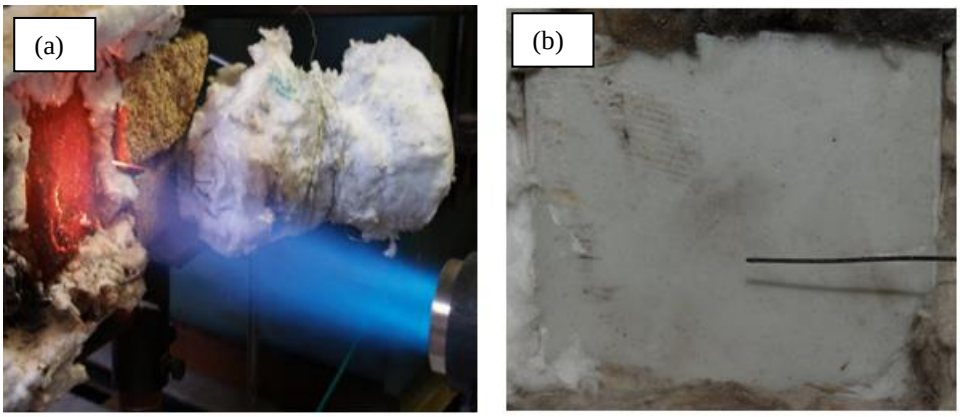

Figure 5. 6 Fire testing set-up: (a) propane burner used to provide constant heat flux of 116 kW/m^2 with the sample secured around the metal frame using a ceramic blanket; (b) front view of sample with a type-K thermocouple to monitor the flame temperature

The temperature profile was recorded using type K thermocouple placed 1 cm from the sample's hot surface. An additional type K thermocouple was inserted through a small drilled hole, to the mid-thickness of the steel plate's rear face. The data was collected by an IO data acquisition unit, Tech DAQ Shuttle 55, connected to a computer.

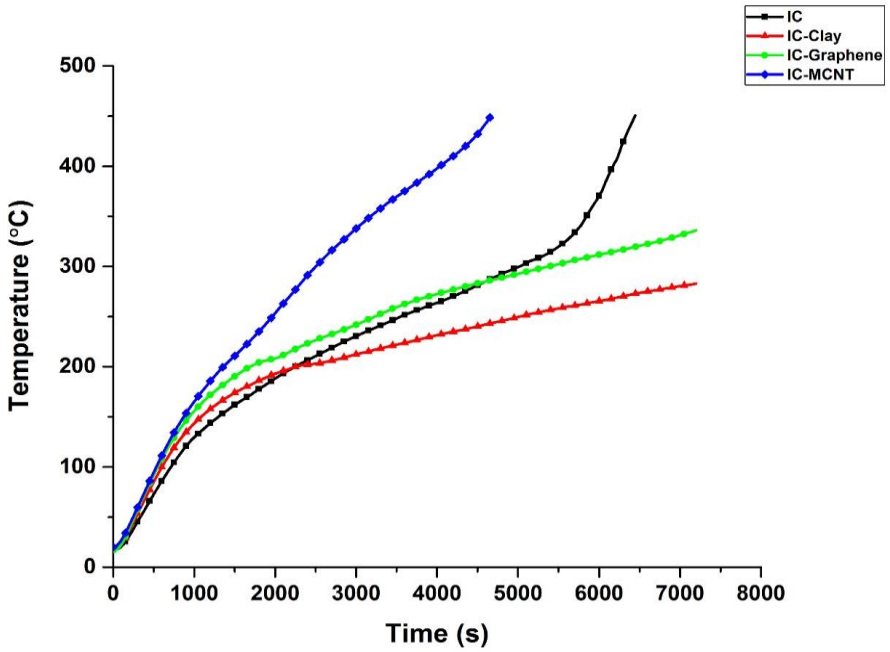

Figure 5. 7 Representation of one of two specimens for each sample rear face temperature profiles of different formulations exposed to 116 kW/m^2 heat flux. The fire testing was stopped if either the sample temperature reached 450 °C or the duration of testing reached 2 hours, whichever came first

Test was repeated twice for each formulation. Similar temperature profile observed for both specimens hence the best curve for each sample selected for further discussions. Rapid increments of temperature were observed in all coatings within 1000s before the backface temperature reached 200 °C as displayed in figure 5.7.

It is believed that, at this stage, chemical reactions within the intumescent constituent have not started to decompose, but have only caused some of the formulations to melt. Similar swelling in all coatings was observed within 10s of fire ignition. Small bubbles and burst bubbles were observed especially on the IC and IC-MCNT. Bubbles formed on the surface were volatile content and gases escaping of from underneath. The thermal conductivity of the protective layer is affected by changes in the chemical composition from interactions between the flame retardant additives during the degradation of the intumescent system (Lecouvet *et al.*, 2013a), which influence fire protection performance.

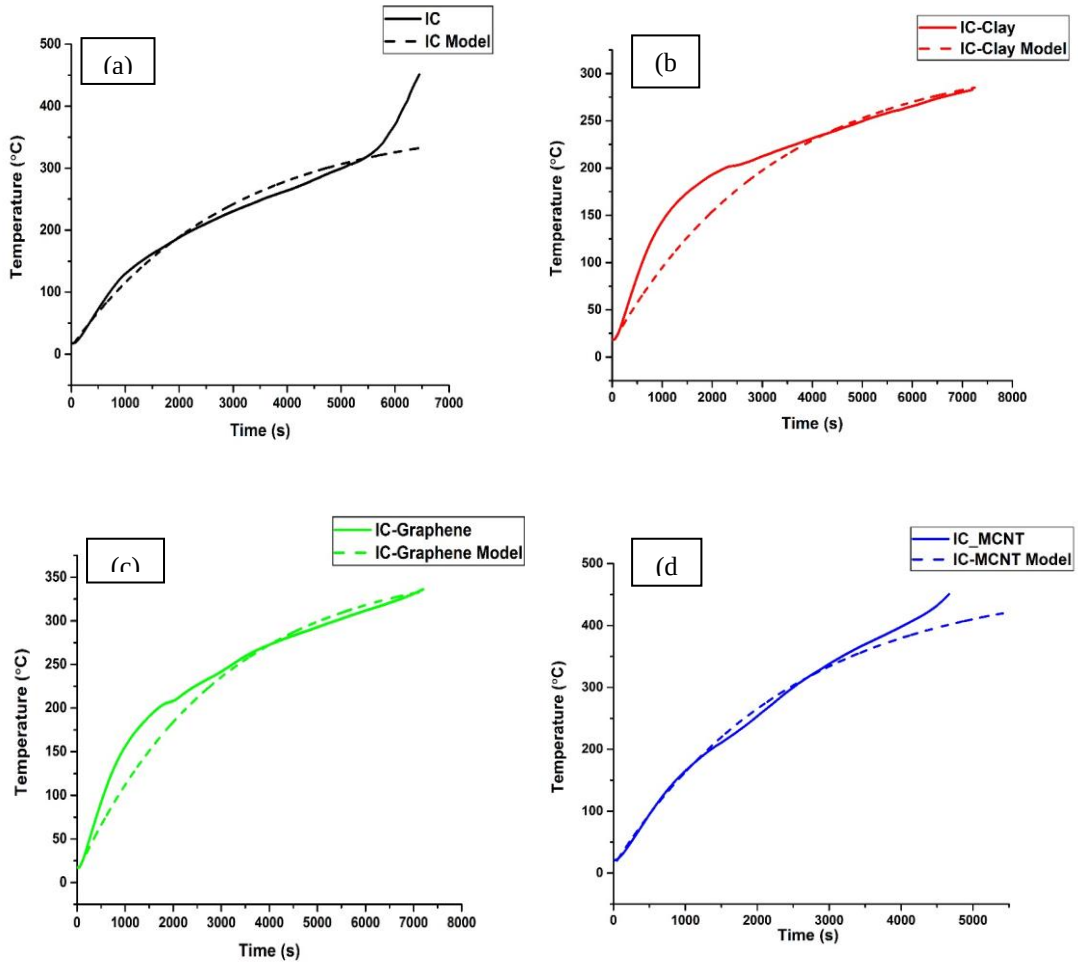

Figure 5. 8 Comparisons of experimental and modelled results of steel substrate temperature profiles of different intumescence formulations at 116 kW/m^2 heat flux

The modelled temperature profiles are basically in fairly good agreement with the experimental data with 50 s induction time. IC and IC-MCNT models fit properly with the experimental results up to a temperature of ~300 °C. It is observed during the testing, at this temperature, some parts of the coating having big voids and some of the char might have fallen off, exposing the steel substrate directly to the fire. This could explain the sudden increase in steel temperature seen in figure 5.8.

The experimental temperature profiles for the IC-Clay and IC-Graphene curves show some variations around 75 to 250 °C due to pyrolysis decomposition that leads to swelling and the expansion of the coatings. Since Model II does not take changes in thickness into consideration, this part of the temperature profile was not properly modelled.

Table 5.3 shows results for thermal conductivity using estimations from the temperature profile slope of each sample. The thermal diffusivity then calculated based on the thermal conductivity value. The heat transfer coefficient later, was speculated on two specimens by using the calculated thermal conductivity and thermal diffusivity as in equation 4.11. Both specimens show agreement with the speculated heat transfer coefficient.

	Thermal Conductivity,k (W/m.K)	**Thermal Diffusivity, α (mm^2/s)**	**Heat Transfer Coefficient, h ($W/m^2.K$)**
IC	0.05	1.34	7.90
IC-Clay	0.04	8.33	7.90
IC-Graphene	0.04	8.3 3	7.90
IC-MCNT	0.07	1.11	7.90

Table 5. 3 Estimation of thermal parameters used in Model II

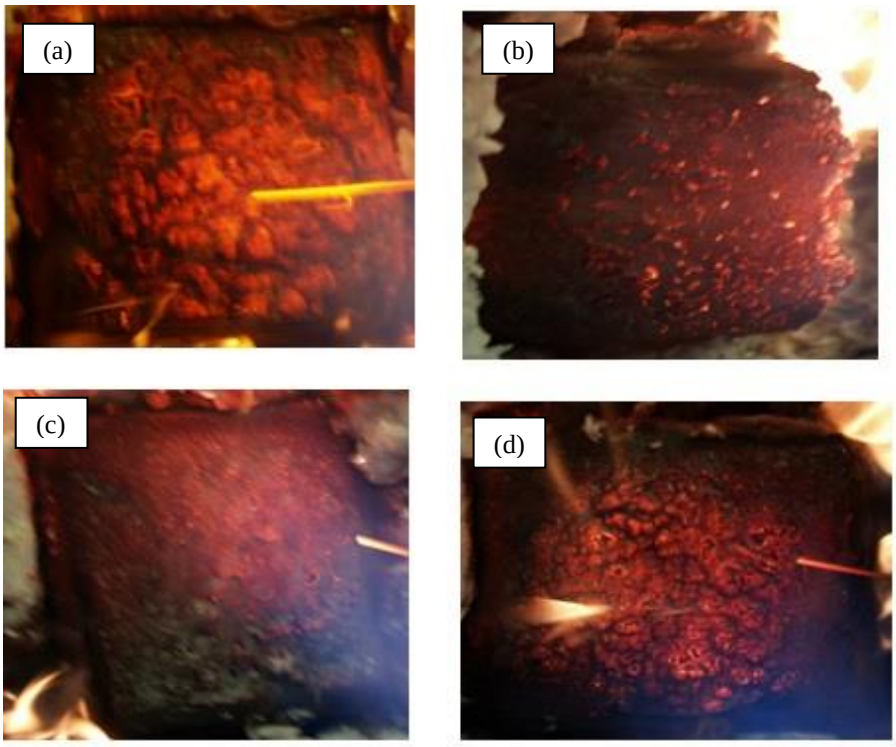

Figure 5. 9 Images of test sample surface during 40 mins of fire testing at 116 kW/m^2 heat flux with different types of nanoparticle additives as follows (a) IC; (b) IC-Clay; (c) IC-Graphene; (d) IC-MCNT

The photograph in figure 5.9 taken after 40 minutes of testing indicate different reactions observed in each sample. At this time, the backface temperature of the samples had reached more than 200 °C, where basic intumescent additives like APP and PER begin to interact with each other and nanomaterials forming carbonaceous chars.

The coatings started to intumesce at this stage, and hence different responses were observed for each coating. The top surfaces of the IC and IC-MCNT seem to have smaller bubbles than the other coatings with little swelling, while IC-graphene and IC-Clay had expanded to create thick chars.

According to Mohammadi *et al.* (2015), voids found in intumescent char are formed by the presence of internal gas in the matrix generated through the burning process of volatile substances. More voids are created by the increasing amount of degraded substances. Larger voids found at the outer layer of the coating could disrupt the formation of a char barrier.

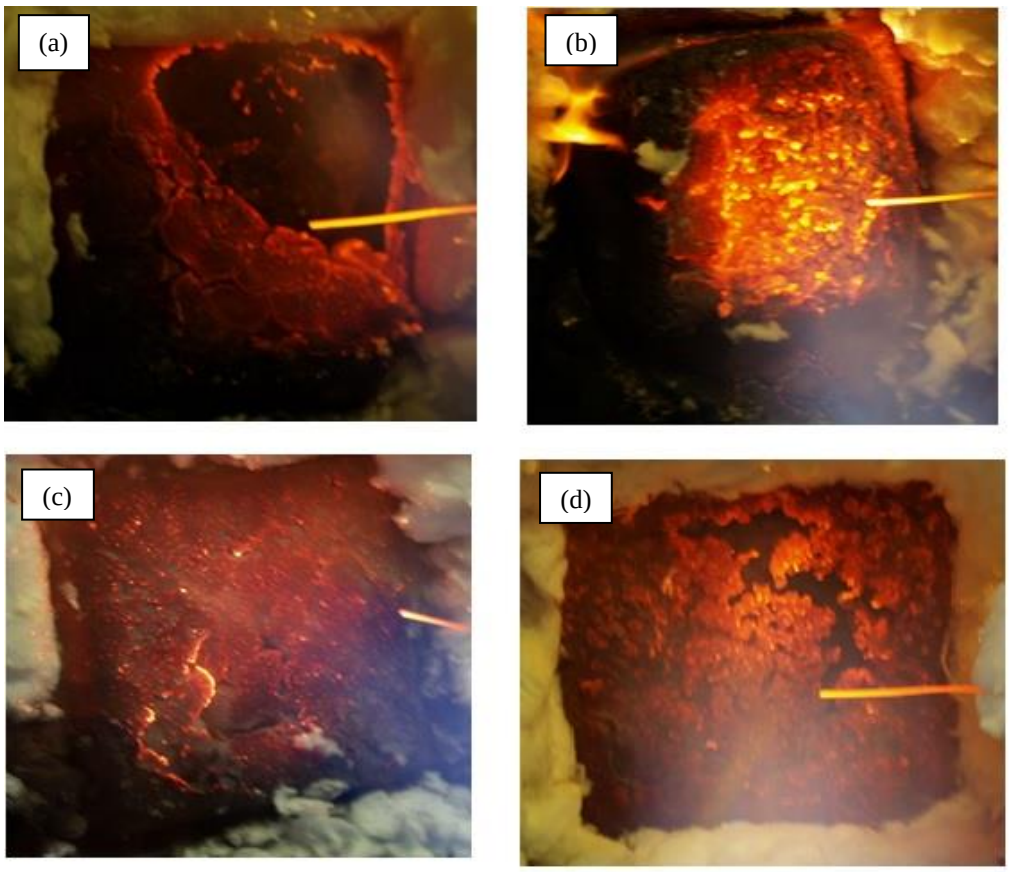

Figure 5. 10 Images of test sample surface during 1 hour of fire testing at 116 kW/m^2 heat flux with different types of nanoparticle additives as follows: (a) IC; (b) IC-Clay;(c) IC-Graphene; (d) IC-MCNT

Surprisingly, the temperature of IC-MCNT reached 375 °C within 1 hour compared to other samples which were still at between 220-260 °C (Figure 5.10). The backface temperature of IC-MCNT continued to increase rapidly until the test stopped when it reached 450 °C as with other samples. For this reason, the fire protection of IC-MCNT is worse than the IC sample. The best protection was given by IC-Clay, which reached 283 °C followed by IC-Graphene (336 °C) after 2 hours of fire testing.

According to previous studies, the main cause of the poor fire protection of IC-MCNT is the high thermal conductivity of the carbon nanotubes which transfer more heat to the steel rather than slowing it down. IC-MCNT also tends to clutter up and prevent the coating system from swelling and developing (Du and Fang, 2011; Beheshti and Heris, 2016). Strong mechanical bonding in the CNT network might also be a reason for the char structure to be blown away before the testing ended. This is supported by Isitman and Kaynak (2010), who found that the char development with CNT addition during initial combustion was dense and without cracks. Du and Fang (2011) and Beheshti and Heris (2016) have also reported that the development of a three-dimensional network structure enhanced the flame retardancy of polymer mixed with CNT, but unfortunately it also produced large cracks which allowed heat and mass transfer, which defeats the system's main purpose.

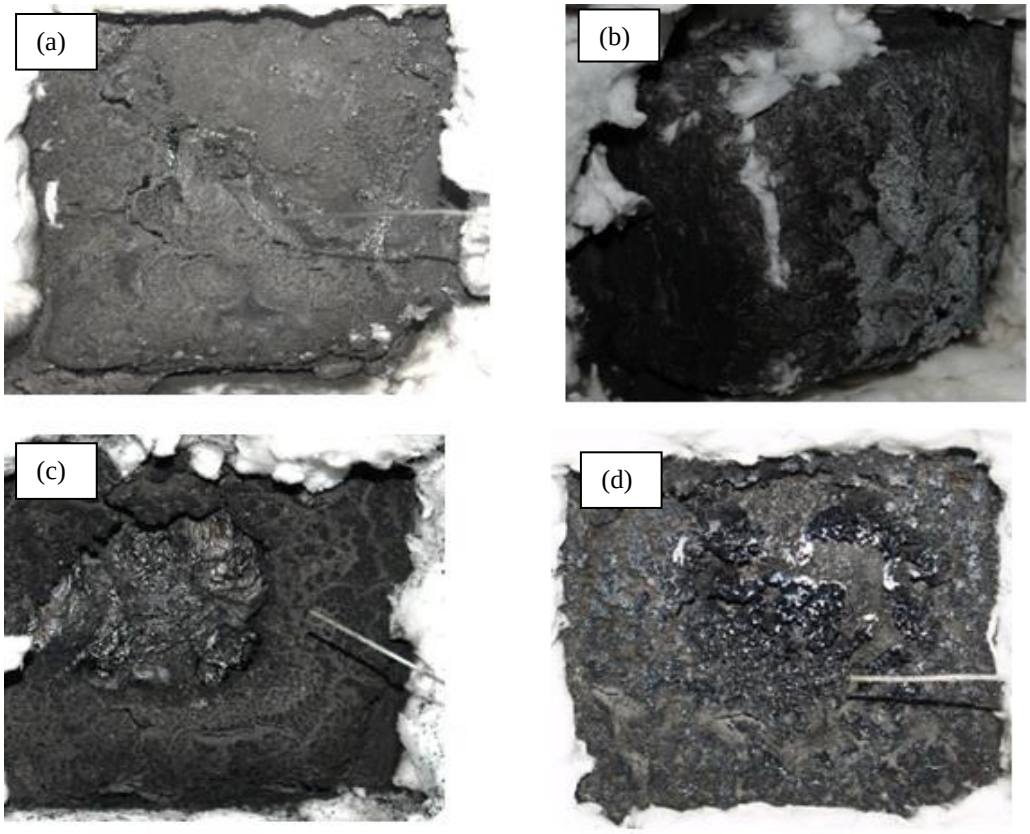

Figure 5. 11 Images of sample surface after exposure to 116 kW/m^2 heat flux. Complete burn-out is observed in all samples with different amounts of char residue depending on the type of nanoparticle additives (a) IC; (b) IC-Clay; (c) IC-Graphene; (d) IC-MCNT

The photographs in figure 5.11 taken after fire testing on all samples show the complete burn-out of the coatings. IC-Clay produced compact and uniform char compared to the other additives. It is also obvious that this char has the strongest structure, as manifested in the final weight of the residues after testing shown in table 5.4.

The steel substrate was fully covered by the char until the end of the testing. Weak char strength observed in IC and IC-MCNT resulted in more than half of the char falling off by the end of the tests. Due to the weak and brittle char structure with IC, IC-Graphene and IC-MCNT, part of it broke off during removal from the steel frame and the actual thickness could not be ascertained.

	Sample Weight (g)		**Sample Thickness (mm)**	
	Before Test	**After Test**	**Before Test**	**After Test**
IC	907	775	11	-
IC-Clay	894	766	10	62
IC-Graphene	899	781	10	-
IC-MCNT	900	779	11	-

Table 5. 4 Sample parameters before and after testing

The low strength of char also resulted in poor adhesion bonds between it and the steel substrate. The char residues also appeared to be porous with small holes on the surface and large void structure inside which contributed to a reduction in the expected heat barrier effect.

Even and dense char with fewer holes and lower crack depth is a more effective and efficient heat blocker compared to char with larger holes. Larger holes reduced char strength, making it easier to crack and expose the substrate to heat.

The development of uniform swelling and high quality char of the coating acts as a protective barrier and thermal insulator for the substrate, delays the diffusion of oxygen gas, volatile substances and providing a shield for the substrate from heat flux (Du and Fang, 2011; Mohammadi *et al.*, 2015).

The swelling and expansion of char is a result of trapped volatile gases. If these escape during decomposition, they will contribute to the development of the fire. High expansion with low amounts of weight loss indicate gases trapped inside the samples (Gérard *et al.,* 2012).

Lecouvet *et al.* (2013a) reported that halloysite minimizes the cell size of char by preventing the evolution and release of gas bubbles. Consequently it prevents the development of intumescent char structures with open micro-channels that increase the heat barrier properties. This observation may be due to the effect of heat stabilization produced in intumescent char with clay at high temperatures.

The fire protection of IC-MCNT deteriorated due to the "cage effect" from a strong and continuous nanotube network developed on the hot surface during combustion (Isitman and Kaynak, 2010). The nanotube network, unfortunately transfers more heat to the substrate compared to coatings with other nanomaterials.

On the other hand, graphene nanosheet with high surface area managed to create a uniform char with a crumpled structure that acted like a thermal insulator and a mass barrier preventing the escape of volatile content (Liu *et al.*, 2014).

5.6 Micrograph Examination

Coatings that give the best curved from the fire test for each formulation were selected for micrograph examinations. Micrograph examinations before and after testing were conducted using a Scanning Electron Microscope (SEM). Samples were coated with a carbon layer to improve the conductivity surface. The analysis was conducted twice for each sample with different observation spots.

The cross sections microstructures of untested and tested coatings were checked under SEM to observe the level of dispersion or agglomeration of nanoparticles since the efficiency of nanoparticles as flame retardant additives is strongly influenced by their dispersion in the matrix. Due to the different physical properties of the coatings, different magnifications were used on the micrographs in order to get good images. The morphology of char in terms of size and cell shape is important, as it has been observed that this directly influences heat transfer.

Voids observed on the char surface are developed during combustion when the polymer matrix degrades, and volatile content accumulates at the thermal degradation temperature. Bubbles grow underneath the polymer and are later released to the gas phase which will disturb the char development (Liu *et al.*, 2014).

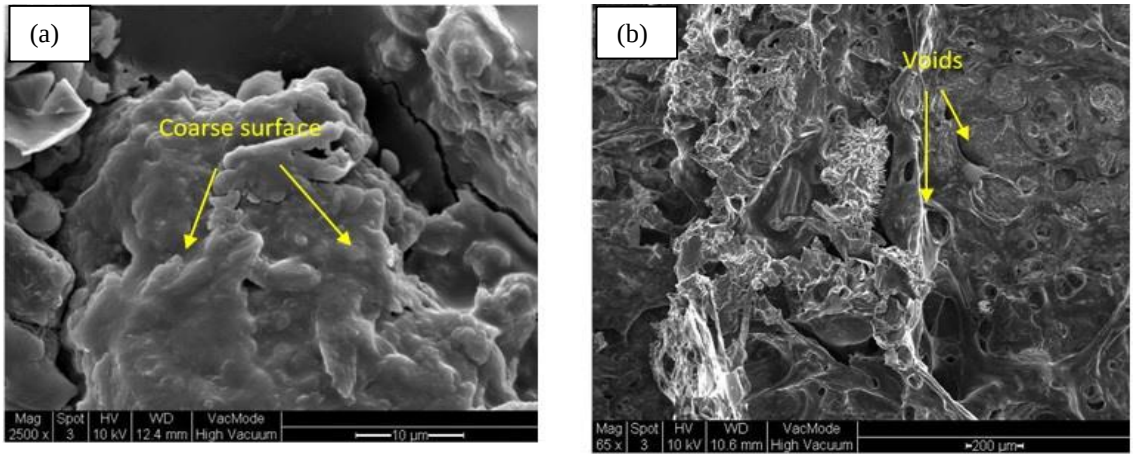

Figure 5. 12 Images of SEM micrograph of IC sample cross-sections (a) Before testing: Coarse and irregular surface with some microcracks observed on the untested sample; (b) After testing: Non-uniform voids found scattered all over the irregular on the tested sample surface

The SEM image of IC (see figure 5.12 (a)), reveals a coarse and irregular surface with some microcracks and possibly agglomerations. The microcracks could possibly have formed during the curing process, which introduced some shrinkage stress on the coating surface. The sample does not have any other distinctive appearance. The microstructure of IC after fire testing (see figure 5.12 (b)), reveals an irregular surface with non-uniform voids distributed all over the surface.

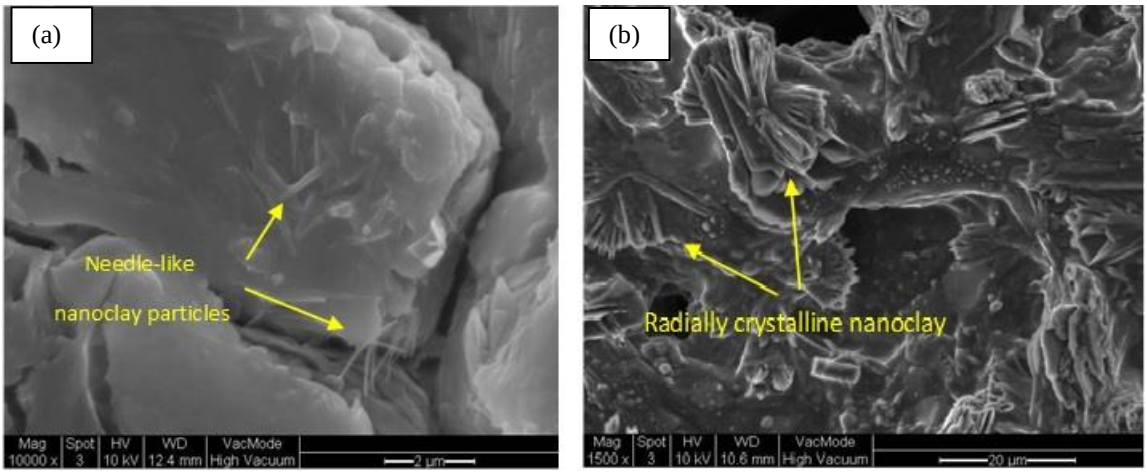

Figure 5. 13 Images of SEM micrograph of IC-Clay sample cross-sections: (a) Before testing: Cluster of nanoclay particles were noticed on the untested sample; (b) After testing: Radially crystalline nucleation of halloysites observed on the tested sample

Needle-like nanoclay particles are clearly visible in figure 5.13 (a) above. It appears that a cluster of nanoclay particles agglomerated at certain areas of the coating with a few microcracks. Some of these randomly oriented particles also stick out from the surface. Figure 5.13 (b) shows the radial crystalline nucleation of amorphous nanoclay after exposure to fire. This crystallization phase is believed to have strengthened the char structure compared to that in the other nanomaterials.

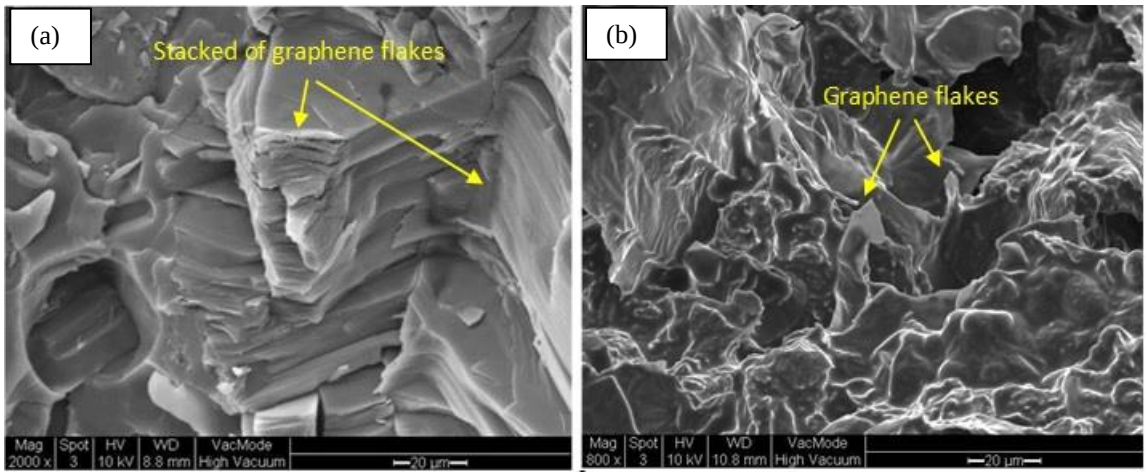

Figure 5. 14 Images of SEM micrograph of IC-Graphene sample cross-sections: (a) Before testing: Stacked of graphene flakes were observed on the untested sample; (b) After testing: Graphene flakes were noticed scattered on the tested sample

An irregular surface was observed on IC-Graphene with stacks of graphene flakes shown in figure 5.14 (a) as a result of poor dispersion. Coating morphology seems flaky compared to other samples.

The char morphology shown in figure 5.14 (b) for IC-Graphene shows an irregular and rugged surface with fewer voids. It could also be observed that flakes are distributed inside the char with some sticking out from the surface. As reported by Ullah and Ahmad (2014), the presence of more flakes creates a stronger and denser char microstructure. A porous microstructure decreases heat transfer to the substrate compared to a solid microstructure with air acting as an insulation between the hot surface and the substrate.

This is supported by Liu *et al.* (2014) who found, that 0.3 wt.% and 0.5 wt.% graphene content developed a kind of rugged surface char residue with smaller holes compared to epoxy without graphene. The movement of the melting polymer was efficiently reduced and constrained with the addition of 0.5 wt.% graphene.

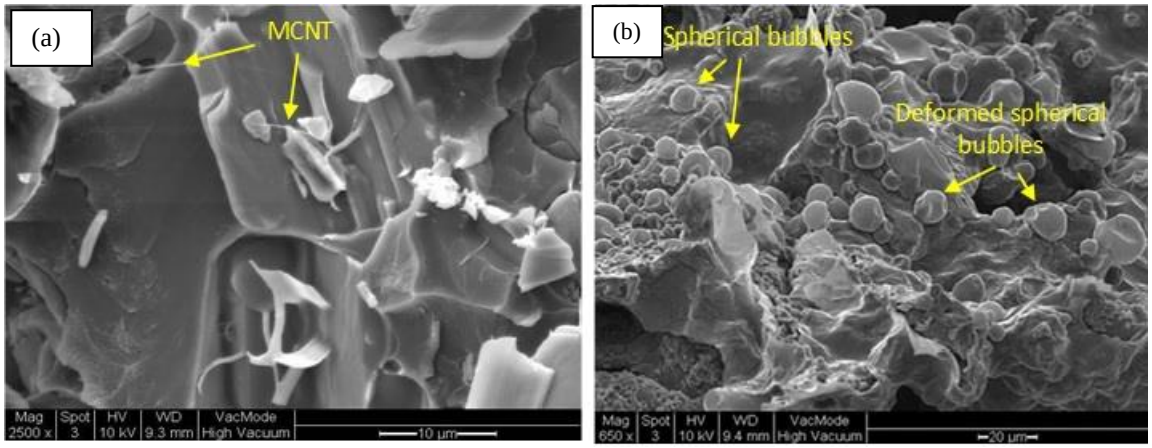

Figure 5. 15 Images of SEM micrograph of IC-MCNT sample cross-sections: (a) Before testing: Rope-like CNTs found on the untested sample surface; (b) After testing: Spherical bubbles distributed on the tested sample surface

For IC-MCNT before testing (see figure 5.15 (a)) shows rope-like CNTs are distributed on the irregular surface of the coating. Under the SEM the IC-MCNT char (see figure 5.15(b)) showed a large number of spherical bubbles present on the surface. Some of these bubbles seem to be deformed.

The formation of these bubbles might be attributed to an excessive gas phase in the polymer matrix influenced by MCNT. Kashiwagi *et al.* (2005b) have reported that this strong bubbling during combustion can be reduced with the presence of nanoclay particles.

The results also revealed that entanglement between the nanotubes interrupts the char morphology structure and network, which later produces poor char structure and a weak bond to the steel.

5.7 Conclusion

A thermal analysis study reveals that carbon-based nanomaterials like graphene and MCNT promote the carbonization process resulting in higher amounts of final residue >20 %. IC-MCNT has the highest amount of remaining char at 26.6 % followed by IC-Graphene (21.1 %), IC-Clay (19.0 %) and IC (17.9 %).

IC-Clay attained the lowest temperature (283 °C) after two hours of the fire test. A different reaction was observed by the addition of 0.5 % MCNT, where it caused degradation in the flame retardancy of the IFT, which was worse than a formulation without the addition of nanoparticles. However, the thermal analysis results showed that IC-MCNT promoted the generation of the most carbonaceous char. Nevertheless, the high thermal conductivity of CNT defeats the purpose of using it as a intumescence fire barrier.

There was no significant different in IC sample microstructures before and after the test unlike coatings with nanomaterials additives. The char produced from the IC-Clay formulation was the sturdiest in terms of maintaining its form and structure during removal from the testing frame, which suggests better char structure was formed during the combustion process.

Agglomerations of halloysite clays were observed, with some of them sticking out from the surface. Radial crystalline nucleation of halloysite was observed on IC-Clay char under the SEM, indicating the crystallization of the char structure which is believed to help strengthen the char.

Stacked flaky graphene was observed on the IC-Graphene samples before the fire tests. A coarse and flaky microstructure was detected on the IC-Graphene char samples after the test, with some of the graphene flakes having bonded onto the matrix.

The spherical bubbles found in IC-MCNT char samples observed through SEM could have contributed to its weaker fire protection. The formation of these bubbles is due to the strong bond between nanotubes that may have contributed to excessive bubble formation during combustion.

SEM examination of all samples before the fire test showed agglomerations of nanoparticles. It is recommended to use specific dispersion techniques with different nanoparticle-matrix combinations, as the agglomeration and dispersion processes of various nanoparticles are not similar. It can be concluded that the addition of 0.5 wt. % of halloysite and graphene is able to effectively reduce the heat flux on the substrate.

Chapter 6. Conclusion

6.1 Overall Conclusion

Different mechanisms of passive fire protection has been determined and established through the studies. One of the major findings is that the thin and light weight multi-layered laminate developed able to be used as a new form of PFP on aluminium substrate without adding significant weight to the structure. The main consideration of using aluminium as a structure is due to its weight saving factor compare to the steel structure. Excess PFP weight on the aluminium structure will defeat the purpose of using aluminium. The use of high melting point foil as a front surface in the multi-layered laminate is recommended as to increase the fire protection and prevent the front surface from broken upon exposure to high temperature (~1000^{o}C).

Metallic foils are widely available making the price is more affordable compared to other conventional PFP such as intumescent coating. The used of non fire-retardant resin as a binder in the laminate open the option to various type of resin in the market. The resin application on the laminate is much easier than the application of intumescent coating because of the low viscosity of the resin.

In structural application that required high temperature material performance, steel is still favourable than aluminium because of its higher temperature degradation. In this case, weight of the PFP usually is not a critical factor, but the duration of protection is more important. There are a wide range of PFP systems available commercially, and these PFPs are required to undergo a stringent large-scale commercialization test before entering the market. The recently developed models based on small-scale propane burner testing is relevant to any new development of PFP as initial assessment before proceeding with the expensive large-scale test.

The general conclusions of each project are listed below.

The multi-layered laminates were successfully developed and conclusion of the thermal properties and effect of using metallic foils as PFP can be drawn as follows:

- Ti/Al and SS/Al provide better fire protection than Al/Al either on aluminium or carbon laminate substrate upon exposure to a direct propane burner flame at 35 or 116 kW/m^2 constant heat flux. This is supported by the step-change experimental results which indicate that Al/Al has higher thermal diffusivity

- The low melting point of aluminium caused the Al/Al to soften and tear during fire testing, which became the route for heat to be transferred to the substrate. Whereas for Ti/Al and SS/Al the front face is still intact due to the higher melting temperature.

- The fire under tensile load test revealed that the failure temperatures for all samples were between 181 to 266℃ which is around the recrystallization temperature (200℃) of aluminium. At this temperature, the strength of aluminium is significantly reduced to 50% of its yield strength. The failure temperature found in Al/Al is higher compared to those in Ti/Al and SS/Al although the failure time shows no significant difference.

- The fire under compression load test indicated that the time to failure of all samples are close. This could be due to the fact that the small size of the compression sample (50mm x 50mm) minimise the differences in fire protection given by the different multi-layered laminates.

- The horizontal testing in the cone calorimeter revealed that Al/Al performed better than Ti/Al and SS/Al on either aluminium or carbon laminate substrate. It is assumed that the low thermal conductivity of Ti and SS led to the hot gases from the pyrolysis being trapped within the samples. This indicates that the fire protection performance of multi-layered laminates depends on the orientation of testing which affects the heat transfer mode, thermal flows and heat flux direction to the exposed surface.

The main objectives of the second project was to evaluate the new models, Model I (Insulated Rear Face) and Model II (Uninsulated Rear Face), using different types of PFP (commercial intumescent coating, ceramic wool and furan microsphere composite). The following conclusions were drawn from this study:

- The three PFP materials show similar temperature-time profiles even though they reacted differently upon exposure to fire. The furan microsphere shows good thermal stability with high levels of final residue compared to the intumescent coating, according to the TGA results.

- Furan microsphere formed a fragile char after fire testing due to the degradation of the biodegradable resin. It does not produce observable smoke compared to intumescent coating during the fire test, which is beneficial to the environment.

- The simulation results using Model I and Model II demonstrate a good fit with the experimental results for all samples especially for furan microsphere and kaowool. Data gathered from this study suggested that both Model I and Model II are able to simulate the temperature profile of steel with different kinds of PFP.

The final project aimed to determine the influence of nanoparticles, halloysite, multiwall carbon nanotube and graphene in the intumescent coating upon exposure to constant heat flux. The effects of the addition of nanoparticles on the intumescent coating fire protection can be summarised as follows:

- TGA results indicate that the graphene and MCNT developed extra carbonization reaction resulting in higher amounts of final residues >20% compared to the addition of halloysite.

- After 2 hours of constant heat flux exposure, IC-Clay was able to offer better protection compared to the other samples with a steel temperature of 283°C. The addition of MCNT was found to increase the thermal conductivity of the intumescent coating, thus increasing the steel temperature.

- The char produced from the IC-Clay formulation was the sturdiest and still maintained its structure even after removal from the testing frame, while the IC-MCNT and IC char were the weakest.

- SEM images of all coatings before the fire test indicate agglomerations of nanoparticles due to poor dispersion. Observation of the coatings char under SEM indicate different char microstructures. IC-Clay char shows the radial crystalline nucleation of halloysite char, which is believed to strengthen the char, while the IC-Graphene char has a more flaky and coarse microstructure. IC-MCNT, on the other hand is revealed to have a microstructure of spherical bubbles that could be formed due to the strong bond between the nanotube particles.

- The temperature profile of the steel was simulated using Model II established in the second project. Overall the simulation results indicate a fairly good fit with the experimental results

6.2 Recommendations for Future Work

It is recommended that the multi-layered laminate results should be simulated in order to give a better understanding and to validate the findings, although the experimental results do show consistency from test repetitions.

Due to the limitation of Universal Testing Machine (UTM), the small size of the compression sample implied a minimal effect of multi-layered protection on the aluminium plate. Therefore, it is suggested that the compression test is conducted on a different UTM that could perform with bigger sample size and give more justification of multi-layered protection performance.

It would be interesting to further evaluate Model I and Model II on other PFP materials such as cementitious coatings or calcium silicate board with different thicknesses. It is also suggested that changes in material thickness are included in the models to capture the thickness changes in certain type of PFP.

The main improvement needed for the third project is to improve the dispersion of the nanoparticles. Therefore, a better dispersion technique such as ball milling or centrifugal milling combined with ultrasound sonication might help to properly disperse the nanoparticles.

References

1. Afaghi Khatibi, A., Kandare, E., Feih, S., Lattimer, B.Y., Case, S.W. and Mouritz, A.P. (2014) 'Finite element modelling of tensile deformation and failure of aluminium plate exposed to fire', Computational Materials Science, 95, pp. 242-249.
2. Alongi, J., Han, Z.D. and Bourbigot, S. (2015) 'Intumescence: Tradition versus novelty. A comprehensive review', Progress in Polymer Science, 51, pp. 28-73.
3. Babrauskas (2003) 'Ignition Handbook: Principles and Applications to Fire Safety Engineering, Fire Investigation, Risk Management and Forensic Science'.
4. Babrauskas, V. (1992) The Cone Calorimeter. In: Heat Release in Fires. London: Elsevier Applied Science.
5. Babrauskas, V. and Peacock, R.D. (1991) 'Heat Release Rate: The Single Most Important Variable in Fire Hazard', Fire Safety Journal, 18, pp. 255-272.
6. Beheshti, A. and Heris, S.Z. (2016) 'Is MWCNT a good synergistic candidate in APP–PER–MEL intumescent coating for steel structure?', Progress in Organic Coatings, 90, pp. 252-257.
7. Bertomeu, D., García-Sanoguera, D., Fenollar, O., Boronat, T. and Balart, R. (2012) 'Use of eco-friendly epoxy resins from renewable resources as potential substitutes of petrochemical epoxy resins for ambient cured composites with flax reinforcements', Polymer Composites, 33(5), pp. 683-692.
8. Biedermann, M. and Grob, K. (2006) 'Phenolic resins for can coatings: I. Phenol-based resole analysed by GC–MS, GC×GC, NPLC–GC and SEC', LWT - Food Science and Technology, 39(6), pp. 633-646.
9. Bodzay, B., Bocz, K., Bárkai, Z. and Marosi, G. (2011) 'Influence of rheological additives on char formation and fire resistance of intumescent coatings', Polymer Degradation and Stability, 96(3), pp. 355-362.
10. Bourbigot, S., Le Bras, M., Dabrowski, F., Gilman, J.W. and Kashiwagi, T. (2000) 'PA-6 Clay Nanocomposite Hybrid as Char Forming Agent in Intumescent Formulations', Fire and Materials, 24, pp. 201-208.
11. Bourbigot, S., Turf, T., Bellayer, S. and Duquesne, S. (2009) 'Polyhedral oligomeric silsesquioxane as flame retardant for thermoplastic polyurethane', Polymer Degradation and Stability, 94(8), pp. 1230-1237.
12. Browne, T.N.A. (2006) A model for the structural integrity of composite laminates in fire. Newcastle University.

13. BS, B.S. (2009) EN 1999-1-2: 2007. Eurocode 9-design of aluminium structures-Part 1-2: Structural fire design British Standard
14. Burianek, D.A. and Spearing, S.M. (2000) 'Durability of titanium-graphite hybrid laminates', in Dardon, H., Fukuda, H., Reifsnider, K.L. and Verchery, G. (eds.) Recent Developments in Durability Analysis of Composite Systems. Netherlands: A.A.Balkema, pp. 465-472.
15. Bwalya, A. (2008) 'An Overview of Design Fires for Building Compartments', Fire Technology, 44(2), pp. 167-184.
16. Camino, G., Costa, L. and Martinasso, G. (1989) 'Intumescent fire-retardant systems', Polymer Degradation and Stability, 23(4), pp. 359-376.
17. Camino, G., Costa, L. and Trossarelli, L. (1984) 'Study of the mechanism of intumescence in fire retardant polymers: Part II—Mechanism of action in polypropylene-ammonium polyphosphate-pentaerythritol mixtures', Polymer Degradation and Stability, 7(1), pp. 25-31.
18. Camino, G. and Luda, M.P. (1998) 'Mechanistic Study On Intumescence', in Fire Retardancy of Polymers. Woodhead Publishing, pp. 48-63.
19. Campaner, P., D'Amico, D., Longo, L., Stifani, C. and Tarzia, A. (2009) 'Cardanol-based novolac resins as curing agents of epoxy resins', Journal of Applied Polymer Science, 114(6), pp. 3585-3591.
20. Chatterjee, S., Wang, J.W., Kuo, W.S., Tai, N.H., Salzmann, C., Li, W.L., Hollertz, R., Nüesch, F.A. and Chu, B.T.T. (2012) 'Mechanical reinforcement and thermal conductivity in expanded graphene nanoplatelets reinforced epoxy composites', Chemical Physics Letters, 531, pp. 6-10.
21. Christke, S., Gibson, A.G., Grigoriou, K. and Mouritz, A.P. (2016) 'Multi-layer polymer metal laminates for the fire protection of lightweight structures', Materials & Design, 97, pp. 349-356.
22. Davies, J.M., Wang, Y.C. and Wong, P.M.H. (2006) 'Polymer composites in fire', Composites Part A: Applied Science and Manufacturing, 37(8), pp. 1131-1141.
23. Desgrosseilliers, L., Groulx, D. and White, M.A. (2013) 'Heat conduction in laminate multilayer bodies with applied finite heat source', International Journal of Thermal Sciences, 72, pp. 47-59.

24. Ding, X., Fang, F., Du, T., Zheng, K., Chen, L., Tian, X. and Zhang, X. (2016) 'Carbon nanotube-filled intumescent multilayer nanocoating on cotton fabric for enhancing flame retardant property', Surface and Coatings Technology, 305, pp. 184-191.
25. Dittrich, B., Wartig, K.-A., Hofmann, D., Mülhaupt, R. and Schartel, B. (2013) 'Flame retardancy through carbon nanomaterials: Carbon black, multiwall nanotubes, expanded graphite, multi-layer graphene and graphene in polypropylene', Polymer Degradation and Stability, 98(8), pp. 1495-1505.
26. Drysdale, D. (1999) An introduction to fire dynamics. 2nd edn. Chichester: Wiley
27. Du, B. and Fang, Z. (2011) 'Effects of carbon nanotubes on the thermal stability and flame retardancy of intumescent flame-retarded polypropylene', Polymer Degradation and Stability, 96(10), pp. 1725-1731.
28. Du, B., Guo, Z. and Fang, Z. (2009) 'Effects of organo-clay and sodium dodecyl sulfonate intercalated layered double hydroxide on thermal and flame behaviour of intumescent flame retarded polypropylene', Polymer Degradation and Stability, 94(11), pp. 1979-1985.
29. Duncan, J. (2001) Fire Protection Systems. Second Edition edn. United States of America: American Society of Plumbing Engineers.
30. Duquesne, S., Magnet, S., Jama, C. and Delobel, R. (2004) 'Intumescent paints: fire protective coatings for metallic substrates', Surface and Coatings Technology, 180-181, pp. 302-307.
31. Easby, R.C. (2007) Fire Behaviour of Pultruded Composites. Newcastle University
32. Faggiano, B., De Matteis, G., Landolfo, R. and Mazzolani, F.M. (2004) 'Behaviour of aluminium alloy structure under fire', Journal of Civil Engineering and Management 10(3).
33. Feih, S. (2005) Finding kinetic parameter from TGA curves with a Multi-branch least square fit. Ltd.
34. Feih, S., Mouritz, A.P., Mathys, Z. and Gibson, A.G. (2007) 'Tensile Strength Modeling of Glass Fiber Polymer Composites in Fire', Journal of Composite Materials, 41(19), pp. 2387-2410.
35. Fogle, E.J., Lattimer, B.Y., Feih, S., Kandare, E., Mouritz, A.P. and Case, S.W. (2012) 'Compression load failure of aluminum plates due to fire', Engineering Structures, 34, pp. 155-162.

36. Formosa, J., Chimenos, J.M., Lacasta, A.M. and Haurie, L. (2011) 'Thermal study of low-grade magnesium hydroxide used as fire retardant and in passive fire protection', Thermochimica Acta, 515(1-2), pp. 43-50.
37. Gaetano, L.D. (2010) Aerospace composite materials in fire. Newcastle University.
38. Gandini, A. and Lacerda, T.M. (2015) 'From monomers to polymers from renewable resources: Recent advances', Progress in Polymer Science, 48, pp. 1-39.
39. Gérard, C., Fontaine, G., Bellayer, S. and Bourbigot, S. (2012) 'Reaction to fire of an intumescent epoxy resin: Protection mechanisms and synergy', Polymer Degradation and Stability, 97(8), pp. 1366-1386.
40. Gibson, A.G., Feih, S. and Mouritz, A.P. (2011) 'Developments in Characterising the Structural Behavior of Composite in Fire', in Composite Material A Vision for the Future. Springer, pp. 187-218.
41. Gibson, A.G., Jusoh, W.W., Kotsikos, G., P., D.M. and S., C. (2016) 'Model for the Characterisation and Design of Passive Fire Protection (PFP) Systems for Steel Structures'.
42. Gibson, A.G., Torres, M.E.O., Browne, T.N.A., Feih, S. and Mouritz, A.P. (2010) 'High temperature and fire behaviour of continuous glass fibre/polypropylene laminates', Composites Part A: Applied Science and Manufacturing, 41(9), pp. 1219-1231.
43. Gibson, A.G., Wu, Y.S., Chandler, H.W., Wilcox, J.A.D. and Bettes, P. (1995) 'A model for the thermal performance of thick composite laminate in hydrocarbons fires', Revue de L'Institut Francais du Petrole, 50, pp. 69-74.
44. Gibson, A.G., Wu, Y.S., Evans, J.T. and Mouritz, A.P. (2006) 'Laminate theory analysis of composites under load in fire', Journal of Composite Materials, 40(7), pp. 639-658.
45. Gibson, N. (1994) Hazards: European Advances in Process Safety 12th United Kingdom. The Institution of Chemical Engineers.
46. Gilman, J.W., Jackson, C.L., Morgan, A.B. and Harris, R.J. (2000) 'Flammability Properties of Polymer-Layered-Silicate Nanocomposites. Polypropylene and Polystyrene Nanocomposites'.
47. Gomez-Mares, M., Tugnoli, A., Landucci, G., Barontini, F. and Cozzani, V. (2012a) 'Behavior of intumescent epoxy resins in fireproofing applications', Journal of Analytical and Applied Pyrolysis, 97, pp. 99-108.

48. Gomez-Mares, M., Tugnoli, A., Landucci, G. and Cozzani, V. (2012b) 'Performance Assessment of Passive Fire Protection Materials', Industrial & Engineering Chemistry Research, 51(22), pp. 7679-7689.
49. Gómez-Mares, M., Zárate, L. and Casal, J. (2008) 'Jet fires and the domino effect', Fire Safety Journal, 43(8), pp. 583-588.
50. Greene, E. Marine Composites.
51. Griffin, G.J. (2010) 'The Modeling of Heat Transfer across Intumescent Polymer Coatings', Journal of Fire Sciences, 28(3), pp. 249-277.
52. Grigoriou, K. and Mouritz, A.P. (2016) 'Comparative assessment of the fire structural performance of carbon-epoxy composite and aluminium alloy used in aerospace structures', Materials & Design, 108, pp. 699-706.
53. Grober, H., Erk, S. and Grigull, U. (1961) Fundamentals of Heat Transfer. New York,: McGraw-Hill Book Company Inc.
54. Guigo, N., Mija, A., Zavaglia, R., Vincent, L. and Sbirrazzuoli, N. (2009) 'New insights on the thermal degradation pathways of neat poly(furfuryl alcohol) and poly(furfuryl alcohol)/SiO2 hybrid materials', Polymer Degradation and Stability, 94(6), pp. 908-913.
55. Guo, Y., Bao, C., Song, L., Yuan, B. and Hu, Y. (2011) 'In Situ Polymerization of Graphene, Graphite Oxide, and Functionalized Graphite Oxide into Epoxy Resin and Comparison Study of On-the-Flame Behavior', Industrial & Engineering Chemistry Research, 50(13), pp. 7772-7783.
56. Gupta, A.K., Kumar, R., Yadav, P.K. and Naveen, M. (2001a) 'Fire safety through mathematical modelling ', Current Science 80(1), pp. 18-26.
57. Gupta, A.K., Lloyd, D.J. and Court, S.A. (2001b) 'Precipitation hardening processes in an Al–0.4%Mg–1.3%Si–0.25%Fe aluminum alloy', Materials Science and Engineering: A, 301(2), pp. 140-146.
58. Gupta, A.P., Ahmad, S. and Dev, A. (2011) 'Modification of novel bio-based resin-epoxidized soybean oil by conventional epoxy resin', Polymer Engineering & Science, 51(6), pp. 1087-1091.
59. Heisler, M.P. (1947) 'Temperature Charts for Induction Heating and Constant-Temperature, Trans', ASME, 69, pp. 227-236.
60. Henderson, J.B., Tant, M.R., Doherty, M.P. and O'Brien, E.F. (1987) 'Characterization of the high-temperature behaviour of a glass-filled polymer composite', Composites, 18(3), pp. 205-215.

61. Henderson, J.B., Wiebelt, J.A. and Tant, M.R. (1985) 'A model for the thermal response of polymer composite materials with experimental verification', Journal of Composite Materials, 19, pp. 579-595.
62. Hergenrother, P.M., Thompson, C.M., Smith, J.G., Connell, J.W., Hinkley, J.A., Lyon, R.E. and Moulton, R. (2005) 'Flame retardant aircraft epoxy resins containing phosphorus', Polymer, 46(14), pp. 5012-5024.
63. Hornsby, P.R. (2007) 'The Application of Fire-Retardant Fillers for Use in Textile Barrier Materials', in Duquesne, S., Magniez, C. and Camino, G. (eds.) Multifunctional Barriers for Flexible Structure. Textile, Leather and Paper. Berlin, Germany Springer.
64. Horrocks, A.R., Anand, S.C. and Sanderson, D. (1996) 'Complex char formation in flame retarded fibre-intumescent combinations: 1. Scanning electron microscopic studies', Polymer, 37(15), pp. 3197-3206.
65. Hull, T.R. and Kandola, B.K. (2008) 'Introduction. Polymers and Fire', pp. 1-14.
66. Hull, T.R. and Stec, A.A. (2009) 'Introduction Polymers and Fire', in Hull, T.R. and Kandola, B.K. (eds.) Fire Retardancy of Polymers: New Strategies and Mechanisms. The Royal Society of Chemistry, pp. 1-14.
67. Hull, T.R., Witkowski, A. and Hollingbery, L. (2011) 'Fire retardant action of mineral fillers', Polymer Degradation and Stability, 96(8), pp. 1462-1469.
68. Hung, W.Y. and Chow, W.K. (2002) 'Review on the requirements on fire resisting construction ', International Journal on Engineering Performance-Based Fire Codes 4(3), pp. 68-83.
69. IMO, I.M.O. (1998) Resolution A.754(18). Recommendation on fire resistance tests for "A", "B" and "F" class division. FTP code - international code for application of fire test procedures London
70. Isitman, N.A. and Kaynak, C. (2010) 'Nanoclay and carbon nanotubes as potential synergists of an organophosphorus flame-retardant in poly(methyl methacrylate)', Polymer Degradation and Stability, 95(9), pp. 1523-1532.
71. Jimenez, M., Duquesne, S. and Bourbigot, S. (2006a) 'Characterization of the performance of an intumescent fire protective coating', Surface and Coatings Technology, 201(3-4), pp. 979-987.
72. Jimenez, M., Duquesne, S. and Bourbigot, S. (2006b) 'Intumescent fire protective coating: Toward a better understanding of their mechanism of action', Thermochimica Acta, 449(1-2), pp. 16-26.

73. Kahraman, H.T., Gevgilili, H., Pehlivan, E. and Kalyon, D.M. (2015) 'Development of an epoxy based intumescent system comprising of nanoclays blended with appropriate formulating agents', Progress in Organic Coatings, 78, pp. 208-219.
74. Kandare, E., Feih, S., Kootsookos, A., Mathys, Z., Lattimer, B.Y. and Mouritz, A.P. (2010a) 'Creep-based life prediction modelling of aluminium in fire', Materials Science and Engineering: A, 527(4-5), pp. 1185-1193.
75. Kandare, E., Feih, S., Lattimer, B.Y. and Mouritz, A.P. (2010b) 'Larson–Miller Failure Modeling of Aluminum in Fire', Metallurgical and Materials Transactions A, 41(12), pp. 3091-3099.
76. Kandare, E., Luangtriratana, P. and Kandola, B.K. (2014) 'Fire reaction properties of flax/epoxy laminates and their balsa-core sandwich composites with or without fire protection', Composites Part B: Engineering, 56, pp. 602-610.
77. Kandola, B., Ebdon, J. and Chowdhury, K. (2015) 'Flame Retardance and Physical Properties of Novel Cured Blends of Unsaturated Polyester and Furan Resins', Polymers, 7(2), pp. 298-315.
78. Kashiwagi, T., Du, F., Douglas, J.F., Winey, K.I., Harris, R.H., Jr. and Shields, J.R. (2005a) 'Nanoparticle networks reduce the flammability of polymer nanocomposites', Nat Mater, 4(12), pp. 928-33.
79. Kashiwagi, T., Du, F., Winey, K.I., Groth, K.M., Shields, J.R., Bellayer, S.P., Kim, H. and Douglas, J.F. (2005b) 'Flammability properties of polymer nanocomposites with single-walled carbon nanotubes: effects of nanotube dispersion and concentration', Polymer, 46(2), pp. 471-481.
80. Kashiwagi, T., Harris Jr, R.H., Zhang, X., Briber, R.M., Cipriano, B.H., Raghavan, S.R., Awad, W.H. and Shields, J.R. (2004) 'Flame retardant mechanism of polyamide 6–clay nanocomposites', Polymer, 45(3), pp. 881-891.
81. Kashiwagi, T., John R. Shields, Richard H. Harris, J. and Davis, R.D. (2002) 'Flame-Retardant Mechanism of Silica: Effects of Resin
82. Molecular Weight', Journal of Applied Polymer Science, Vol. 87, pp. 1541–1553.
83. Keles, O. and Dundar, M. (2007) 'Aluminum foil: Its typical quality problems and their causes', Journal of Materials Processing Technology, 186(1-3), pp. 125-137.
84. Kim, D. and Ramulu, M. (2007) 'Study on the Drilling of Titanium/Graphite Hybrid Composites', Journal of Engineering Materials and Technology, 129(3), p. 390.
85. Kontogeorgos, D.A. and Founti, M.A. (2012) 'Gypsum board reaction kinetics at elevated temperatures', Thermochimica Acta, 529, pp. 6-13.

86. Laachachi, A., Burger, N., Apaydin, K., Sonnier, R. and Ferriol, M. (2015) 'Is expanded graphite acting as flame retardant in epoxy resin?', Polymer Degradation and Stability, 117, pp. 22-29.
87. Landucci, G., Rossi, F., Nicolella, C. and Zanelli, S. (2009) 'Design and testing of innovative materials for passive fire protection', Fire Safety Journal, 44(8), pp. 1103-1109.
88. Langhelle, N.K. and Amdahl, J. (2001) Eleventh (2001) International Offshore and Polar Engineering Conference. Stavanger, Norway. The Interational Society of Offshore and Polar Engineers.
89. Laoutid, F., Bonnaud, L., Alexandre, M., Lopez-Cuesta, J.M. and Dubois, P. (2009) 'New prospects in flame retardant polymer materials: From fundamentals to nanocomposites', Materials Science and Engineering: R: Reports, 63(3), pp. 100-125.
90. Lecouvet, B., Sclavons, M., Bailly, C. and Bourbigot, S. (2013a) 'A comprehensive study of the synergistic flame retardant mechanisms of halloysite in intumescent polypropylene', Polymer Degradation and Stability, 98(11), pp. 2268-2281.
91. Lecouvet, B., Sclavons, M., Bourbigot, S. and Bailly, C. (2013b) 'Thermal and flammability properties of polyethersulfone/halloysite nanocomposites prepared by melt compounding', Polymer Degradation and Stability, 98(10), pp. 1993-2004.
92. Lee, C.-W., Liu, L. and Holmes, W.J. (2013) 'Experimental Investigation of Mode I Fatigue Crack Growth
93. Behavior of Titanium Foils', 13th International Conference on Fracture
94. June 16–21, 2013, Beijing, China. Beihing, China.
95. Liang, J.-Z. (2013) 'Thermal conductivity of PP/Al(OH)3/Mg(OH)2 composites', Composites Part B: Engineering, 44(1), pp. 248-252.
96. Lindholm, J., Brink, A. and Hupa, M. (2012) 'Influence of decreased sample size on cone calorimeter results', Fire and Materials, 36(1), pp. 63-73.
97. Liu, S., Yan, H., Fang, Z. and Wang, H. (2014) 'Effect of graphene nanosheets on morphology, thermal stability and flame retardancy of epoxy resin', Composites Science and Technology, 90, pp. 40-47.
98. Liukov, A.V. (1968) Analytical heat diffusion theory New York,: Academic Press,.
99. Lu, H. and Wilkie, C.A. (2010) 'Study on intumescent flame retarded polystyrene composites with improved flame retardancy', Polymer Degradation and Stability, 95(12), pp. 2388-2395.

100. Lyon, R.E. (1998) 'Pyrolysis kinetics of char forming polymers', Polymer Degradation and Stability, 61(2), pp. 201-210.
101. Maljaars, J., Fellinger, J. and Soetens, F. (2005) 'Fire exposed aluminium structures', HERON Journal 50(4).
102. Maljaars, J., Soetens, F. and Snijder, H.H. (2009a) 'Local buckling of aluminium structures exposed to fire. Part 1: Tests', Thin-Walled Structures, 47(11), pp. 1404-1417.
103. Maljaars, J., Twilt, L., Fellinger, J., Snijder, H.H. and Soetens, F. (2010) 'Aluminium structure exposed to fire conditions-an overview', HERON Journal, 55(2).
104. Maljaars, J., Twilt, L. and Soetens, F. (2009b) 'Flexural buckling of fire exposed aluminium columns', Fire Safety Journal, 44(5), pp. 711-717.
105. Marchal, A., Delobel, R., Le Bras, M., Leroy, J.-M. and Price, D. (1994) 'Effect of intumescence on polymer degradation', Polymer Degradation and Stability, 44(3), pp. 263-272.
106. McManus, H.L.N. and Springer, G.S. (1992) 'High Temperature Thermomechanical Behavior of Carbon-Phenolic and Carbon-Carbon Composites, I. Analysis', Journal of Composite Materials, 26(2).
107. Mesquita, L.M.R., Piloto, P.A.G., Vaz, M.A.P. and Pinto, T.M.G. (2009) 'Decomposition of Intumescent Coatings: Comparison between a Numerical Method and Experimental Results', Acta Polytechnica, 49(1/2009), pp. 60-65.
108. Mhike, W., Ferreira;, I.V.W., Li;, J., Stoliarov;, S.I. and Focke, W.W. (2014) 'Flame Retarding Effect of Graphite in Rotationally MoldedPolyethylene/Graphite Composites'.
109. Milke, J. (2016) 'Fire protection as the underpinning of good process safety programs', Journal of Loss Prevention in the Process Industries, 40, pp. 329-333.
110. Moghtaderi, B., Novozhilov, V., Fletcher, D. and Kent, J.H. (1997) 'An integral model for the transient pyrolysis of solid materials. ', Fire and Materials, 21(1), pp. 7-16.
111. Mohammadi, S., Shariatpanahi, H. and Taromi, F.A. (2015) 'Influence of hybrid functionalized graphite nanoplatelets-tripolyphosphate on improvement in fire protection of intumescent fire resistive coating for steel structures', Polymer Degradation and Stability, 120, pp. 135-148.
112. Monti, M., Hoydonckx, H., Stappers, F. and Camino, G. (2015) 'Thermal and combustion behavior of furan resin/silica nanocomposites', European Polymer Journal, 67, pp. 561-569.

113. Mouritz, A.P. and Gibson, A.G. (2006). Fire Properties of Polymer Composite Materials. Springer Netherlands.
114. Mouritz, A.P., Mathys, Z. and Gibson, A.G. (2006) 'Heat release of polymer composites in fire', Composites Part A: Applied Science and Manufacturing, 37(7), pp. 1040-1054.
115. Mróz, K., Hager, I. and Korniejenko, K. (2016) 'Material Solutions for Passive Fire Protection of Buildings and Structures and Their Performances Testing', Procedia Engineering, 151, pp. 284-291.
116. Nazir, M.S., Mohamad Kassim, M.H., Mohapatra, L., Gilani, M.A., Raza, M.R. and Majeed, K. (2016) 'Characteristic Properties of Nanoclays and Characterization of Nanoparticulates and Nanocomposites', pp. 35-55.
117. Paulik, F., Paulik, J. and Arnold, M. (1992) 'Thermal decomposition of gypsum', Thermochimica Acta, 200, pp. 195-204.
118. Quang Dao, D., Luche, J., Richard, F., Rogaume, T., Bourhy-Weber, C. and Ruban, S. (2013) 'Determination of characteristic parameters for the thermal decomposition of epoxy resin/carbon fibre composites in cone calorimeter', International Journal of Hydrogen Energy, 38(19), pp. 8167-8178.
119. Rahatekar, S.S., Zammarano, M., Matko, S., Koziol, K.K., Windle, A.H., Nyden, M., Kashiwagi, T. and Gilman, J.W. (2010) 'Effect of carbon nanotubes and montmorillonite on the flammability of epoxy nanocomposites', Polymer Degradation and Stability, 95(5), pp. 870-879.
120. Rivero, G., Fasce, L.A., Ceré, S.M. and Manfredi, L.B. (2014) 'Furan resins as replacement of phenolic protective coatings: Structural, mechanical and functional characterization', Progress in Organic Coatings, 77(1), pp. 247-256.
121. Rivero, G., Pettarin, V., Vázquez, A. and Manfredi, L.B. (2011) 'Curing kinetics of a furan resin and its nanocomposites', Thermochimica Acta, 516(1-2), pp. 79-87.
122. Schartel, B., Bartholmai, M. and Knoll, U. (2005) 'Some comments on the use of cone calorimeter data', Polymer Degradation and Stability, 88(3), pp. 540-547.
123. Shan, G., Jin, W., Chen, H., Zhao, M., Surampalli, R., Ramakrishnan, A., Zhang, T. and Tyagi, R.D. (2015) 'Flame-Retardant Polymer Nanocomposites and Their Heat-Release Rates', Journal of Hazardous, Toxic, and Radioactive Waste, 19(4), p. 04015006.

124. Sinmazçelik, T., Avcu, E., Bora, M.Ö. and Çoban, O. (2011) 'A review: Fibre metal laminates, background, bonding types and applied test methods', Materials & Design, 32(7), pp. 3671-3685.
125. Snegirev, A.Y., Talalov, V.A., Stepanov, V.V. and Harris, J.N. (2013) 'A new model to predict pyrolysis, ignition and burning of flammable materials in fire tests', Fire Safety Journal, 59, pp. 132-150.
126. Staggs, J.E.J., Crewe, R.J. and Butler, R. (2012) 'A theoretical and experimental investigation of intumescent behaviour in protective coatings for structural steel', Chemical Engineering Science, 71, pp. 239-251.
127. Summers, P.T., Case, S.W. and Lattimer, B.Y. (2014) 'Residual mechanical properties of aluminum alloys AA5083-H116 and AA6061-T651 after fire', Engineering Structures, 76, pp. 49-61.
128. Suzuki, J., Ohmiya, Y., Wakamatsu, T., Harada, K., Yuasa, S. and Kohno, M. (2005) 'Evaluation of fire resistance of aluminium alloy members', Fire Science and Technology 24(4), pp. 237-255.
129. Tant, M.R., Henderson, J.B. and Boyer, C.T. (1985) 'Measurement and modelling of the thermochemical expansion of polymer composites', Composites, 16(2), pp. 121-126.
130. Tsai, K.C. (2009) 'Orientation effect on cone calorimeter test results to assess fire hazard of materials', J Hazard Mater, 172(2-3), pp. 763-72
131. Ullah, S. and Ahmad, F. (2014) 'Effects of zirconium silicate reinforcement on expandable graphite based intumescent fire retardant coating', Polymer Degradation and Stability, 103, pp. 49-62
132. Vandermeer, R.A. and Hansen, N. (2008) 'Recovery kinetics of nanostructured aluminum: Model and experiment', Acta Materialia, 56(19), pp. 5719-5727.
133. Vincenzo, U.M. (2011) Modelling composite fire behaviour using apparent thermal diffusivity. Newcastle University
134. Wan Jusoh, W., Kotsikos, G. and Gibson, A.G. (2017) 'A propane burner test to characterise the performance of passive fire protection (PFP) formulations', 16th European Meeting on Fire Retardant Polymeric Materials. Manchester, UK
135. Wang, D. and Wilkie, C.A. (2006) 'Fire Properties of Polymer Nanocomposites ', in Gladwell, G.M.L. (ed.) Fire Properties of Polymer Composite Materials Netherlands: Springer, pp. 287-312.

136. Wang, L., Wang, Y.C. and Li, G.Q. (2010) Structure in Fire Sixth International Conference. Michigan, USA. DEStech Publications, Inc.
137. Weil, E.D., Hirschler, M.M., Patel, N.G., Said, M.M. and S.Shakir (1992) 'Oxygen index: Correlations to other fire tests', Fire and Materials, 16, pp. 159-167.
138. Xu, J. and Fang, T. (2013) 'Experimental Study on Combustion Characteristics for Polyurethane-aluminum Composite Insulation Material under Different Heat Fluxes', Procedia Engineering, 62, pp. 837-843.
139. Yovanovich, M.M. (1996) Simple explicit expressions for calculation of the Heisler-Grober charts. Canada University of Waterloo.
140. Yuan, B., Bao, C., Song, L., Hong, N., Liew, K.M. and Hu, Y. (2014) 'Preparation of functionalized graphene oxide/polypropylene nanocomposite with significantly improved thermal stability and studies on the crystallization behavior and mechanical properties', Chemical Engineering Journal, 237, pp. 411-420.
141. Zaman, I., Phan, T.T., Kuan, H.-C., Meng, Q., Bao La, L.T., Luong, L., Youssf, O. and Ma, J. (2011) 'Epoxy/graphene platelets nanocomposites with two levels of interface strength', Polymer, 52(7), pp. 1603-1611.
142. Zhang, P., Hu, Y., Song, L., Ni, J., Xing, W. and Wang, J. (2010) 'Effect of expanded graphite on properties of high-density polyethylene/paraffin composite with intumescent flame retardant as a shape-stabilized phase change material', Solar Energy Materials and Solar Cells, 94(2), pp. 360-365.
143. Zhu, J., Uhl, F.M., Morgan, A.B. and Wilkie, C.A. (2001) 'Studies on the Mechanism by Which the Formation of Nanocomposites Enhances Thermal Stability', Chemistry of Material 13, pp. 4649-4651.